

# Characterization of acidic and basic properties of heterogeneous catalysts by test reactions

Von der Fakultät für Mathematik und  
Naturwissenschaften der



zur Erlangung des Grades eines  
Doktors der Naturwissenschaften  
- Dr. rer. nat. -

angenommene

Dissertation

Von

M.Sc. Murad Alsawalha

Geboren am 14.03.1973 in Kuwait (Kuwait)

Betreuender Erstgutachter: Prof. Dr. Frank Rößner

Korreferent: Prof. Dr. Katharina Al-Shamery

Tag der Disputation: 10. Dezember 2004

*For my Parents,  
sisters and brothers*

## Acknowledgements

The completion of this thesis would not have been possible without the support of numerous people. I would like to use this opportunity to thank all of them.

I would like to thank Professor Frank Rößner for the specification of the research topic, his permanent readiness for discussion and his great interest in the success of this work at the University of Oldenburg (Germany). I thank Professor Rößner for his great organisation and for realising the financing of my Ph.D. As a member of the group of Professor Rößner, I appreciate deeply his spiritual support and his motivation for all his students. My thanks belong also to Professor Katharina Al-Shamery and Professor Axel Brehm being referee of this thesis.

I would like to thank the members of the group Technische Chemie II of the University of Oldenburg for many inspiring talks and social hours and for the warm welcome and for supporting me during my study in Germany.

Many thanks go to Dipl.-Chem. Andreas Rausch for great cooperation and critical discussions about this thesis. I thank him again and Gustavo Ota from Brazil for running the  $\text{NH}_3$ -TPD measurements.

I would like to thank Dr. Elke Heitling and Dipl.-Chem. Arne Kuhlmann for allowing me to call on their help whenever needed and Mr. Gerold Bruns and Mr. Frank Rolfes-Busch for their help in the gas phase methyl butynol apparatus and for their support while rearranging and repairing it.

My special thanks go to Mr. Walter Böhringer at the University of Cape Town for the benefit discussion in the kinetic part in my study.

I would like to thank all members of the Faculty of Chemistry, Jagiellonian University of Cracow (Poland) for analytical measurements for the part of hydrotalcites, special thanks for Dr. Piotr Kuśtrowski.

I thank Sasol Germany GmbH (Brunsbüttel) for giving me the opportunity to combine my Ph.D. thesis with industrial work and the financial support. My thanks also go to DAAD for their financial support in part of my study.

My special thanks go to my parents for their patience and love, my sisters and brothers for the backing and the support that I experienced during my study in Germany.

Lastly my thanks also belong to the first people who gave me overall support at the start of my education stage, and Uncle Adel Al-Qasem (Jordan) for the part of financial help at the start of my study and Uncle Fahri Al Thaher who gave me his support before his death.

# Contents

<b>1. Introduction.....</b>	<b>1</b>
<b>2. Literature review.....</b>	<b>4</b>
2.1 The importance of catalysis .....	4
2.2 Base catalysts in chemical reactions.....	7
2.3 Generation of Basic Sites.....	8
2.4 Characterization of basic surfaces.....	10
2.5 Reactions on heterogeneous basic catalysts.....	16
2.6 Heterogeneous basic and acidic catalysts .....	21
<b>3. Experimental part.....</b>	<b>29</b>
3.1 Investigated catalysts.....	29
3.2 Conditions for methyl butynol conversion and experimental apparatus.....	35
3.3 Verification of carbon deposit for MBOH test reaction.....	38
3.4 Conditions for isopropanol test reaction.....	40
3.5 Experimentals for test reaction in liquid phase.....	40
3.6 Analysis and calculations.....	42
3.7 Values of relative response factors.....	45
3.8 Characterization methods.....	49
3.8.1 Characterization of solids with different silica alumina ratios calcined at different temperatures and metal oxides supported on alumina.....	49
3.8.2 Characterization methods for hydrotalcites derived from mixed magnesium aluminium .....	53
<b>4. Results and discussion .....</b>	<b>55</b>
4.1 Temperature programmed desorption of ammonia from silica alumina.....	55
4.2 Acid properties of the metal oxides supported on alumina.....	58

4.3 Hydrotalcite derived from mixed Mg-Al oxides.....	61
4.3.1 Acid-base properties of the hydrotalcite derived from mixed magnesium aluminium oxides.....	63
4.3.2 X-ray diffraction (XRD).....	64
4.3.3 Infrared spectroscopy (FTIR).....	66
4.3.4 Structural and chemical composition of the mixed magnesium aluminium oxides...	68
4.3.5 BET measurements.....	69
4.4. Methyl butynol conversion.....	73
4.4.1 Catalytic activity of methyl butynol over different silica alumina with different ratios at different reaction temperatures 120 °C, 180 °C.....	73
4.4.2 Influence of reaction temperature and treatment preparations of the sample reaction behavior.....	77
4.4.3 Influence of the deactivation process on the methyl butynol catalytic activity .....	83
4.4.4 The dependency of the selectivity of 3-methyl-3-buten-1-yne as a function of the conversion depending on the silica content over different l ratios.....	86
4.4.5 The formation of 3-methyl-3-butyn-2-one as a function of the conversion depending on the silica content over different silica alumina ratios.....	87
4.4.6 Correlations and formation of 3-methyl-3-butyn-2-one as primary product over silica alumina solids.....	89
4.5 Effect of water on the conversion of methyl butynol.....	93
4.6 Determination of activation energy in the methyl butynol conversion.....	96
4.7 Basicity of hydrotalcite derived from mixed magnesium oxides studied by methyl butynol test reaction.....	104
4.8 Conversion of isopropanol.....	108
4.9 Knoevenagel condensation.....	112
<b>5. Conclusions.....</b>	<b>118</b>
<b>6. References.....</b>	<b>122</b>
<b>7. Appendix.....</b>	<b>128</b>

# 1. Introduction

The current standard of living shapes to a considerable degree the new developments in chemistry. Tailor-made products are not part of these everyday life concerns. Manufactory (synthesis) of these products is tied to a multitude of single procedural steps.

However, the necessary reactivity of the intermediate stages if these reagents make no contribution to the structure of the final product, they must be detoxified correspondingly. From the observation of the data gathered in table 1 it is evident that in the single refining steps, the formation of refuse materials is different.

**Table 1. Accrue ment of by products**

	Amount of product / t	kg intermediate product / kg product	Amount of scrap / t
Refinery	$10^6$	< 0,1	$10^5$
Intermediate products	$10^4 - 10^6$	< 1 ... 5	$10^4$
Fine chemicals	$10^2 - 10^4$	5 ... 50	$5 * 10^5$
Pharmaceuticals	$10 - 10^3$	25 ... 100	$10^5$

One of the most important possibilities to mitigate this accrue ment is the transition from stoichiometric to catalytic conversions whereby a high atom efficiency is striven for.

At the same time two fundamentally different systems can be chosen for example: homogeneous and heterogeneous catalysts. Each catalyst system has its advantages and disadvantages.

From an industrial point of view the good detachability and the high space-time ratio would make heterogeneous catalysts particularly attractive. Heterogeneous catalyzed reactions play an exceptional role in the petrochemical industry; at the same time all isomerization and oligomerization reactions are catalyzed by acid centers. Accordingly the characteristics of such centres were determined comprehensively in the past four decades.

A multitude of characterization methods were developed for investigating the question about nature, strength and amount of the acidic centres. At the same time test reactions play a central role as their great advantage lies incontestably in the fact that the catalyst is examined

under real, as practice-near as possible conditions. Besides the clarification of structural questions, the main goal pursued is the estimation of the acid strength.

With the use of heterogeneous catalysts for the manufacture of intermediate products and fine chemicals, the following problems arise in the conversion over acidic centres:

- \* the molecules are constructed more complexly (for example: hetero-compound)
- \* the acidic centres very often catalyze undesirable secondary reactions
- \* deactivation takes place in an early stage of the reaction.

To avoid these problems, basic catalysts came at the center of interest. In literature, some test reactions have been described for basic systems. In gas phases the following reactions are predominant:

alkylation of toluol with methanol and isomerization of 1-buten (1, 2). On the other hand, test reactions prevail in liquid phases like Knoevenagel condensation (3, 4) and Michael addition (5).

As regards the test reactions reported above, a correlation with the base's strength of the catalyst has so far not been described in literature. A new extension was recently introduced by Laurent-Pernot (6). The conversion of methylbutynol should permit a distinction between the acidic and basic characteristics of a catalyst (7). In contrast to the conversion of isopropanol also amphoteric characteristics of the catalyst should become comprehensible.

The use of 2-methyl-3-buten-2-ol (also known as methylbutynol) for a test reaction was proposed and tested by Lauron *et al.* (6). Here acid, amphoteric and basic catalysts, respectively, show a very suitable reaction by producing different products for each pathway reaction. Further examinations of the mechanism of the conversion of 2-methyl-3-buten-2-ol on  $ZrO_2$  were published by Audry *et al.* (7).

In a comparison of different test reactions Aramendía *et al.* (8) found that the conversion of methylbutynol is a suitable test reaction for the characterisation of the catalyst due to the large spectrum of products, which are formed at different sites of the catalyst (acidic, basic, amphoteric). Consequently the conversion of methylbutynol is suited for the use as test reaction for a classification of catalysts according their acid- base properties (9).



In the present study, a detailed investigation of the conversion of methylbutynol should be conducted at a broad variety of catalysts. The question should be addressed if the problems described in previous literature, such as adsorption of products or the explanations of the formation of by products, can actually be assigned to the nature of the different center types.

This approach implies the following studies in this PhD thesis:

- (a) Establish test reactions for the classification of catalysts, (b) examine the test reactions such as methyl butynol conversion in detail, and (c) Compare methyl butynol test reaction with other test reactions like isopropanol conversion in gas phase and in liquid phase to clarify which reaction characterises which strength. The study aims on different types of catalysts such as silica-aluminas with different ratios calcined at different temperatures, hydrotalcite-like layered double hydroxides and bulk metal oxides supported on alumina. Moreover, the catalytic characteristics should be correlated with the results of other characterisation methods applied to the surface centers like BET, temperature programmed desorption of ammonia ( $\text{NH}_3$ -TPD) and carbon dioxide ( $\text{CO}_2$ -TPD), FTIR spectroscopy and XRD, respectively.

## 2. Literature review

### 2.1 The importance of catalysis

The principal theme in catalysis is the desire to control chemical test reactions and the secondary theme is to understand the mechanisms of the control.

Catalysis is of crucial importance for the environment and for chemical industry, the number of catalysts applied in industry is very large and catalysts come in many different forms, from heterogeneous catalysts in the form of porous solids over homogeneous catalysts dissolved in the liquid reaction mixture to biological catalysts in the form of enzymes.

#### *- Environmental impact*

Progress towards environmentally responsibility is marked by the reduced dependence on hazardous chemicals and by-product generation. The key to both is often provided by catalytic processes as alternatives to stoichiometric processes.

Heterogeneous catalysis, long established in bulk-chemical processing, is beginning to make inroads into the fine chemicals industry also.

In the past, the need to reduce costs was the driving power for improvements in process efficiency, science wasteful processes are also uneconomic. However, recent public concern about the environment, leading to regulatory activity by governments has accelerated this tendency.

Two useful measures of the environmental impact of chemical process (10) are the E-factor defined by the mass of waste to desired product, and the atom utilization, calculated by dividing the molecular weight of the desired product by the sum of molecular weights all substances produced in the stoichiometric redox reagents, represent the major sources of waste production in the form of salts and heavy metals and high E-factors allow high atom utilization.

Reactions of this type, employed in the fine-chemicals industry particularly, include Friedel-Crafts alkylations mediated by Lewis acids such as aluminium chloride, reductions with metal hydrides or dissolving metals such as zinc or iron, and stoichiometric oxidations with

dichromate or permanganate, all of which generate prohibitive amounts of metal-containing wastes.

The elimination of such wastes is the first goal of environmentally friendly processing; the second is the reduction dependence on the use of hazardous chemicals such as phosgene, dimethyl sulphate, peracids, and sodium azide.

A good example of an environmental benefit occurring from the introduction of heterogeneously catalysed process is provided by the petrochemical ethylene (EO), in which the direct oxidation of ethene over silver catalyst replaced the old chlorohydrin process. The direct process has an atom utilization of 100% and a E-factor of zero (1, 2).

#### *- Impact of catalysis on economy*

Catalysis can be an important step in removing key contaminants, both from power plant effluent and from process plants, contributing to efficient energy production and utilization. Catalysis is also important to the chemical and petroleum industries, where advances in catalysis have created many new products and processes.

Catalysis, as it is applied to the industrial production of materials, is both, broad and complex. It has significant implications on process costs and product properties, thereby affecting the competitiveness of the catalytic technology (via intellectual property). Catalysis is responsible for the efficient, low cost manufacture of products as diverse to each other as gasoline is to aspirin. A foundation so deep that can be state that "most of the global economy and societal gains over the last 100 years would not have been possible without it (10).

Catalysis is an important scientific and technological area for the development of environmentally friendly chemical processes, and fundamental to process optimization, waste reduction and pollution prevention. These in turn underlie cleaner industrial development and are key elements in an overall philosophy of industrial pollution prevention. New, less polluting processes together with optimization of existing processes depend greatly on improvement of catalyst performance in heavy and fine chemical production lines

Catalysts and the products made with them are all around us, even though most people know neither what a catalyst is nor what they do. Some experts claim that catalysts are involved in the manufacture of products that represent about one-quarter of the entire U.S. Gross National Product. Considering that a high percentage of chemical and refined petroleum products are made via catalytic reactions (some experts put the percentage at 90% or higher for chemicals), this value seems logical (10).

Virtually every polymer, whether it is a synthetic fiber, a plastic resin, or an elastomer, is made with a catalytic process. Other chemicals, from pharmaceuticals to pesticides, are produced catalytically. In petroleum refining, it is catalytic processes that allow refiners to produce the broad mix of fuels and other products that drive today's economy and there is an entire body of catalysis, outside the scope of this report, in environmental correction; the most obvious examples are catalytic converters on automobiles that clean up auto exhausts. Even our bodies are operated by catalysts, the biological catalysts called enzymes, another important area of bio-catalysis that is outside our scope as well (11).

Catalysts have been used commercially for more than a century, dating from the Deacon and contact processes, first used in the late 1800ies. Fritz Haber's ammonia synthesis of 1908 can be considered the process that heralded the birth of modern industrial catalysis.

Catalysis thus has a strong impact on the global economy and the economy of developing countries, since it is widely applied, in sectors including polymer production, agricultural production, and the petrochemical, pharmaceutical and fine chemicals industries.

Within the industrialization programmes of many developing countries, the transfer of the latest know-how and technologies on catalytic systems and processes and their industrial application and adoption is recognized as urgent. In order to optimize an industrial process, special attention should be given to recycling and reuse of specific fluids or semi-products into the mainstream of the process line, introduction of innovative clean technologies into the process cycle, use of new catalysts to give better kinetics of critical process reactions, thereby improving process and product efficiency as well as environmental quality of the waste by-product, development and use of new catalysts in small and medium enterprises .

Both homogeneous and heterogeneous catalysis may offer advantages in particular cases. Heterogeneous catalysts generally offer the advantage of simple separation and recovery, are employed for both gas and liquid-phase operations, and lend themselves for continuous reactor operations. The advantages of heterogeneous catalysis were first appreciated in the petroleum refining and bulk-chemical industries. However, fine chemicals operations, although of smaller scale, are more numerous and on the average. Their E-factors are of the order of 5-50 kg waste per kg product, compared with values of <1-5 for bulk chemicals and about 0.1 for refinery operations (12).

The small-scale operations of the fine-chemicals industry make the costs of developing a catalysts, and possibly installing specialized equipment, for specific reaction slow recoup.

Nevertheless, environmental imperatives have recently produced an increasing degree of penetration of heterogeneous catalysis into fine-chemicals production.

The increasing complexity of the reactions for which is desired to design heterogeneous catalysts has placed increasing demands on the catalysts themselves. In particular, the molecules of fine chemicals, being in general larger, more poly-functionals and less stable than those of bulk petrochemicals, impose requirements for activity under milder conditions and higher selectivity on catalysts.

In general, acid and base are paired concepts; a number of chemical interactions have been understood in terms of acid-base interaction. Among chemical reactions which involve acid-base reactions are acid catalysed and base catalyzed reactions which are initiated by acid-base interactions followed by catalytic cycles. In contrast, relatively few studies solid basic catalysts. One of the reasons why the studies of heterogeneous basic catalysts are not as extensive as those of heterogeneous acidic catalysts seems to be the requirement for severe pretreatment conditions for active basic catalysts (13).

Solid basic catalysts are becoming extensively studied in the past years and the scientific literature on the subject is becoming more and more abundant because of their necessity for the chemical industry. For more insight to the role of base catalysis in chemical reaction, the next point presents some examples.

## **2.2 Base catalysts in chemical reactions**

Solid base catalysts exhibit high activities and selectivities for many kinds of reactions, including some condensation, alkylation, cyclization and isomerization which are carried out using liquid bases as catalysts in industrial applications. Many of these applications require stoichiometric amounts of the liquid base for conversion to the desired product.

Replacement of these liquid bases with solid base catalysts would allow easier separation from the product as well as possible regeneration and reuse of the catalyst (14).

Examples of commercially applied solid base catalysts are fewer than of solid acids. However, in this area also, newer solids including basic zeolites and related aluminosilicate, layered-structure materials such as hydrotalcite, and immobilized organic bases are enabling applications to be extended.

The next advance in the manufacture of the bulk chemical styrene may come from processes in development for the side-chain alkylation of toluene with methanol, employing solid basic catalysts such as Cs-X zeolites. The feed stock costs are lower than for benzene alkylation, while the fact that methanol is preferentially produced from natural gas, and from renewable resources, gives this process an environmental premium (15).

Additionally, the use of alkali-exchanged zeolites such as K-Y and Cs-X can be used as effective base catalysts for the methylation of aniline and phenylacetonitrile with methanol or dimethyl carbonate. For bulky substrates, caesium-exchanged mesoporous MCM-41 prove and to be effective mild basic solid catalyst for Knoevenagel condensation (15).

Hydrotalcite clays are built of positively charged brucite layers; upon calcinations they become active as solid bases useful for reactions such as aldolization and Knoevenagel condensation, exemplified by the reaction of benzaldehyde with ethylcyanoacetate (16).

### **2.3 Generation of basic sites**

At present, several classes of basic catalysts can be distinguished according how they are synthesized. A first class would contain unmodified oxide solids, i.e. intrinsically basic oxides, namely alkaline earth oxides like MgO or CaO, and Al<sub>2</sub>O<sub>3</sub> or ZrO<sub>2</sub> that have both acid and basic centers. The basic site of these solids is either an oxygen or a basic hydroxyl.

A second group of basic solids could be modified oxides (17).

$\gamma$ -Alumina is widely used as catalyst and catalyst supports. Its catalytic activity is closely related to certain "acid" sites developed when chemisorbed water is removed from the surface. From the classical Lewis definition, the base strength of a solid catalyst is determined by its ability to donate an electron pair to an adsorbed molecule. These sites are believed to be aluminium ions (Lewis acids) exposed at the surface in small amounts as a result of condensation of surface hydroxyl groups. The surface hydration and catalytic activity of  $\gamma$ -alumina has been discussed in the literature (18). Ionic surfaces, unless highly dried, are usually covered with hydroxyl groups formed by chemisorption of water. Removal of such groups from alumina leaves a strained surface on which strained oxide linkages have been postulated as active sites. Active sites on  $\gamma$ -Alumina have also been identified to be cation defects arising from its presumed defect spinel structure, whereas such defects which have captured protons, or with aluminium ions are abnormally exposed as a result of surface

dehydration (19). Other catalysts that could be classified in this second group are zeolites where the structural basic sites are the framework oxygens bearing the negative charge of the lattice; their basicity (Other modifications of alumina are ascribed in this work in a separate point).

The surface properties of heterogeneous basic catalysts have been studied by various methods by which the existence of basic sites has been realized. Different characterization methods give different information about the surface properties.

Surfaces of solids are covered either with carbon dioxide, water or oxygen and therefore show no activity for base catalyzed reactions. Generation of basic sites requires high temperature pretreatment to remove the adsorbed species (19).

In 1980 proposed a surface model for MgO. There exist several Mg-O ion pairs with different coordination numbers. Ion pairs of low coordination numbers exist at corners, edges. Ion pairs with low coordination numbers are stronger sites than the pairs with high coordination numbers, see figure 1 (20). The appearance of basic sites depends on pretreatment temperature, higher temperature generates stronger basic sites.

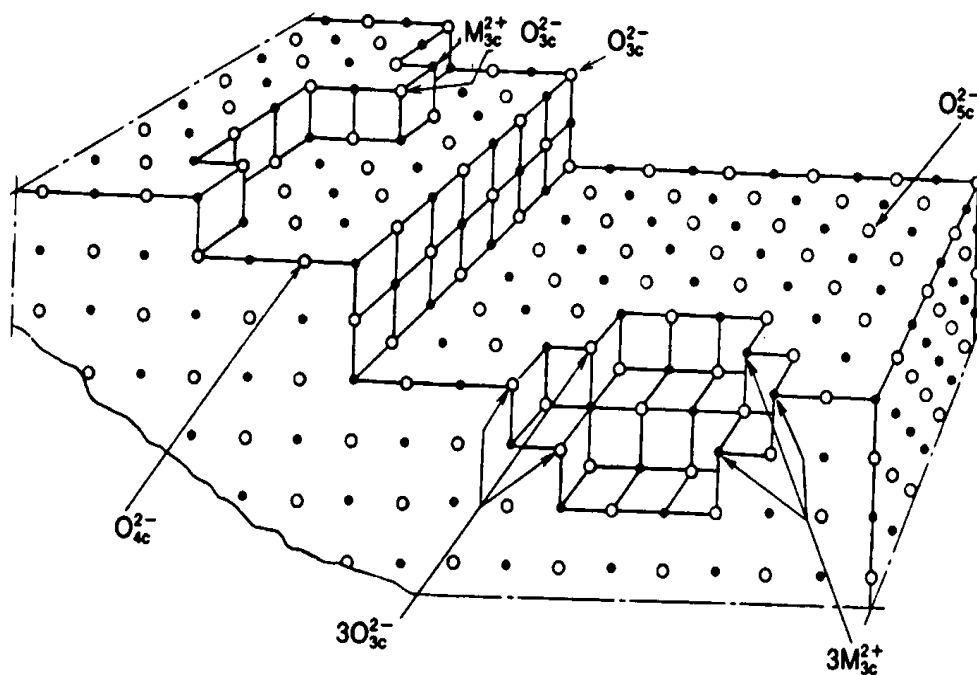


**Figure 1. Ions in low coordination on the surface of MgO**

Among the ion pairs of different coordination numbers, the ion pair of 3-fold bonded  $\text{Mg}^{2+}$ -3-fold  $\text{O}^{2-}$  ( $\text{Mg}_{3c}^{2+}$ - $\text{O}_{3c}^{2-}$ ) is most reactive and adsorbs carbon dioxide most strongly. To reveal the ion pair  $\text{Mg}_{3c}^{2+}$ - $\text{O}_{3c}^{2-}$ , the highest pre-treatment temperature is required (12).

It was prepared Mg-Al oxides with Mg/Al molar ratios of 0.5-9.0 were obtained by thermal decomposition of precipitated hydrotalcite precursors (12). The effect of composition on structure studied by different characterizations methods like x-ray photo electron spectroscopy, temperature program desorption of carbon dioxide, BET surface area and x-ray diffraction.

It was found that addition of small amounts of Al to MgO diminished drastically the density of surface basic sites because of a significant Al surface enrichment. Formation of surface amorphous  $\text{AlO}_y$  structures in samples with low Al content ( $5 > \text{Mg}/\text{Al} > 1$ ), the basic site density increased because the  $\text{Al}^{3+}$  cation within the MgO lattice created a defect in order to compensate the positive charge generated, and the adjacent oxygen anions became coordinatively unsaturated. In samples  $\text{Mg}/\text{Al} < 1$ , segregation of bulk  $\text{MgAl}_2\text{O}_4$  spinels occurred and caused the basic site density to diminish. The dehydrogenation of ethanol to acetaldehyde and the aldol condensation to n-butanol both involved the initial surface ethoxide formation on a lewis acid-strong base pair. Pure MgO exhibited poor activity because of the predominant presence of isolated  $\text{O}^{2-}$  basic centers hindered formation of the ethoxide intermediate by ethanol dissociative adsorption (12).

## 2.4 Characterization of basic surfaces

There are many methods allowing determination of acidic and basic properties of solids as described above. Apart from titration and spectroscopic techniques (FTIR, XPS, NMR) (21 - 24) temperature-programmed desorption is often used (89 - 90). The most widely applied molecular probes are ammonia (to study acidic sites) and carbon dioxide (basic sites). Recently, the application of catalytic test reactions for characterization of acidic and basic properties of solids has been intensively developed (25). The attention is paid on model substrates which are transformed into different products depending on a type of centers present on the catalyst surface, like 2-methyl-3-butyn-2-ol (MBOH) or isopropanol.



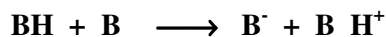
### 2.4.1 Indicator methods

Typical measurements of basicity have been obtained by using titration of adsorbed indicators having a wide range of  $pK_a$  values.

Acid–base indicators change their colours according to the strength of the surface sites of the catalysts. The strengths of the surface sites are expressed by an acidity function ( $H_-$ ) proposed by Paul and Long (7). The  $H_-$  function is defined by the following equation (26, 27):

$$H_- = pK_{BH} + \log [B^-]/[BH]$$

Where  $[BH]$  and  $[B^-]$  are, respectively, the concentration of the indicator BH and its conjugated base, and  $pK_{BH}$ , is the logarithm of the dissociation constant of BH. The reaction of the indicator BH with the basic site ( $B_-$ ) is :



One problem with using adsorbed indicators to evaluate basicity is the interference of indicator reactions that are not due to acid-base chemistry. In addition, evidence of reaction is often provided by a color change, which requires the use of colorless catalyst. Clearly, there is a need for other methods to probe surface basic sites.

### 2.4.2 Temperature programmed desorption (TPD)

This method is used to measure the number and base strengths of sites found on solid base catalysts. Since strongly bound probe molecules have high binding energies, increases temperatures are necessary to desorb these adsorbates. Experiments are typically performed under identical experimental conditions (heating rates and sample size) so that a qualitative comparison can be made between samples. During a TPD experiment, the amount of desorbed molecules is often monitored by mass spectrometry and the surface interactions are explored with infrared spectroscopy. Numerous texts describe in detail the TPD method (28, 29, 30).

### *Temperature programmed desorption (TPD) of carbon dioxide*

The desorption of carbon dioxide is often used in order to determine the strength and amount of basic centers. The strength of the centers calculated then correlated with the desorption temperature. At the same time it is found to be difficult because of the large amount of the received area peaks, quantitative results. Often qualitative measurements are carried out for different experiments under same conditions.

TPD of adsorbed carbon dioxide has been widely used to probe basic materials. For example, rubidium-modified supports have been investigated using stepwise TPD of CO<sub>2</sub>. The addition of Rb species to supports like MgO, Al<sub>2</sub>O<sub>3</sub>, TiO<sub>2</sub> and SiO<sub>2</sub>, via the decomposition of supported rubidium acetate, increases the surface density of adsorbed CO<sub>2</sub> over that pure support. The high desorption temperatures required to liberate CO<sub>2</sub> from RbO/MgO indicated the formation of very strong basic sites.

Carbon dioxide temperature programmed desorption has also been used to measure the base strengths of various alkali metals-containing (exchanged and occluded) zeolites (31).

TPD plots of carbon dioxide desorbed from alkaline earth oxides are compared in figure 2. Before each TPD run, adsorption of carbon dioxide and the following treatment were done under the same conditions (32).

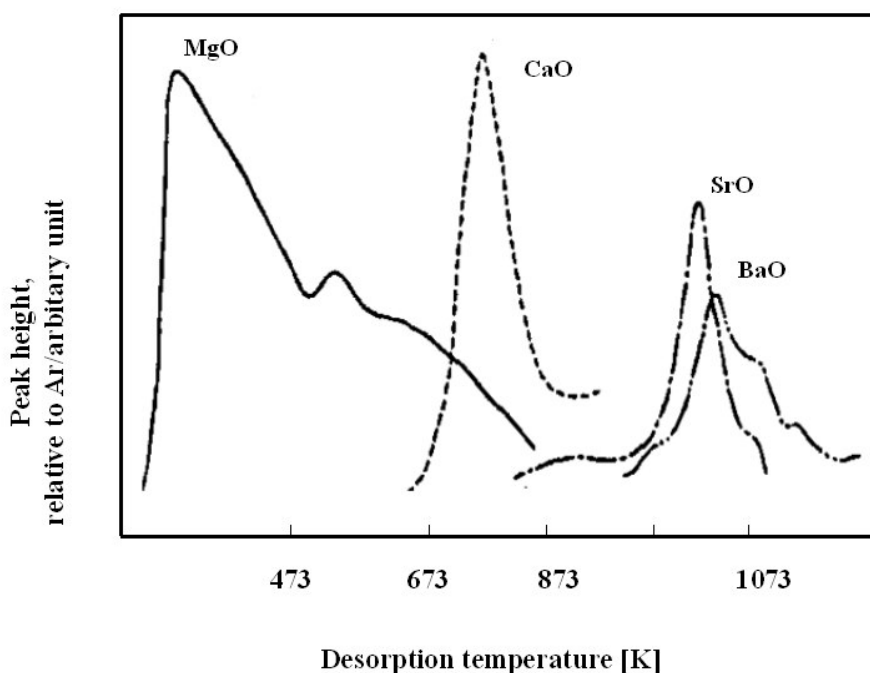


**Figure 2. TPD plots of carbon dioxide desorbed from the alkaline earth oxide (32)**

The TPD of adsorbed CO<sub>2</sub> has also been used to characterize the basicity of alkali metal and alkaline earth-modified metal oxide catalysts (33, 34).

*- Temperature programmed desorption (TPD) of hydrogen*

This method gives information about the coordination state of the surface ion pairs when combined with other methods such as UV absorption and luminescence spectroscopy.

Hydrogen is heterolytically dissociated on the surface of MgO to form H<sup>+</sup> and H<sup>-</sup> which are adsorbed on the surface O<sup>2-</sup> and Mg<sup>2+</sup> ions (35). The adsorption sites on MgO are pretreated at different temperatures, a heterolytical dissociation of hydrogen on the MgO surface can be verified by IR spectroscopies (36).

Temperature-programmed desorption of hydrogen spectroscopy was used to characterize such catalysts prepared from the  $\gamma$ -Al<sub>2</sub>O<sub>3</sub>-supported bimetallic precursors. TPD was used to determine desorption energies and ( $E_d$ ) pre-exponential factors (A) characterizing the desorption process as a function of initial surface coverage. The coverage dependences of indicate marked dif-  $E_d$  ferences between samples made from bimetallic precursors and those made from a single platinum-containing precursor or a combination of monometallic precursor. The data indicated that desorption energy distribution functions and compensation plots determined from TPD are helpful in characterizing the surface heterogeneity of highly dispersed supported metals and provides a relatively simple and reliable determination of desorption energy distributions (37).

*- Temperature programmed desorption of Pyrrole*

Pyrrole adsorption has been found to be useful for probing the basicity of zeolites. An increase in solid base strength has been correlated to a shift in the NH vibration frequency to lower wavenumbers in the IR spectrum for numerous alkali-exchanged zeolites (38) and for various metal oxides (39).

When the O<sup>2-</sup> species is highly basic, the surface OH species are unperturbed and the H atom of the pyrrole molecule is localized near the basic oxygen, undergoing dissociative chemisorption. When the O<sup>2-</sup> species are less basic, the surface oxygen forms an NH-O bridge with pyrrole.

Complexities in the IR spectrum result from interaction with surface hydroxy and pyrrole since hydroxy species are as both a basic surface species and as product formed from pyrrole dissociation (40).

### 2.4.3 Spectroscopic methods

#### *- X-ray absorption spectroscopy*

The lack of long range order associated with supported phases often prevents structural characterization by techniques like X-ray diffraction, which require samples with substantial crystallinity X-Ray absorption spectroscopy (XAS) is a technique that is able to investigate the local structure near a particular element. When using a standard of known composition, the oxidation state, coordination number, nearest-neighbor interatomic distance(s) and factors can be determined.

X-ray absorption spectroscopy has been used to study many catalytic materials like alkali metal-support interactions for rubidium deposited on pure oxides. In fact, the reduced intensity of the Rb-O peak in the radial structure function for rubidium-modified SiO<sub>2</sub> indicated the formation of highly disordered rubidium silicate phase due to the strong interaction between silica and the supported alkali species.

X-ray absorption spectroscopy has also been used to study cesium in catalytic materials for the determination of the Cs-O distance in Cs-ZSM-5- zeolites (41). Dokocil and Davis recently published a study of the Cs-containing compounds and catalysts, comparison of CsX and Cs<sub>2</sub>CO<sub>3</sub> was also analyzed by this method. Apparently, the bonding in Cesium carbonate is more covalent than in the zeolites, which results in a greater density of filled s-type states for the bulk compound. Both impregnated and ion-exchanged cesium catalysts showed a more intense white line than any Cs compound investigated (42).

#### *- UV absorption and luminescence spectroscopies*

UV absorption and luminescence spectroscopies give information about the coordination states of the surface atoms. High surface area MgO absorbs UV light and emits luminescence, which is not observed with MgO single crystal. Nelson and Hale first observed the absorption at 5.7 eV, which is lower than the band gap (8.7 eV, 163 nm) for bulk MgO at 3 eV.

Tench and Pott observed photoluminescence. The UV absorption corresponds to the following electron transfer process involving surface ion pairs (18,19).



Absorption bands were observed at 230 nm and 274 nm, which are considerably lower in energy than the band at 163 nm for bulk ion pair. The bands at 230 nm and 274 nm are assigned to be due to the surface  $\text{O}^{2-}$  ion of coordination numbers 4 and 3 respectively. Luminescence corresponds to the reverse process of UV absorption, and the shape of the luminescence spectrum varies with the excitation light frequency and with absorption of molecules. Emission sites and excitation sites are not necessarily the same. Excitations move on the surface and emit at the ion pair of low coordination numbers where emission efficiency is high. Ion pairs of low coordination numbers responsible for UV absorption and luminescence exist at corners edges.

The surface model for MgO shown in figure 1 was proposed on the basis of UV absorption and luminescence spectrum excited by the 274 nm light and was it much more severely influenced by hydrogen adsorption than that excited by the 230 nm light. Hydrogen molecules interact more strongly with the ion pairs of coordination number 3 than with those of coordination number 4 are heterolytically dissociated on these sites.

The UV absorption and luminescence spectroscopies give us useful information about the coordination state, but it is difficult to quantify the sites of a certain coordination state (16).

#### *- IR spectroscopy*

$\text{CO}_2$  interact strongly interaction with the basic centers of a surface. IR-spectroscopy can measured the tie strength so that conclusions are possible on the tie condition. Three species of adsorbed  $\text{CO}_2$  shown as figure 3, correspond with three different types of surface basic sites:

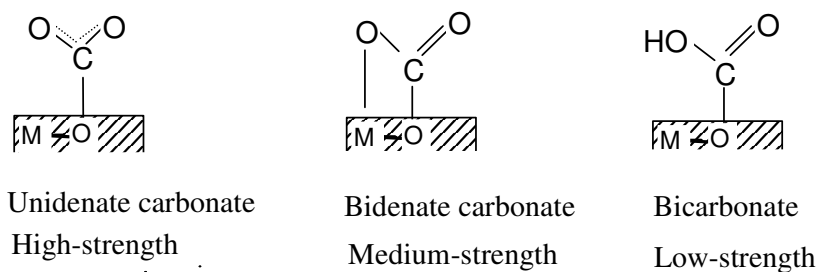


**Figure 3. IR bands of adsorbed CO<sub>2</sub> surface species**

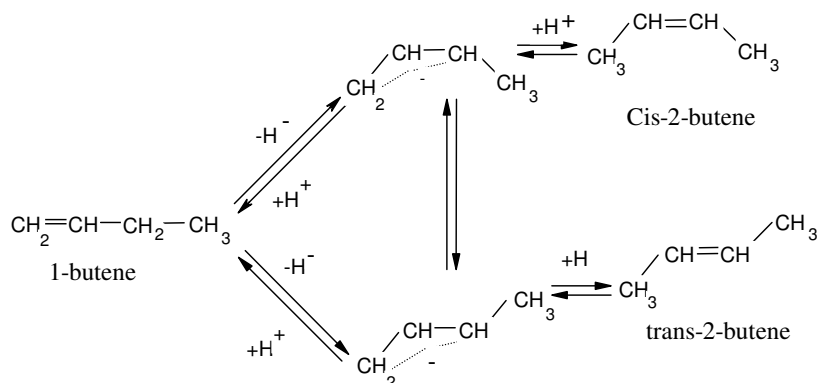
At the formation of the bidentate carbonates, also a metal ion is involved. Three species of adsorbed CO<sub>2</sub>, which are shown in figure 3, were detected on samples of MgO and Al<sub>2</sub>O<sub>3</sub>. Apparently reflecting three different types of surface basic sites. Unidentate and bidentate carbonate formation requires surface oxygen atoms. Unidentate carbonate exhibits symmetric O-C-O stretching at 1360–1400 cm<sup>-1</sup> asymmetric O-C-O stretching at 1510-1560 cm<sup>-1</sup>. Bidentate carbonate shows symmetric O-C-O stretching at 1320 – 1340 cm<sup>-1</sup> and asymmetric O-C-O stretching at 1610- 1630 cm<sup>-1</sup>. Bicarbonate species formation involves surface hydroxyl groups showing C-OH bending mode at 1220 cm<sup>-1</sup> as well as symmetric and asymmetric O-C-O stretching modes at 1480 cm<sup>-1</sup> and 1650 cm<sup>-1</sup>, respectively (30). The basic characteristics can therefore be led back to the available metal atoms and not alone to the surface oxygen atoms. same although the strength of the tie changes and therefore the waves number

The oxygen exchange between CO<sub>2</sub> and MgO surface basic sites suggest an important aspect of the nature of surface basic sites. The basic sites are not fixed on the surface but are able to move over the surface when carbon dioxide is adsorbed and desorbed. The position of the basic site (surface O atom) changes as CO<sub>2</sub> migrate over the basic site. In addition, it became clear that not only O<sup>2-</sup> basic sites but also adjacent Mg<sup>2+</sup> sites participate in CO<sub>2</sub> adsorption. Therefore, it is reasonable to consider that the metal cations adjacent to the basic site participate in the base-catalyzed reactions (16, 17).

## 2.5 Reactions on heterogeneous basic catalysts

### 2.5.1 Double bond migration

1-butene isomerization to 2-butenes has been extensively studied over many heterogeneous basic catalysts to elucidate the reaction mechanisms and to characterize the surface basic properties. The reaction proceeds at room temperature over most of heterogeneous basic catalysts. The reaction mechanisms for 1-butene isomerization are shown in scheme 1.

**Scheme 1.** Reaction mechanism of 1-Butene isomerization

The reaction is initiated by abstraction of allylic hydrogen by basic sites to form cis- or trans- form 2-butene of the allyl anion. Coisomerization of butene- $\text{d}_0$  and  $\text{d}_8$  is an useful method to determine the reaction mechanisms (43). In the coisomerization, a mixture containing equal amounts of nondeuteriobutene ( $\text{d}_0$ ) and perdeuteriobutene ( $\text{d}_8$ ) is allowed to react.

If the reaction proceeds by proton addition-abstraction mechanisms, an intermolecular hydrogen (or D) transfer is involved and the products will be composed of  $\text{d}_0$ ,  $\text{d}_1$ ,  $\text{d}_7$ ,  $\text{d}_8$  isotopic species. On the other hand, if the reaction proceeds by hydrogen abstraction-addition mechanisms, an intramolecular H (or D) transfer is involved, and the products will be composed of  $\text{d}_0$  and  $\text{d}_8$  isotopic species. Since an  $\text{H}^+$  is abstracted first for base-catalyzed isomerization to form allyl anions to which the  $\text{H}^+$  returns at different C atom, an intramolecular H (or D) transfer is expected (44, 45). Therefore, an intramolecular H (or D) transfer and high cis/trans ratio are characteristic features for 1-buten double bond isomerization over heterogeneous basic catalyst.

If acidic catalyst were used, the ring –opening reactions would easily occur, and the selectivities for double migration should markedly decreases. A characteristic feature of heterogeneous basic catalyst is lack of C-C bond cleavage ability. The double bond migration occurs without bond cleavages over heterogeneous basic catalysts.

### 2.5.2 Dehydration and dehydrogenation

In general, alcohols undergo dehydration to olefins and ethers over acidic catalysts, and dehydrogenation to aldehydes or ketones over basic catalysts. In some cases, heterogeneous basic catalysts promote dehydration of alcohols in which the mechanisms and product distribution differ from those for acid-catalyzed dehydration (26).

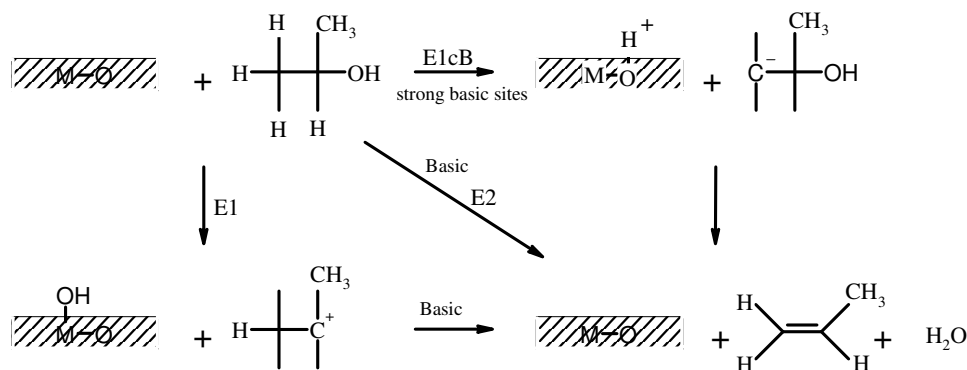
The product of the conversion of 2-butanol over the rare earth oxides ThO<sub>2</sub>, and ZrO<sub>2</sub> consists mainly of 1-butene (20, 21). This is in contrast to the preferential formation of 2-butenes over acidic catalysts.

A commercial scale was attained for the dehydration of 1-cyclohexylethanol to vinylcyclohexane with ZrO<sub>2</sub> as a catalyst. In the dehydration of 2-alcohols to the corresponding 1-olefins over ZrO<sub>2</sub> the selectivity for 1-olefins depends on the amount of Si contained in ZrO<sub>2</sub> as an impurity. Silicon, contained in zirconia as an impurity contaminates the zirconia by generating acidic sites. By treatment of ZrO<sub>2</sub> with NaOH to eliminate the acidic sites, formation of 2-olefins, a typical by-product of acid catalysed reaction, is markedly reduced and 1-olefins is increased. It is widely accepted that the interaction between an alcohol and the surface of a metal oxide yields a mixture of adsorbed alcohol molecules and alkoxide species (46, 47).

Aramendia *et al.* (48) proposed a mechanism for the decomposition of 2-propanol over magnesium oxides. The mechanism involves strong basic sites that effect the withdraw of protons, whether from the  $\beta$  carbon or alcohol function (E1cB), scheme 2.

The E1 elimination mechanism is a two-step pathway, the rate determining step is the ionization of the substrate to a carbenium ion (by releasing OH<sup>-</sup>). In the E2 mechanism, both the leaving group and the proton depart simultaneously, the proton being pulled off by the base. The results which obtained by Aramendia (48) show that the final reactivity of the reaction at MgO depends largely on the preparation method and the precursor used.

**Scheme 2.** Mechanism of dehydrogenation of 2-propanol





### 2.5.3 Isopropanol and methylbutynol test reactions

The transformation of 2-propanol is a widely used test reaction for characterizing both acidic and basic properties of solids (49). On contact with an acidic or basic solid, 2-propanol undergoes two types of competitive reactions namely: (a) intramolecular dehydration, which yields to propene and this is characteristic for acidic properties of the catalyst, subsequent dehydration of propene leads to di-isopropyl ether (b) dehydrogenation to acetone and hydrogen and this is characteristic for basic properties (50).

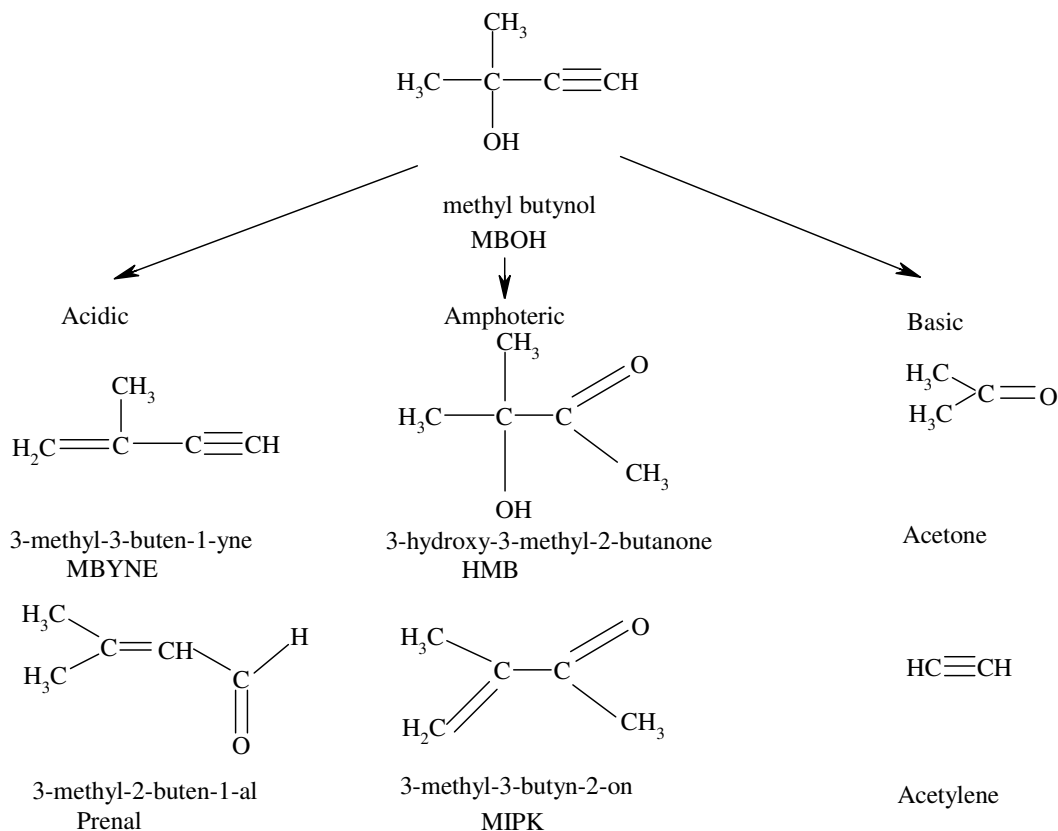
Lahousse, *et al.* (51) used two test reactions to characterize the acid-base properties of metal oxides: isopropanol and methylbutynol decomposition under He stream, at 180 °C and 210 °C with MgO and ZnO and the family of mixed oxides generated with alumina as catalysts. The results have shown that these two test reactions do not characterize the same surface properties because basicity of isopropanol dehydrogenation requires additional redox ability, otherwise acetone is not formed. Catalyst for isopropanol dehydrogenation should activate hydrogen, one of the reaction products. Hydrogen adsorption on ZnO has been widely studied by IR spectroscopy (52). At least two types of dissociated species have been evidenced at higher temperature. In contrast MgO, is unable to activate hydrogen except if it is activated at very high temperature.

Lauron Pernot *et al.* (6) have investigated a new test reaction, using methylbutynol (MBOH) that undergoes dehydration to yield 3-methyl-3-buten-1-yne (MBYNE) on acid catalysts such as acidic activated alumina or P<sub>2</sub>O<sub>5</sub>/SiO<sub>2</sub>. By-products such as 3-hydroxy-3-methyl-2-butanone (HMB) and the corresponding dehydrated product 3-methyl-3-buten-2-one (MIPK) were found in the reaction of MBOH in concentrated sulfuric acid. The reactivity of MBOH over solids and bases and the mechanisms are shown in scheme 3. The MBOH conversion differs from other test reactions by the unique property to give product distribution which are characteristic for entirely acid, basic and amphoteric sites, respectively (6). Since the different products can be formed at the same temperature no additional activation barriers have to be considered for interpretation.

This reactivity test using MBOH gives good results in the characterization of basic properties (7, 8). It can also be used for estimating the basic property of weak bases such as lithium hydroxide supported on alumina (53). The transformation of MBOH towards HMB involves residual surface hydroxyl groups or traces of water which either is contained in the MBOH

reactant or formed by MBOH condensation on residual hydroxy groups or by condensation of acetone which is a by-product of the reaction (54, 55, 56, 57).

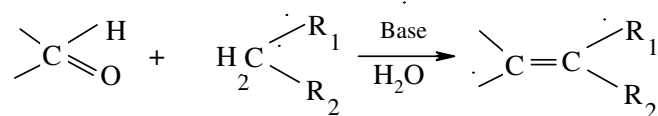
**Scheme 3.** Overall reactivity of MBOH



**2.5.4 Basic test reaction in the liquid phase (Knoevenagel Condensation)**

Knoevenagel condensation involves the formation of a C-C bond via the reaction of aldehyde or ketone with an active methylene compound, scheme 4 (58). Usually, this reaction employs compounds containing a methylene group activated by two electron-withdrawing moieties.

**Scheme 4.** Scheme for the Knoevenagel Condensation



Both  $R_1$  and  $R_2$  : possibly CHO, COR, COOH, CN, NO<sub>2</sub>, SOR, SO<sub>2</sub>R, SO<sub>2</sub>R, or similar groups.

The versatile Knoevenagel condensation have numerous applications in the elegant synthesis of chemicals and are classically catalysed by bases in the liquid system (59). On the laboratory scale many catalysts have been known to effect the Knoevenagel condensation and include alumina (60), hydrotalcites (61), zeolites (62). Table demonstrates different examples for the Knoevenagel condensation (59). In the present work for the Knoevenagel condensation was performed on the example of benzaldehyde with malononitrile which gives the condensation product benzylidenmalononitrile

**Table 1.** Examples for Knoevenagel condensation

Initial compound (Aldehyde, ketone)	Initial compound (methyl compounds)	Product
Benzaldehyde	Acetaldehyde	Zimtaldehyde
Benzaldehyde	n-heptanal	Jasminaldehyde
Benzaldehyde	Malononitrile	benzylidenmalononitrile
Benzaldehyde	Malono-diethylester	Benzylidenmalno di-ethylester
Crotonaldehyde	Malono acid	Sorbic acid
Vanillin	Malono acid	Ferulene acid

## 2.6 Heterogeneous basic and acidic catalysts

### 2.6.1 Non-oxidic catalysts

Most of heterogeneous basic catalysts are metal oxides. The basic sites are  $O^{2-}$  ions with different environments. If the basic sites are constituted by elements other than  $O^{2-}$  the catalysts are expected to show catalytic properties different than those of the oxide form (63). Potassium fluoride supported on alumina ( $KF/Al_2O_3$ ), a typical base catalyst (64, 65), has been applied as a catalyst to a number of organic reactions as Michael addition (66, 67, 68), Wittig-Honner reactions, Knoevenagel condensation (65), and alkylation at C, O, N, and S atoms with aldehydes and dimethyl sulfate (66).

Other non oxide catalysts show high activity too as presented by Ando (69), who compared  $KF$  and  $NaF$  supported on alumina. The formation of strong base fluoride with alumina can not totally explain the extremely high reactivity of  $KF$ -alumina as a heterogeneous base for

catalytic as well as non-catalytic reactions. Because of this high basicity the applications of KF-Al<sub>2</sub>O<sub>3</sub> will increase.

### 2.6.2 Heterogeneous super basic catalysts

Super acids are reagents which have a higher protonating effect than 100% sulfuric acid. In analogy to these acids, those reagents which have a very high deprotonating effect are called super basics, whether no clear definition of these compounds exists. They can be used to activate a reactant at mild conditions (49). There have been some attempts to prepare a strong or as reported in the literature super basic catalyst basic catalyst for example by addition of alkali hydroxides to alumina (51) followed by further addition of alkali metals. Ushikubo *et al.* prepared a super basic catalysts by addition of metallic sodium to MgO (70). After pretreating MgO at high temperature it was mixed with NaN<sub>3</sub> and heated to 355 °C to decompose NaN<sub>3</sub> to evolve metallic sodium. The resulting catalyst acts as an efficient catalyst for decomposition of methyl formate to CO and methanol. The activity was much higher than that of MgO. Others like Suzukamo *et al.* (71) have prepared strong basic catalysts by addition of alkali hydroxides to alumina. and catalyses various base catalyzed reactions such as double bond migration and side alkylations of alkylbenzenes at the reaction temperature 293-433 K.

### 2.6.3 Aluminas

In the past aluminas were used as adsorbents and active catalysts supports. In industrial catalytic processes, aluminas have mostly been used as catalyst supports although pure alumina is important for the Claus process. In general aluminas are still used for several groups of reactions, as summarized in table 2 (72).

The reactions compiled in the table show that aluminas are able to activate hydrogen-hydrogen, and carbon-carbon bonds, although with varying efficiency (72).

Alumina (Al<sub>2</sub>O<sub>3</sub>) occurs in various crystallographic modifications, among which the  $\eta$  and  $\gamma$ -phases are the catalytically most important (73).

Experiments clearly show that the catalytic activity of  $\eta$ -Al<sub>2</sub>O<sub>3</sub> usually turns out to be higher than that of  $\gamma$ -Al<sub>2</sub>O<sub>3</sub>, and that the aluminas have to be pretreated at elevated temperatures of 300 – 400 °C in vacuum for the development of catalytic activity. Peri (74) modified a surface

model for  $\gamma$ -Al<sub>2</sub>O<sub>3</sub> which seemed to account for most of the experimental information using dehydroxylation process, and attributing the five OH-stretching bands which were observed during the process of  $\gamma$ -alumina to OH groups in distinct lateral surface environments. The process was simulated by statistical methods (74).

**Table 2.** Reactions catalyzed by alumina

Reaction	Temperature (°C)
H <sub>2</sub> +D <sub>2</sub> → 2 HD	150
Alkene+ D <sub>2</sub> → Alkene-d+ HD	300
Benzene+D <sub>2</sub> → benzene-d+ HD	300
Double-bond isomerization of alkenes	300
Cis/trans isomerization of alkenes	300
Cyclopropane → propene	375
Alcohols → alkenes+ H <sub>2</sub> O	350
2-alcohols → ether+ H <sub>2</sub> O	400
Skeletal isomerization of alkenes	600
O-xylene isomerization	770

A general classification of the various modifications of aluminum hydroxides is shown in figure (4). The best defined *crystalline forms* are the three trihydroxides, Al(OH)<sub>3</sub>: gibbsite, bayerite, and nordstrandite. In addition two modifications of aluminum oxide–hydroxide, AlO(OH), exist: boehmite and diaspore. Besides these well-defined crystalline phases, several other forms have been described in the literature. However, there is controversy as to whether they are truly new phases or simply forms with distorted lattices containing adsorbed or interlamellar water and impurities (75).

Gelatinous hydroxides may consist of predominantly x-ray indifferent aluminum hydroxide or pseudoboehmite. The x-ray diffraction pattern of the latter shows broad bands that coincide with strong reflections of the well-crystallized oxide–hydroxide boehmite.

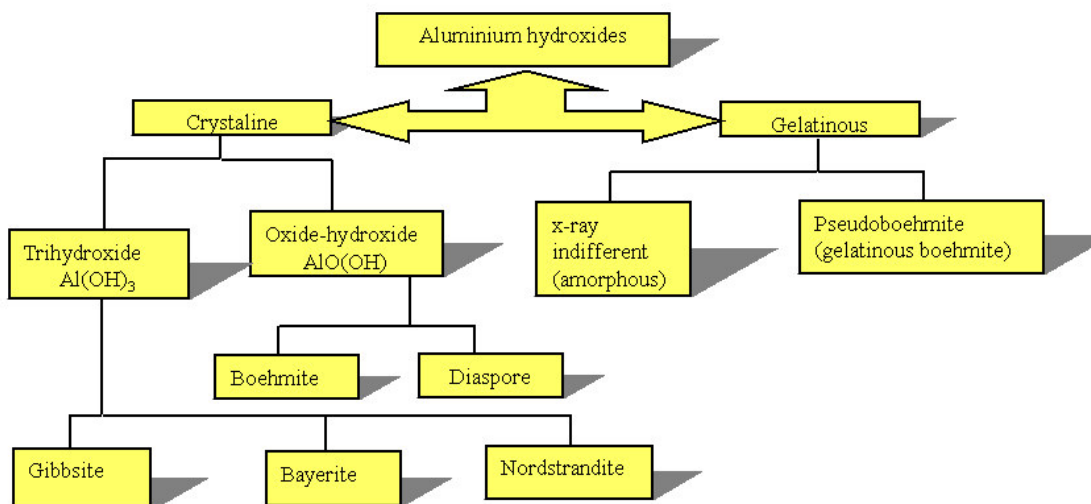


**Figure 4. Classification of aluminium hydroxides**

The aluminum hydroxides found abundantly in nature are gibbsite, boehmite, and diaspor. Gibbsite and bayerite have similar structures. Their lattices are built of layers of anion octahedra in which aluminum occupies two thirds of the octahedral interstices. In the gibbsite structure, the layers are somewhat displaced relative to one another in the direction of the  $a$  axis. The hexagonal symmetry of this lattice type (brucite type) is lowered to monoclinic. In bayerite the layers are arranged in approximately hexagonally close packing. Because of shorter distances between the layers, the density is higher than in the case of gibbsite. The individual layers of hydroxyl ion octahedra in both the gibbsite and the bayerite structure are linked to one another through weak hydrogen bonds only. Bayerite does not form large single crystals. The most commonly observed growth forms are spindle- or hourglass-shaped somatoids.

The long axis of these somatoids stands normal to the basal plane, i.e. the somatoids consist of stacks of  $\text{Al}(\text{OH})_3$  layers. Nordstrandite, the third form of  $\text{Al}(\text{OH})_3$ , was described by Van nordstrand and others. The structures of nordstrandite and bayerite were investigated and compared with those of the monoclinic and triclinic gibbsite. The lattice of nordstrandite is built of the same, electrically neutral  $\text{Al}(\text{OH})_3$  octahedral layers that form the structural elements of gibbsite and bayerite The ideal

nordstrandite structure consists of alternating double layers, in which the OH octahedral are arranged once in the packing sequence of bayerite.

*Pseudoboehmite* is formed during aging of x-ray indifferent hydroxide gels as a precursor of trihydroxide. The reflexes of pseudoboehmite are broadened not only because of the very small particle size, but also because of variable distances of the AlO(OH) double chains, which form the structural element of pseudoboehmite as well as of well-crystallized  $\gamma$ -AlO(OH) (75, 76).

#### *-Thermal Decomposition of Aluminum Hydroxides*

When aluminum hydroxides or oxide hydroxides are heated in air at atmospheric pressure, they undergo a series of compositional and structural changes before ultimately being converted to  $\alpha$ -Al<sub>2</sub>O<sub>3</sub>. These thermal transformations are topotactic. Despite a loss of 15 or 34 % of mass for the trihydroxides or oxide hydroxides, respectively, the habit of the primary crystals and crystal aggregates changes very little and the simplest transformation is that of diasporite to corundum. The thermal transformation, at ambient pressure, of  $\gamma$ -AlO(OH) and the trihydroxides to  $\alpha$ -Al<sub>2</sub>O<sub>3</sub> requires considerably more structural rearrangements and is generally not completed until the temperature reaches at least 1375 – 1400 °C figure (5). The first step in the reaction sequence is the diffusion of protons to adjacent OH groups and the subsequent formation of water. This process begins at a temperature near 475 °C. If this water cannot diffuse rapidly out of larger trihydroxide particles, hydrothermal conditions may develop locally, resulting in the formation of  $\gamma$ -AlO(OH). With increasing loss of water, a large internal porosity develops

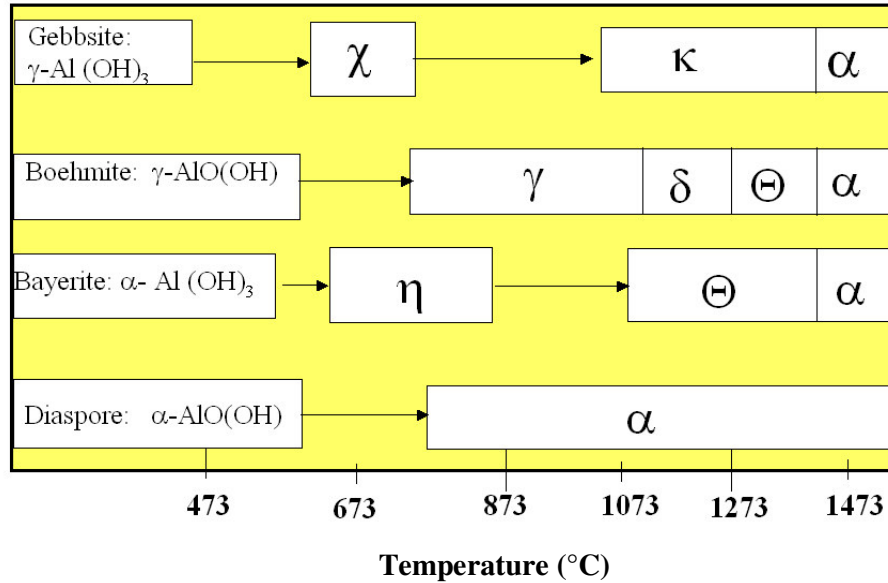


**Figure 5. Thermal decomposition of alumina**

The lattice voids left by the escaping water are not readily healed because of the slow diffusion in this low temperature range.

Alumina oxides formed at lower temperatures are mostly two-dimensionally, short-range ordered domains within the texture of the decomposed hydroxides. Extensive three-dimensional ordering begins at about 1050 °C. Until completely converted to corundum, the solid retains considerable amounts of OH<sup>-</sup> ions. Most likely protons are retained to maintain electro neutrality in areas deficient of cations. The presence of protons therefore may retard the re-ordering of the cation sublattice. Addition of fluorine to the furnace atmosphere removes protons. As a result, rapid transition to  $\alpha\text{-Al}_2\text{O}_3$  occurs at temperatures as low as 1150 °C. Markedly tabular corundum crystals are formed possibly because the preceding transition alumina is mostly two-dimensionally ordered (75). Knözinger (77) described that the formation of Gibbsite and Bayerite to Boehmite is favored by pressures exceeding 1 bar, moist air, heating rates higher than 1 K min<sup>-1</sup> and particle sizes higher than 100  $\mu\text{m}$ . while, the formation of Gibbsite to  $\chi$ - alumina or Bayerite to  $\eta$  alumina is favored by pressures of 1 bar, dry air, heating rates below 1 K min<sup>-1</sup> and particle sizes about 10  $\mu\text{m}$ .



#### 2.6.4 Oxynitride catalysts

One of the ways for modifying the acid–base properties of solids can be the nitridation of oxides. The nitridation of an oxide consists in substituting an oxygen atom by a nitrogen atom. A common way for achieving this reaction is a thermal treatment of the oxide under a flow of ammonia for a prolonged time. If the substitution is complete the solid is called a nitride. In the case of partial substitution it is an oxynitride (5). However, this method can take place only on the surface of oxide because it is hard to get a nitride from bulk oxide by treating with ammonia.

The influence of the nitrogen content on the acid–base properties of aluminophosphate oxynitrides (ALPON) have been reported in the literature (79-81). An increase of nitrogen content in the bulk leads to a decrease in the acidity and to an augmentation in the catalytic conversion in the Knoevenagel condensation reaction, indicating that the surface exhibits a more basic character (82, 83).

#### 2.6.5 Base catalysis by alkali-modified zeolites

The use of alkali–exchanged zeolites for base catalysis has received little attention and even less attention was directed toward the development and characterization of these sieves as solid bases (84). However, it is known that the alkali cation exchanged zeolites have little activity to promote any reactions proceeding through a carbonium ion. It has been found that the alkali-exchanged zeolites have appreciable catalytic activity in dehydration of alcohols (85) methylenation of anisole, dealkylation of cumene and the reaction of acetic anhydride with hydrogen sulfide (86, 87)

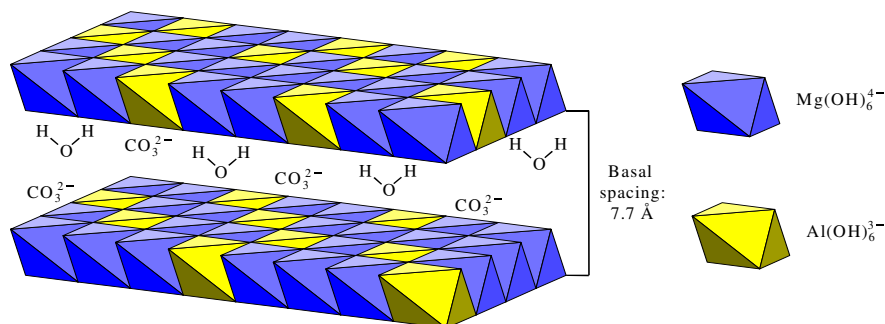
Other researches (88) have studied in detail the alkylation of toluene with methanol and with formaldehyde on various alkali-exchanged X and Y zeolites to examine the correlation between the selective formation of alkylates and the catalyst properties. It was found that the xylenes were formed by alkylation of the benzene ring of toluene on Li-exchanged zeolites.

#### 2.6.6 Hydrotalcites

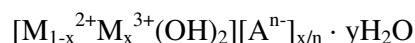
Hydrotalcite-like layered double hydroxides (LDHs), also known as anionic clays, are natural or synthetic materials consisting of positively charged brucite-like sheets. The structure of hydrotalcite can be visualized as the structure of brucite,  $Mg(OH)_2$ , in which some of the

$\text{Mg}^{2+}$  cations, coordinated octahedrally by hydroxyl groups, are substituted by trivalent ions such as  $\text{Al}^{3+}$  (scheme 4).

**Scheme 4.** Structure of double layered hydroxaltes intercalated with  $\text{CO}_3^{2-}$  anions.



The excess of positive charge in the LDHs' layers is compensated by anions located together with water in the interlayer space. The general formula of hydroxaltes is:



where  $\text{M}^{2+}$  and  $\text{M}^{3+}$  represent divalent and trivalent cations in the octahedral sites within the hydroxyl layers,  $x$  is equal to the ratio  $\text{M}^{3+}/(\text{M}^{2+} + \text{M}^{3+})$  with a value varying in the range of 0.17-0.50, and  $\text{A}$  is an exchangeable interlayer anion. It is very important that  $\text{M}^{2+}$  and  $\text{M}^{3+}$  cations should have ionic radii not too different from 0.65 Å (characteristic of  $\text{Mg}^{2+}$ ) to form a stable structure of hydroxaltes (89 - 91). In naturally occurring hydroxaltes, carbonate is the interlayer anion. However, the number of counterbalancing ions is essentially unlimited, and LDHs intercalated by various simple inorganic (92, 93), polyoxometalate (94 - 96), complex (97 - 99) as well as organic anions (100 - 102) have been synthesized. Therefore, it seems to be possible to prepare tailor-made materials for specific applications by changing the cationic and anionic compositions of hydroxaltes. Unique basic properties of LDHs, which behave as solid bases, make these materials very useful for catalytic purposes. The replacement of homogeneous basic catalysts by solid bases would make separation and recovery of catalysts easier and allow to avoid corrosion and environmental problems. Thus, LDHs as well as mixed metal oxides formed by calcination of hydroxaltes have been studied as basic catalysts in many chemical processes including aldol and Knoevenagel condensation (93, 102), Michael addition (103), alkylation (104) and transesterification (105). Catalysts derived from hydroxaltes have been the subject of a recent review by Sels *et al.* (24).

### 3. Experimental

#### 3.1 Investigated catalysts

##### 3.1.1 Silica-alumina catalysts

Table 3 shows the data for the examined silica alumina with different silica alumina ratios obtained by Sasol Germany GmbH. In this work these catalysts are named by the abbreviation Si/Al and a number referring to the content of SiO<sub>2</sub> and Al<sub>2</sub>O<sub>3</sub> measured in wt.%. The calcination process proceeded by the supplier.

**Table 3.** Composition and texture data of silica–alumina catalysts with different silica alumina ratio

As-synthesized sample	Al <sub>2</sub> O <sub>3</sub> wt. %	SiO <sub>2</sub> wt. %	BET surface area m <sup>2</sup> /g	Pore volume cm <sup>3</sup> /g	Pore size Å
Si/Al 5 Calcined 3h at 550 °C	95.19	4.81	315	0.9	36
Si/Al 10 Calcined 3h at 550 °C	89.92	10.08	339	1.0	32
Si/Al 20 Calcined 3h at 550 °C	80.46	19.54	398	0.9	24
Si/Al 40 Calcined 3h at 550 °C	61.32	38.68	438	0.7	20
Si/Al 5 Calcined 3h at 900 °C	95.06	4.94	237	1.0	44
Si/Al 10 Calcined 3h at 900 °C	89.88	10.12	270	1.0	36
Si/Al 20 Calcined 3h at 900 °C	80.78	19.22	296	0.9	27
Si/Al 40 Calcined 3h at 900 °C	90.1	39.03	285	0.7	20

### 3.1.2 Puralox catalysts

The investigated samples were prepared and supplied by Sasol Germany GmbH and their properties are shown in table 4.

**Table 4.** Different studied types of puralox with a specific surface area

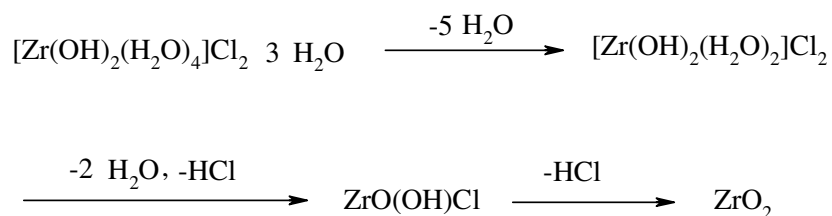
As-synthesized samples	Chemical composition	BET surface area m <sup>2</sup> /g
Puralox MG 30	MgAl <sub>2</sub> (OH) <sub>8</sub> *H <sub>2</sub> O MgO:Al <sub>2</sub> O <sub>3</sub> = 30:70	219
Puralox HT MG 70 hydrotalcite	Mg <sub>6</sub> Al <sub>2</sub> (OH) <sub>18</sub> *H <sub>2</sub> O MgO:Al <sub>2</sub> O <sub>3</sub> = 70:30	144
Puralox SBA 150	Al <sub>2</sub> O <sub>3</sub> Bulk density: 500-700 kg/m <sup>3</sup>	144
Puralox SBA 200	Al <sub>2</sub> O <sub>3</sub> Bulk density: 550-800 kg/m <sup>3</sup>	146

### 3.1.3 Preparation of bulk metal oxides of TiO<sub>2</sub>, ZrO<sub>2</sub>, and HfO<sub>2</sub> and of the corresponding supported on alumina catalysts

- Preparation of Zirconium oxide, ZrO<sub>2</sub>

Zirconium oxide was prepared by calcination of ZrOCl<sub>2</sub>\*8 H<sub>2</sub>O for 24 h at 500 °C (5 K/min). Dehydration occurs stepwise with the formation of the species [Zr<sub>4</sub>(OH)<sub>8</sub>(H<sub>2</sub>O)<sub>16</sub>]Cl<sub>8</sub>\*12 H<sub>2</sub>O, [Zr<sub>4</sub>(OH)<sub>8</sub>(H<sub>2</sub>O)<sub>16</sub>]Cl<sub>8</sub>\*4 H<sub>2</sub>O, [Zr<sub>4</sub>(OH)<sub>8</sub>(H<sub>2</sub>O)<sub>12</sub>]Cl<sub>8</sub> and finally, ZrO<sub>2</sub>. Scheme 5 shows the thermal decomposition of ZrOCl<sub>2</sub>\*8 H<sub>2</sub>O (108).

**Scheme 5.** Thermal decomposition of ZrOCl<sub>2</sub>\*8 H<sub>2</sub>O



*\* Supported metal oxides with alumina by precipitation*

The alumina used for synthesis of the supported samples, calcined 3h at 900 °C (supplied by Sasol Germany GmbH).

*\* ZrO<sub>2</sub>/Al<sub>2</sub>O<sub>3</sub>*

An amount of 5 g ZrOCl<sub>2</sub>\*8 H<sub>2</sub>O was dissolved in 100 mL deionized water. The addition of Al<sub>2</sub>O<sub>3</sub> to the metal salt solution was performed in the proportion of 95 g. The mixture was heated up to 100 °C under magnetic stirring. Then the precipitating agent, which is aqueous NH<sub>3</sub> solution (25 M), was added till the suspension achieved pH = 7. After that, the gel was filtered and dried in an oven at 200 °C (5 °C/min) for 24 h.

*\* TiO<sub>2</sub>/Al<sub>2</sub>O<sub>3</sub>*

The TiO<sub>2</sub>/Al<sub>2</sub>O<sub>3</sub> samples with a titanium oxide content of 5 % were prepared from 2,5 g titanium chloride (TiCl<sub>4</sub>) and 45 g Al<sub>2</sub>O<sub>3</sub> in 100 mL H<sub>2</sub>O. The subsequent preparation procedure was the same as explained in above point for ZrO<sub>2</sub>/Al<sub>2</sub>O<sub>3</sub>.

*\* HfO<sub>2</sub>/Al<sub>2</sub>O<sub>3</sub>*

Different ratios of hafnium oxide (5, 10, and 15 wt.%) were loaded on alumina. For this, 2,5 g HfO<sub>2</sub> were dissolved in each case in 2 ml HNO<sub>3</sub> (4 mol %) and 100 mL deionized water was added. The solution was heated for about 10 minutes under continuous mixing to solve the metal salt. After cooling to room temperature that amount of alumina 45 g was added which was necessary to achieve a hafnium oxide content of 5, 10 or 15 wt.%. The obtained slurry was neutralized by aqueous NH<sub>3</sub> solution (25 M) to pH = 7. This process was followed by filtration and drying in an oven at 200 °C (5 °C/min) for 24 h. The catalysts were marked with the numeric value indicating the loaded weight percentage of hafnium oxide in the sample (5, 10 and 15 wt.%).

\* *Zirconium hydroxide*  $Zr(OH)_4$

Zirconium hydroxide was prepared from 15 g  $ZrOCl_2 \cdot 8 H_2O$  and 0.5 L of deionized water. Next, NaOH (1 M) was added until pH = 7 was achieved and  $Zr(OH)_2$  precipitates. The gel was washed in water then dried for 24 h under air.  $ZrO_2$  was obtained by calcination of the dried gel in an oven at 500°C (10 °C/min) for 3 hours.

### 3.1.4 Hydrotalcite-like layered double hydroxides (LDHs)

Mg-Al hydrotalcites intercalated with five different interlayer anions –  $CO_3^{2-}$ ,  $SO_4^{2-}$ ,  $Cl^-$ ,  $HPO_4^{2-}$  or terephthalate – were synthesized either by co-precipitation or by ion-exchange method.

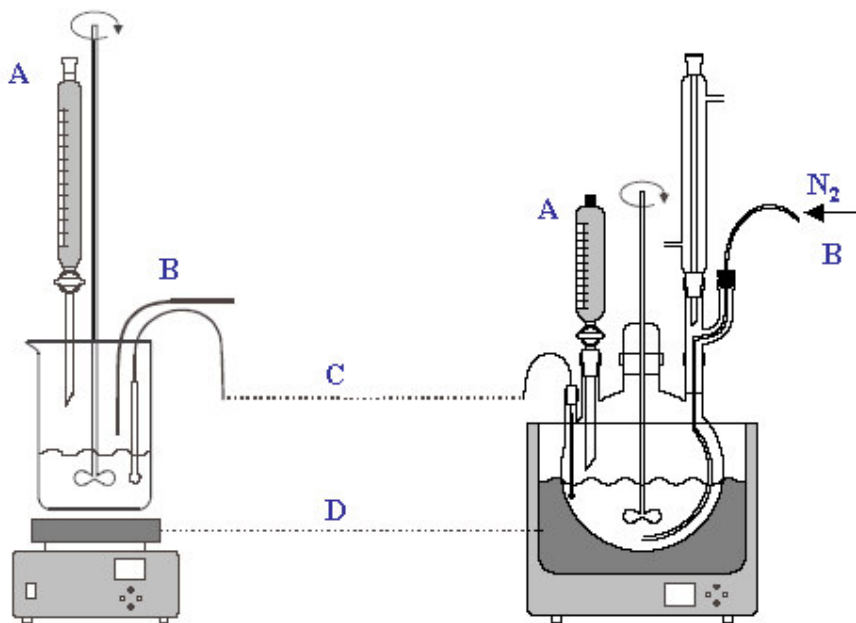
- *Synthesis of hydrotalcite-like layered double hydroxides (LDHs)*

Scheme 6 presents apparatus used for the synthesis of hydrotalcites derived from mixed Mg-Al oxides.

Five differently modified Mg-Al hydrotalcites were synthesized. A presumed Mg/Al molar ratio in all the hydrotalcites was close to 2, but a various type of the interlayer anions - carbonates (HT- $CO_3$ ), sulphates (HT- $SO_4$ ), terephthalates (HT-TA), chlorides (HT-Cl) or phosphates (HT- $HPO_4$ ) – was introduced into the interlayer of the prepared materials.

Taking into account a possibility of contamination with atmospheric  $CO_2$  the synthesis of the chloride-, terephthalate- and phosphate-containing samples was performed in a 1-litre, five-neck, round-bottom flask equipped with a reflux condenser, mechanical stirrer and pH-meter under a constant flow of highly pure nitrogen (scheme 6). Moreover, deionized decarbonated water was used for the preparation of all the aqueous solutions of metal salts as well as for the washing of the obtained precipitates. Scheme 7 presents the synthesis strategy for hydrotalcites derived from mixed Mg-Al oxides.

**Scheme 6.** Apparatus used for the synthesis of hydrotalcites derived from mixed Mg-Al oxides



- A: NaOH solution      B: Salt solution  
C: pH-meter          D: Heating

The HT-CO<sub>3</sub>, HT-SO<sub>4</sub> and HT-Cl samples were prepared by the co-precipitation method at constant pH and temperature in the presence of magnesium and aluminium salts. The metal nitrates (for HT-CO<sub>3</sub>), sulphates (for HT-SO<sub>4</sub>) or chlorides (for HT-Cl) were dissolved in deionized water, respectively. The amounts of metal salts were selected to obtain the total cation concentration of 3.4, 1.8 or 1.5 M, respectively. The solutions were added dropwise under vigorous stirring to the solution of a sodium salt being the source of anions incorporated into the interlayer space of hydrotalcite. The required amounts of Na<sub>2</sub>CO<sub>3</sub>, Na<sub>2</sub>SO<sub>4</sub> or NaCl were calculated according to the relation of  $[A^{x-}] = \frac{1}{x} \cdot [Al^{3+}]$  (where A stands for anion) and taken with an excess of 20 %. The addition was performed over a period of 1.0 - 1.5 h at temperature of about 60 °C and the pH was adjusted close to 10 using a 2 M NaOH solution. The slurries were kept at 60 °C stirred for 1.5 h. The resulting precipitates were isolated by filtration and washed with about 1 L of warm deionized water. The samples were dried at 60 °C for 20 h.

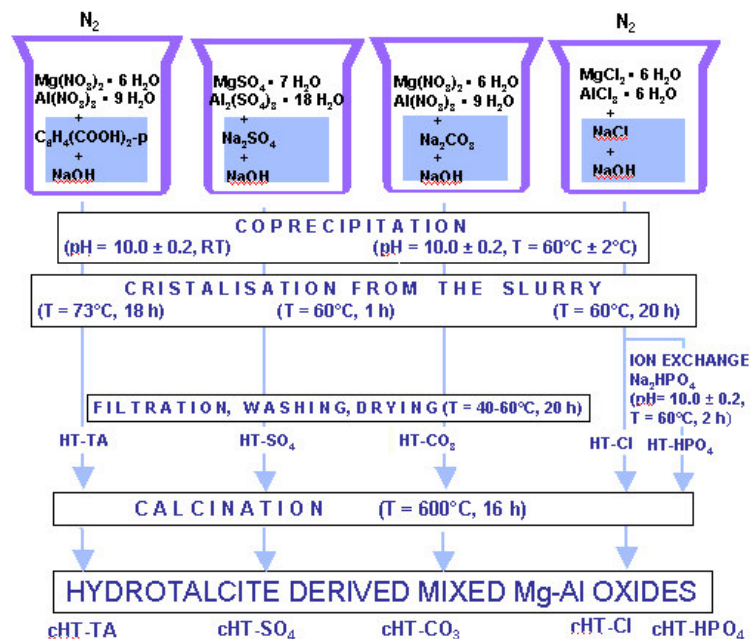
The HT-TA sample was synthesized by a dropwise addition of an aqueous solution of Mg(NO<sub>3</sub>)<sub>2</sub>·6H<sub>2</sub>O and Al(NO<sub>3</sub>)<sub>3</sub>·9H<sub>2</sub>O with the total cation concentration of 1.8 M to an

aqueous solution containing terephthalic acid and NaOH at the molar ratio of 0.11. The amount of terephthalic acid was used with 100 % excess in the relation to the amount which was needed to counterbalance the positive charge of the brucite-like sheets. The precipitation was performed under vigorous stirring at room temperature, and finally the pH of the resulting solution was adjusted to 10 by the addition of 2 M NaOH. The slurry was heated at 73 °C for 18 h under stirring. The product was filtered and washed with about 1 L of warm deionized decarbonated water.

The ion-exchange method was used to the preparation of the HT-HPO<sub>4</sub> sample. As a parent material the chloride-containing hydrotalcite, prepared according to the procedure described above, was chosen. The ion-exchange was carried out by dropwise addition of an aqueous solution of 0.045 M Na<sub>2</sub>HPO<sub>4</sub> to the slurry of the HT-Cl hydrotalcite over a period of 0.5 h. The mixture was stirred at 60 °C and kept at a pH close to 10 using a solution of 2 M NaOH. The slurry was heated at 60 °C for 2 h under stirring. The product was filtered and washed with about 1 L of warm deionised decarbonated water. The resulting precipitate was dried at 60 °C for 18 h in a dryer.

Prior to the studies on textural and acid-base properties, all the samples were calcined at 600 °C for 16 h in static air. The samples after the thermal treatment were kept in an exsiccator in order to avoid a reconstruction of the hydrotalcite structure due to “memory effect”. To distinguish the as-synthesized and calcined samples to the names of thermally treated ones letter “c” was added.

**Scheme 7.** Synthesis of hydrotalcites derived mixed Mg-Al oxides





### 3.2 Experimental set-up and experimental conditions

#### - Conditions for Methyl butynol (MBOH)

Methyl butynol (MBOH) and n-hexane were obtained from Fluka with purity of 99 % and used without further purification.

The test reaction of MBOH conversion was carried out in a fixed-bed, automated bench unit. In pre-experimental runs it was checked that n-hexane, used as internal standard, was not converted over the catalysts. Both mixture of MBOH (95 vol %) and n-hexane (5 vol %) were cooled to 13 °C in a storage vessel. Applying a static nitrogen pressure of 2 bar a constant flow of the mixture (0.02 mL/min) through a capillary into the evaporator was realized.

0.2 g of crashed then sieved catalyst was placed in the centre of quartz tubular reactor. The fraction of the catalyst particles was in the range of 200 -315 µm. Prior to the reaction the catalysts were heated to 500 °C with a rate of 8 °C/min and kept at this temperature for 4 h under nitrogen flow to remove water and carbon dioxide adsorbed on the surface. After the activation of the catalyst (table 5), the reactor was cooled to the reaction temperature. The reaction products were analysed after activation process, see table 5. The products amounts were calculated on the basis of sum peak areas.

**Table 5.** Activation procedure

I	Oxidation in Air	heating rate: 1 h (8 °C/min) to 500 °C air flow: $\dot{v} = 13$ mL/min
II	Inertisation	temperature T = 500 °C N <sub>2</sub> flow : $\dot{v} = 13$ ml/min duration: t = 4 h
III	Cooling	cooling to: T = 200 °C (without T-controlling) N <sub>2</sub> flow : $\dot{v} = 13$ ml/min
IV	Stand-by	temperature T = 200 °C N <sub>2</sub> flow $\dot{v} = 13$ ml/min duration: until the start of reaction

*- Experimental apparatus*

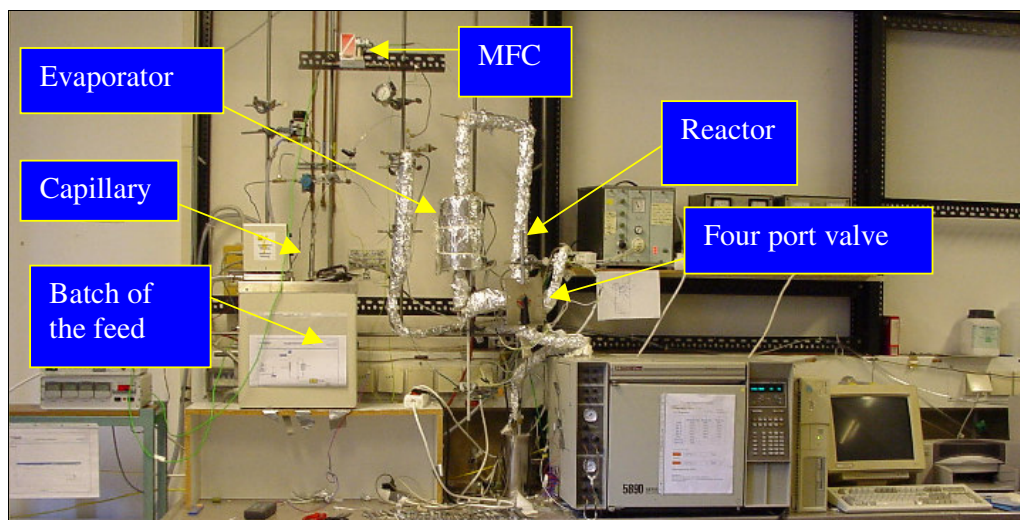
The experimental set-up consists of a feeding unit for the educt, the heatable, catalyst-containing reactor and an analysis unit.

The educt feeding consists of a valve unit which combines a three line valve to enable the time controlled influx of three gases. Two of these valves are used for the gases nitrogen and synthetic air, to allow an over night-activation of the catalyst. The gas flow is controlled by a mass flow controller with corresponding control unit (Bronkhorst company).

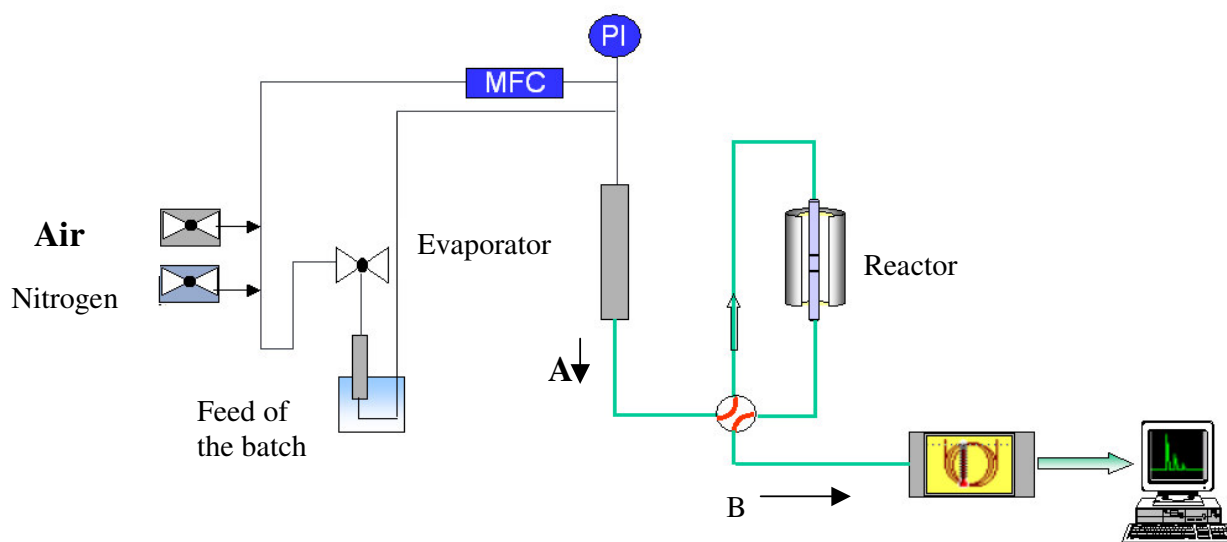
Liquid educts are feed by an evaporator. There, a capillary with a length about 25 cm and diameter 0.3 cm, filled with liquid methyl butynol (MBOH) (95 wt.%) and internal standard n-hexane (5 wt.%). The capillary with substrates is located in the bath filled with water which is temperature 13 °C. This constant temperature insures a constant flow. Outgoing amount of mixture MBOH and n-hexane into the evaporator was measured and found to be 0.02 mL/min. The MBOH and n-hexane proceed then to the evaporator through second and thin capillary, measured length about 300 cm and diameter 1.5 mm.

The evaporator was first covered in a spiral way with heating bands, then wrapped with copper bands for equally heating and finally wrapped with the isolation material. This way of heating insured a continuous transforming from liquid MBOH into gas. The MBOH vapor is carried with an 13 mL/min nitrogen flow through the apparatus. With a pressure indicator (max. 2 bar) arising pressure can be measured inside the system.

In order to insure a steady stream of the substrate over the solid catalysts, a bypass was installed to pass a stream of methyl butynol from the evaporator directly to the gas chromatograph. If a constant educt stream has been established the gas was oriented via a four way valve to the top of the reactor where the solid catalyst is located in the isothermal section of a tubular quartz tube with an inner diameter of 7 mm.



**Scheme 8.** The apparatus for the methylbutynol test reaction



Temperature of transfer lines:

A: 140-145 °C, B: 155 °C

Testing the apparatus with empty reactor was performed and the result are submitted in the appendix point 7.1 ( figure 7-A). This type of experimental test is established to improve that substrates are not reacting with the materials used in the building of the apparatus. The only outgoing peaks were identified to be methyl butynol and n-hexane, this means that no reactions take place between the substrate and the materials used in the apparatus. Additionally, methyl butynol shows a permanent and constant peak. Once established, the constant stream of methyl butynol was oriented to the empty reactor by four-port valve. For

approximately one minute no GC signals can be measured. After this dead time the gas returns to enter the gas chromatograph on the time axis of the chromatogram.

### 3.3 Verification of carbon deposit for MBOH test reaction

With equation (1) the percentage of the deposited carbon can be calculated (106):

$$\text{Carbon deposit (\%)} = 100 \frac{(m_{\text{tot}} - m_{\text{cat}})}{m_{\text{cat}}} \quad \text{equation (1)}$$

$m_{\text{cat}}$  and  $m_{\text{tot}}$  are the mass of the catalyst before and after the reaction, respectively. This way of the calculation is not precise enough due to the unestimated loss of catalyst resulted by transporting before and after the experiment. For that, it is necessary to find another method for calculating the amount of carbon deposit on the catalyst.

Carbon deposition can be calculated easily for the conversion of MBOH at basic catalysts. There, acetylene and acetone are formed as the only products, but both do not arise in the stoichiometric molar ratio of 1 : 1 but a lack of acetone is detected. Assuming that only acetone is responsible for carbon deposition and neither MBOH nor acetylene, the missing amount of acetone can be expected to be carbon deposit. To calculate the amount of carbon deposit the corrected peak areas are calculated for all compounds, using response factors. The corrected area is the peak area which would be obtained if all C-atoms of a compound participate with equal amounts at a FID-Signal, equation (2):

$$\text{Corrected Area} = (\text{Peak Area} / \text{Response factor}) * \text{number of carbon atoms} \quad \text{equation (2)}$$

The actually measured amount of C-Atoms is directly proportional to the sum of the corrected areas, equation (3):

$$\text{Carbon atoms actual} \approx A(\text{MBOH}) + A(\text{acetylene}) + A(\text{acetone})$$

A: corrected area of the compound

If no carbon atoms are deposited the amount of carbon atoms should be:

$$\text{Carbon atoms target} = A(\text{MBOH}) + 2,5 * A(\text{acetylene}) \quad \text{equation (4)}$$

The difference of both can be assumed to be carbon deposit equation (5)

$$\text{Carbon deposit} = \text{Carbon atoms target} - \text{Carbon atoms actual} \quad \text{equation (6)}$$

$$\text{Carbon deposit} = [A(\text{MBOH}) + 2,5 * A(\text{acetylene})] - [A(\text{MBOH}) + A(\text{acetylene}) + A(\text{acetone})] \quad \text{equation (7)}$$

Knowing the target amount of carbon atoms, conversions and selectivities can be calculated. If no carbon deposition takes place, carbon selectivity of acetylene is 40 % and carbon selectivity of acetone is 60 %. Assuming that carbon deposition is only caused by acetone, selectivity of acetylene always stays 40 % and selectivity of acetone decreases. In appendix point 7.2 in table A-1 and A-2 applies the results for the calculation for the example of Puralox MG HT 70. The results plotted against time on stream and presented in figure 6.

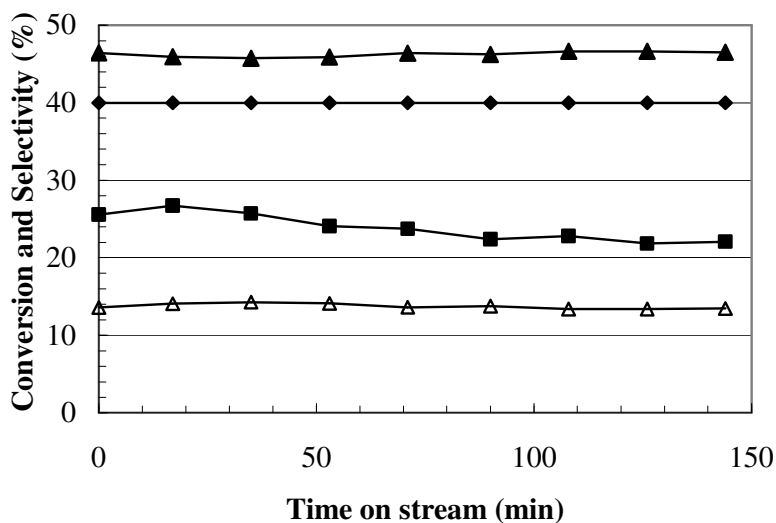


**Figure 6. Carbon balance over Puralox MG HT 70 for the conversion of MBOH  
T = 120 °C**

- ▲ Selectivity of acetone
- ◆ Selectivity of acetylene
- MBOH conversion
- △ Selectivity of carbon deposit

Figure 6 shows that only 45 % of all carbon atoms from converted MBOH could be found in acetone instead of theoretically proposed value of 60 %. About 15 % of all converted carbon atoms could not be detected and are assumed to be deposited as carbon on the catalysts surface. This deposition is constant with time on stream. Taking into consideration the whole amount of MBOH which is lead through the reactor, the part of carbon atoms which are deposited is only 2 %.

### 3.4 Conditions for isopropanol test reaction

In isopropanol test reaction the same activation procedure and conditions were used as described in chapter 3.2 for MBOH test reaction with a few variations:

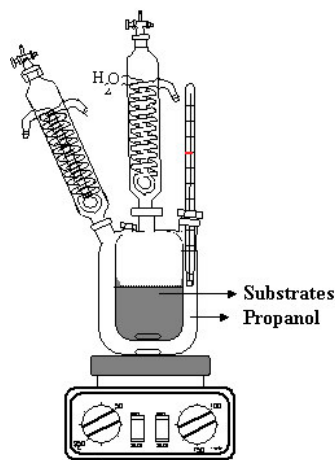
A mixture of 95 wt.% 2-propanol and 5 wt.% dioxane was used as feed with a total liquid flow of  $\dot{v} = 0.01$  mL/min through the capillary, which was at room temperature. The metal reactor was changed for a quartz glass reactor.

### 3.5 Experimentals for test reaction in liquid phase

#### - *Experimental apparatus for Knoevenagel condensation*

The reaction was conducted in a reactor which consists of two parts. The outer part serves for the heating medium, maintaining the same reaction temperature in the jacket reactor, while the inner part is fitted with a reflux condenser filled with the reactants, as shown in scheme 6.

**Scheme 9.** The experimental apparatus for Knoevenagel condensation

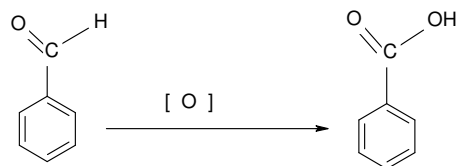


#### - *Reaction conditions*

To prevent oxidation of benzaldehyde to benzoic acid (scheme 10), the reaction was conducted under a nitrogen stream of 34.3 mL/min. Oxidation of benzaldehyde would affect the conversion and benzoic acid would adsorb on the catalysts surface and poison the basic sites (96, 97). For each reaction a mixture of 3.13 g malononitrile (47.4 mmol), 1.6 mL (15.7 mmol) benzaldehyde, and 12 mL of 1,4 dioxane as solvent and 0.2 g of catalyst was filled into

the inner part of the jacket reactor. Zero probe is called the probe which is taken at the time at which the boiling-point of 96 °C was reached. The reaction response time begins with the addition of the catalyst into the reactor during magnetic stirring ( $t = 0$ ).

**Scheme 10.** Oxidation of benzaldehyde



*- Sensivity of the reaction*

An experiment was performed to study the influence of the reactants to produce benzylidenmalononitrile by conducting the reaction as described in the experimental section without catalyst (blind probe). After 4 h the yield of benzylidenmalononitrile was only 1 mol%.

*-Preliminary examinations on the amount of the catalyst*

To find the optimal amount of the catalyst, the experiment was reproduced for 0.2 g, 0.3 g, 0.4 g and 0.5 g. The reaction proceeds very fast and 15 min after the addition of the catalyst to the reactant the yield of benzylidenmalononitrile was 100 mol%. The attained results show that with a low amount of catalyst, the visibility for the comparison in the conversion between different solids is higher and better because the reaction time needed to reach the maximal conversion of 100 % is longer. Hence, the standard amount of catalyst was chosen to be 0.2 g for the investigation of Knoevenagel condensation in the present work. Figure 7 shows the effect of different types of catalyst on the acceleration of the reaction.

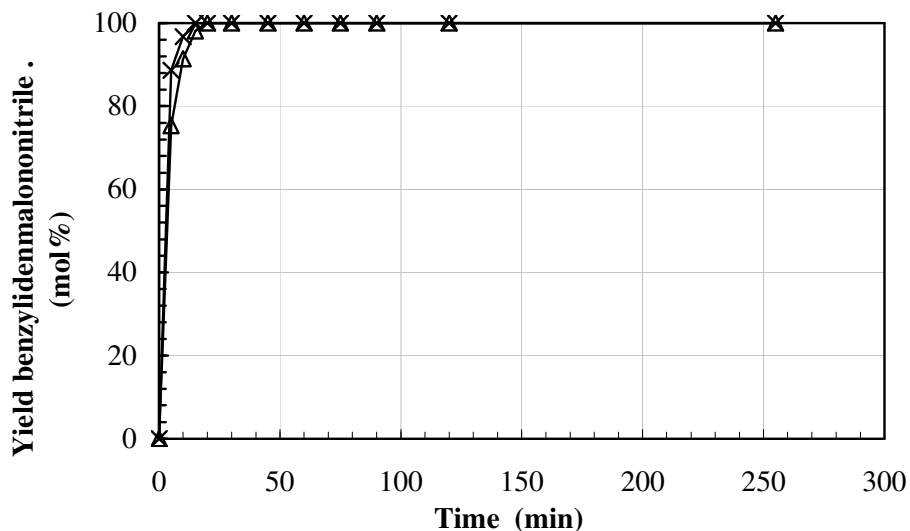


**Figure 7. Influence of the type of catalyst on the maximal conversion of malononitrile**

amount of the catalyst: 0.5 g, malononitrile: 47.5 mmol, benzaldehyde: 15.8 mmol

× Puralox MG 30      ◇ Puralox SBA

#### *- Temperature and reaction time*

The reaction was conducted with 1-propanol as heating medium, realising a constant temperature of 96 °C.

Samples were taken from the reaction mixture in given intervals after the start time: 5, 10, 15, 20, 30, 45, 60, 75, 90, 120, and 255 min. Each sample consist of 25 drops (approx. 1 mL). In order to separate the catalyst the samples were filtered in a glass tube filled with a piece of filter paper and rinsed with 0.2 mL 1,4 dioxane. 1 µl of the eluate was analysed through gas chromatographic analysis with the conditions shown in point 3.5.

### **3.6 Analysis and calculations**

#### **3.6.1 Gas chromatographic parameters for MBOH test reaction**

A HP 890 Series II gas chromatograph with a 60 m Optima Wax capillary column with a 0.25 µm wax film ( $T_{\max} = 270$  °C) was used. The temperature program used to separate all



arising products with nitrogen as carrier gas ( $\dot{v} = 13$  ml/min) was:

$T_{\text{start}} = 45$  °C for 5 min

$dT/dt = 10$  °C/min

$T_{\text{end}} = 90$  °C for 10 min

For identification of MIPK, which is a product of MBOH test reaction HP 6890 GC-MS with mass sensitive detector was used. Analysis was achieved with a 50 m HP-Pona methylsiloxane capillary column (film thickness: 0.50  $\mu\text{m}$ ), helium as carrier gas ( $\dot{v} = 0.6$  mL/min) and the following temperature programm:

$T_{\text{start}} = 40$  °C for 5 min

$dT/dt = 10$  °C/min

$T_{\text{end}} = 200$  °C

The report attained from this injection is presented in appendix, point 7.3.

### 3.6.2 Gas chromatography conditions for isopropanol test reaction

The same GC and column was used as for analysis of MBOH test reaction, only the temperature programm was different:

$T_{\text{start}} = 37$  °C for 5 min

$dT/dt = 20$  °C/min

$T_{\text{end}} = 90$  °C for 10 min

### 3.6.3 Gas chromatography conditions for Knoevenagel condensation

A HP 6890 gas chromatograph with a 60 m HP 5 capillary column with 5% phenylmethyl siloxane (film thickness: 0.25  $\mu\text{m}$ ,  $T_{\text{max}}$ : 360 °C) was used for analysis of the products of Knoevenagel condensation. Nitrogen ( $\dot{v} = 13$  mL/min) was used as carrier gas with the following temperature program:

$T_{\text{start}} = 115 \text{ }^{\circ}\text{C}$  for 7 min

$dT/dt = 30 \text{ }^{\circ}\text{C}/\text{min}$

$T_{\text{end}} = 300 \text{ }^{\circ}\text{C}$  for 5 min

### 3.6.4 Determination of the relative response factors (rRf) for MBOH, isopropanol and Knoevenagel reactions

#### - Empirically determination of the relative response factors (rRf)

The conversion of peak areas into amounts of the corresponding sample component is effected via response factors and is needed for accurate quantitative analysis.

Response factors are usually determined through chromatographic separations, by elution of test mixtures from authentic composition, only. The continuous transfer of the test compound into the detector at a constant concentration in the carrier gas could be an alternative method for evaluation of response factors. The measurements usually performed for the determination of response factors are suited to eliminate secondary errors, e.g. of sampling, by a calibration which is valid only for the analysis performed (98).

The experimental determination of the relative response factor (rRf) was carried out by preparation of three mixtures. Each mixture contains a known mass of 3-methyl-3-buten-1-yne (MBYNE), 3-methyl-2-butenal (Prenal), 3-hydroxy-3-methyl-2-butanone (HMB), methyl butynol (MBOH) and acetone mixed with n-hexane as a solvent. Three times an amount of 1  $\mu\text{l}$  of each mixture was injected and the relative response which was calculated from the following equation (8):

$$\text{rRf} = \frac{m_j A_j}{m_{\text{n-hexane}} A_{\text{n-hexane}}} \quad \text{equation (8)}$$

$m_j$ : mass of component [g]

$m_n$ : mass of related component (n-hexane for MBOH test reaction, dioxane for isopropanol and acetone for Knoevenagel condensation).

$A_j$  : Peak area component j.

$A_n$  : Peak area related component.

*- Calculation of response factors for gas chromatography analysis*

In the present work, all gaschromatography analyses were carried out with a flame ionization detector (FID). There, all organic substances which are eluated of the column by the carrier, are burned in the hydrogen flame whereby ions are formed, which cause the detector signal. The hydrogen flame itself is hardly ionised. When compounds are burned within the flame electrons are formed over a radical reaction. These electrons are caught by the electric field of the collecting electrode and deliver the signal current.



The quantity of the formed ions and electrons and therewith the size of the detector signal depends not only on the quantity, but rather on the type of the respective compound. Compounds which have already carbon-oxygen-bonds deliver a smaller signal per carbon atom than oxygen free compounds. Therefore the signal of the flames ionisation detector has to be multiplied with a correction factor i.e. the response factor, in order to receive the ratio of the amounts of the compounds. For simple compounds, which contain only the elements C, H, O and N, the response factors can be calculated for a flame ionisation detector. The molar response factor is the reciprocal value of the amount of the effectively detected carbon atoms. In order to recieve this amount, one adds the amount of the carbon atoms of the compound whereby the following factors are considered:

- \* The factor of completely indicated carbon atoms, those with just C, H or N bonds, factor: 1.
- \* Carbon atoms with a C-O-single bond, factor: 0.55
- \* Carbon atoms with two C-O single bonds or with a C=O double bond: factor: 0

### **3.7 Values of relative response factors**

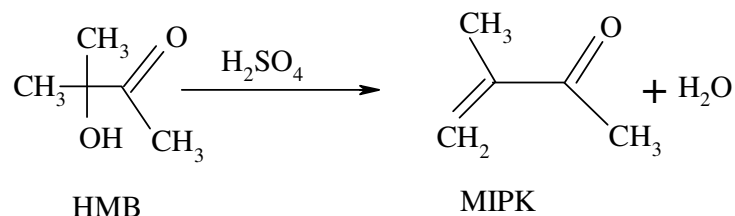
*- Values of the relative response factors (rRf) for MBOH test reaction*

Table 6 presents a comparison between the relative response factors of all compounds arising in MBOH test reaction which were obtained on the basis of the measurements and calculations.

**Table 6.** Comparison of calculated and experimental relative response factors for all components of MBOH test reaction

Substrate	Provenance, Purity (%)	Relative response factor calculated	Relative response factor experimental
MBOH	Fluka (99)	1.28	1.21
Acetylene	Messer (99)	0.95	0.92
Acetone	Acros (99)	1.98	2.00
MBYNE	Aldrich (98)	0.92	0.91
Prenal	Fluka (99)	1.42	1.46
HMB	Aldrich (99)	1.99	2.00
MIPK	-	1.46	n.a.*

Since the MIPK product is not purchasable in the local market which is necessary to indicate its response time, an experiment was performed to produce MIPK. In this aim HMB was dissolved in cyclohexane in a vial of approx. 0.5 mL. A drop of H<sub>2</sub>SO<sub>4</sub> (conc.) was added and the mixture was slightly heated on a heating plate. Two phases were observed. The organic phase in the top contains HMB and MIPK while sulfuric acid and produced water build the second phase in the bottom. The organic phase was yellow and became darker and darker with increasing time.



GC analysis was done (from the organic phase) on GC-MS HP 6890 and on GC HP 5890 series II applying head space technique. From the attained MS report presented in appendix point 7.3 it is shown that MIPK was successfully identified (peak number 4) and by comparing response times of manually injected MIPK and on-line measured product mixture, MIPK was identified without doubt as a product of MBOH conversion.

Because the calculated response factors of MBOH conversion are close to the experimental ones, the calculation for the MBOH conversion was based on the values of the calculated response factors.

\* Not available commercially

- Values of the relative response factors (*rRf*) for isopropanol test reaction

Table 7 presents the provenance and the relative response factors for all components in the isopropanol test reaction.

**Table 7.** Comparison of calculated and experimental relative response factors for all components of isopropanol test reaction.

Substrate	Provenance, Purity (%)	Relative response factor calculated	Relative response factor experimental
Isopropanol	Fluka (99)	1.15	1.16
Propene	Messer (99)	1.30	1.20
Acetone	Acros (99)	0.91	0.92
Isopropylether	Aldrich (98)	2.20	2.10
Dioxane	Basf (99)	1	0.97

- Values of the relative response factors (*rRf*) for Knoevenagel reaction

Table 8 presents the purity, provenance and the relative response factors for all components of Knoevenagel reaction.

**Table 8.** Comparison of calculated and experimental relative response factors all components Knoevenagel reaction

Substrate	Provenance, Purity (%)	Relative response factor calculated	Relative response factor experimental
Benzaldehyde	Acros Organics (98)	1.00	0.99
Malononitrile	Aldrich (99)	1.25	1.26
Benzyliden-malononitrile	Lancaster (98)	0.87	0.90
*Acetone	Acros (99)	1.64	1.62

---

\* Acetone was used as solvent for manual injection.

### 3.7.1 Calculation of data

- MBOH and isopropanol test reactions

If all the response factors are identified for all products we can calculate the conversion (equation 9) and subsequently, the yield (equation 10) and the selectivity (equation 11) in mol%.

$$X = 1 - \frac{A_i \cdot rRf}{\sum A_j \cdot rRf_j} \quad \text{equation (9)}$$

X : Conversion of MBOH or isopropanol

$A_j$  : Chromatogram area of compounds j

$rRf_j$ : relative response factor of compound j

The values of the calculated and experimentally determined relative response factors are very similar (see, table 6, 7, and 8). Therefore, calculation of the conversion was based only on the values of the theoretical method.

$$Y_p = \frac{A_p \cdot rRf_p}{\sum_{i=1}^k A_i R_i} \quad \text{equation (10)}$$

$A_p$  : Peak area of product p

$rRf_p$  : relative Response factor of product p.

k : Number of the components in the chromatogram

$$S_j = \frac{Y_j}{X_{MBOH}} \quad \text{equation (11)}$$

$Y_i$  : Yield of the product

X : Conversion of MBOH or isopropanol

- *Calculation of the conversion of malononitrile for Knoevenagel condensation*

Calculation of the conversion was based on the values of the relative response factors for the theoretical method, which are close to the experimental ones (see table 8).

In Knoevenagel condensation, the stoichiometric component is benzaldehyde and the relationship between benzaldehyde and malononitrile was chosen to be equal 3, this means: if benzaldehyde reacts completely, a conversion of malononitrile of 33 mol % results.

Considering this stoichiometric ratio a normalized conversion of malononitril is calculated according the following equations:

$$X_{\max} = \frac{N_b}{N_m} * 100 \quad \text{equation (12)}$$

$$X_{\max} = 33.2 \text{ mol\%}$$

$$X_{\text{Normalized}} = X_{\text{malononitril}}/X_{\max} \quad \text{equation (13)}$$

Index m, b : Components malononitrile and benzaldehyde, respectively

$X_{\max}$  : Maximal stoichiometrical conversion of malononitrile, for ratio  
benzaldehyde : maolonitrile = 1 : 3

$N_b$  : Amount of benzaldehyde (mmol)

$N_m$  : Amount of malononitrile (mmol)

### 3.8 Characterization methods

#### 3.8.1 Characterization of solids with different Si/Al ratios calcined at different temperatures and metal oxides supported on alumina

The solids silica alumina and metal oxides supported on alumina were characterized at the Univeristy of Oldenburg by BET surface area and temperature programmed desorption of ammonia (NH<sub>3</sub>-TPD).

*a) BET surface area*

The surface area of samples were characterized by the BET method, performing adsorption of nitrogen at  $-196\text{ }^{\circ}\text{C}$  with the apparatus Quantachrome Autosorb-1. The Quantachrome autosorb-1 operates by measuring the quantity of nitrogen adsorbed onto the solid surface at some equilibrium vapour pressure by the static volumetric method. The data are obtained by admitting a known quantity of adsorbate gas, which is nitrogen, into the sample cell containing the solid adsorbent maintained at a constant temperature below the critical temperature of the adsorbate. As adsorption occurs the pressure on the sample cell changes until equilibrium is established. The quantity of gas adsorbed at the equilibrium pressure is the difference between the amount of gas admitted and the amount required to fill the surface of the adsorbent. Data acquisition, reduction and calculating were performed by Quantachrome Autosorb software.

*b) Temperature programmed desorption of ammonia ( $\text{NH}_3$ -TPD)*

Silica alumina and metal oxides (such as titanium oxide, hafnium oxide and zirconium oxide) supported on alumina were characterized by temperature programmed desorption of ammonia with an apparatus constructed from Raczek analyse technic GmbH, Hannover. The apparatus consist of an adjustable oven to heat the sample, gas mixture supplies for helium and a 5 vol.%  $\text{NH}_3/\text{Ar}$  (Messer-Griesheim) and a thermal conductivity detector for gas analysis.

In general, temperature programmed desorption methods give a characteristic “fingerprint” of a solid catalysts which can be used to determine, for example, the distribution of acid site strength of the surface if ammonia is the sorbed gas, or the distribution of basic sites if carbon dioxide is the sorbed gas. In this chapter (3.5/b) the  $\text{NH}_3$ -TPD procedure is explained.

*- Conditioning of the sample*

Figure 8 presents the conditioning diagram of a silica alumina catalyst. For a typical experiment 0.5 g of fresh catalyst was placed within a U-tube in the oven. During the first run, the sample was heated under He stream at a rate of  $20\text{ }^{\circ}\text{C}/\text{min}$  from room temperature up to  $900\text{ }^{\circ}\text{C}$  and the amount of released compounds was measured with a thermal conductivity detector (TCD). At  $900\text{ }^{\circ}\text{C}$  no more compound desorbed from the surface of the sample and the TCD-signal drastically decreases to zero. If one reproduces this procedure for the same



catalyst (run II), no signal is detected anymore which means that the surface of the sample is free from adsorbed compounds after high temperature treatment.

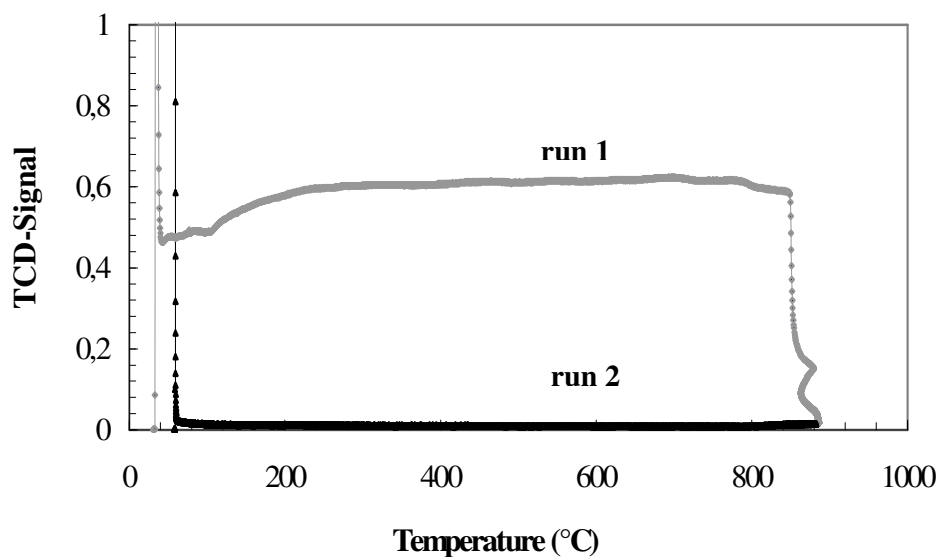


**Figure 8. Conditioning of the sample Si/Al 40 calcined 3h at 900 °C**

*- Ammonia adsorption*

After heating the sample up to 900 °C, it was cooled down to 60 °C, which is the temperature at which ammonia adsorption is conducted. In this process, the sample of catalyst is exposed to 5 vol.% NH<sub>3</sub>/Ar (Messer-Griesheim) stream (50 mL/min) for 30 min at 60 °C.

*- Measuring of physisorption*

Physisorption takes place due to the action of van der Waal's forces between the absorbent and adsorbate. Typical values for the adsorption enthalpy are ca. 20 kJ/mol, which is in the same order of magnitude as the condensation enthalpy. This energy is not sufficient to break chemical bonds and so the molecule does not dissociate during physisorption.

To desorb that part of ammonia which is bond by physisorption, the temperature is increased from 60 °C up to 100 °C, and is kept for 30 min. This should be enough to break the weak forces between the molecules and the surface (figure 9).

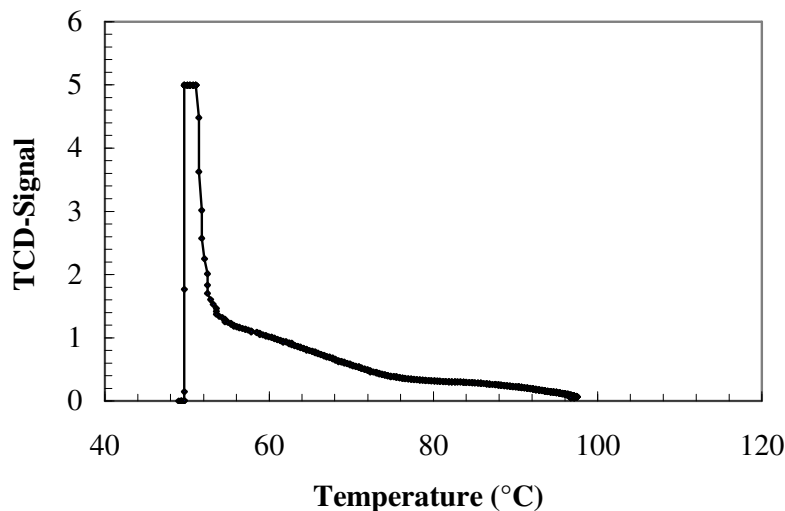


**Figure 9.** Example of TCD- signal of physisorption over Si/Al 10 calcined 3h at 900 °C

*- Measuring of chemisorption*

Chemisorption involves the action of much stronger binding forces, whose strengths are similar to the strength of chemical bonds. These interactions are significantly stronger than the physisorption interactions, but it is only possible to cover the surface with a single monolayer of chemibonded adsorbates. In contrast to the physisorption, the chemisorbed molecules can dissociate on the surface due to the chemical bounding. The adsorption enthalpy for chemisorption can have values up to 200 kJ/mol.

The sample of catalyst is exposed to He stream from 100 °C up to 900 °C at a rate of 20 °C/min, and the NH<sub>3</sub> desorption was monitored. The obtained graph (figure 10) shows a desorption peak within a temperature range from 140 °C to 480 °C. Integrating this peak leads to an area from which the amount of adsorbed ammonia can be calculated according to the equation (14):

$$A.S = \sum TCD_{signal} * C_A \quad \text{equation (14)}$$

AS: amount of ammonia (μmol)

CA: Calibration factor (μmol NH<sub>3</sub>/ area unit)

The calibration factor was determined by leading a known amount of ammonia through the TCD. By these calibrating measurements it was found that one area unit in the graph is equivalent to 1.44  $\mu\text{mol NH}_3$ .

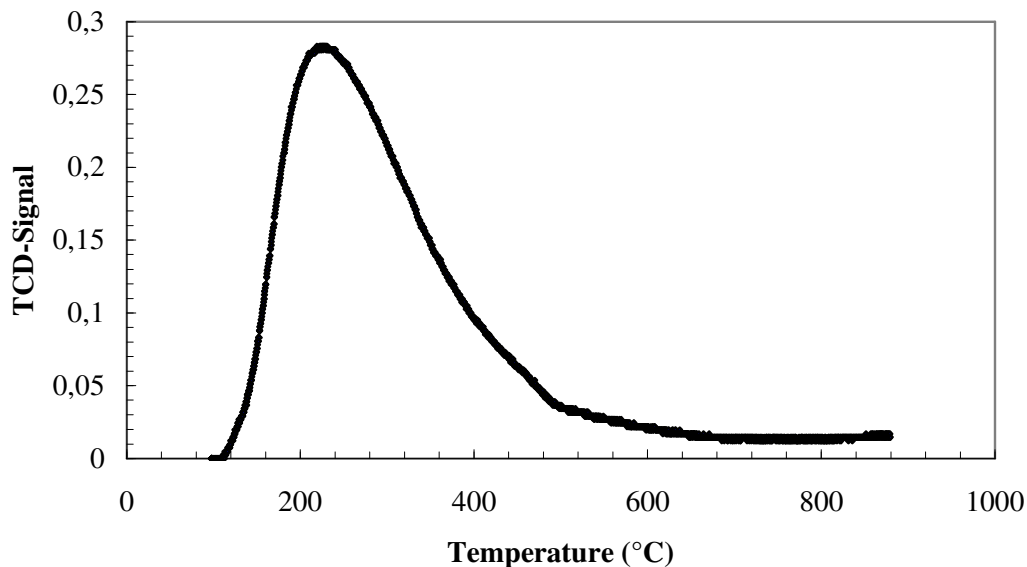


**Figure 10. Example of TCD-signal of chemisorption over Si/Al 10 (10:90) calcined 3h at 900°C**

Knowing the amount of adsorbed ammonia, one can conclude to the amount of acid centres within samples with different Si/Al ratio. This is an important information to predict and explain the chemical behaviour of the catalyst in reactions.

### 3.8.2 Characterization methods for hydrotalcites derived from mixed Mg-Al

The hydrotalcites derived from mixed Mg-Al were characterized as-synthesized at the University of Cracow (Poland) by temperature-programmed desorption of  $\text{NH}_3$  and  $\text{CO}_2$ , BET measurements, X-ray diffraction and FTIR spectroscopy (109).

#### - BET

The texture of the samples was characterized by the BET  $\text{N}_2$  adsorption-desorption method at  $-196^\circ\text{C}$  using Micromeritics 2010 sorptometer. Prior to the experiments the catalysts were outgassed at  $350^\circ\text{C}$  for 12 h under vacuum. The BJH method was applied for determination of pore size distribution.

*-Temperature programm desorption of ammonia and carbon dioxide*

Surface concentrations of acidic and basic centres were determined by temperature-programmed desorption of ammonia (NH<sub>3</sub>-TPD) and carbon dioxide (CO<sub>2</sub>-TPD), respectively. Experiments were carried out in the temperature range of 70 – 650 °C in a fixed-bed flow microreactor. The temperature of the reactor was measured by a K-type thermocouple located in a quartz capillary immersed in the sample bed. The molecules desorbing were monitored on-line by a quadrupole mass spectrometer (VG QUARTZ) connected directly to the reactor outlet via a heated line. Before TPD experiments the calcined hydrotalcites (50 mg) were outgassed at 600 °C for 15 min in a flow of helium (20 mL/min). Subsequently the sample was cooled down to 70 °C and saturated in flow of gas mixture containing 1 vol.% of NH<sub>3</sub> in helium or alternatively 10 vol.% of CO<sub>2</sub> in helium until no adsorption of probe molecules was observed. In both cases the total flow rate was 20 ml/min. Then the sample was purged in the helium flow until a constant baseline level was attained. Desorption was carried out with a linear heating rate (10°C/min) in a flow of He (20 ml/min). Traces of H<sub>2</sub>O and O<sub>2</sub> in pure helium (grade 5.0) used as the eluant gas were removed by appropriate traps (Alltech). The NH<sub>3</sub>-TPD spectra were obtained from the m/z = 16 mass-to-charge signal ratio, while the CO<sub>2</sub>-TPD one from the m/z = 44. A calibration of QMS with commercial test mixtures allowed to recalculate the detector signal into ammonia or carbon dioxide desorption rate.

*- X-ray diffraction*

Powder X-ray diffraction patterns were measured with a PW 3710 Philips X'pert diffractometer using Ni-filtered CuK<sub>α</sub> radiation ( $\lambda=1.54178 \text{ \AA}$ ) over a  $2\theta$  range of 4° to 80° (step size - 0.025°, time per step - 1.5 s).

*- FT-IR spectra*

FT-IR spectra were recorded from 400 to 4000 cm<sup>-1</sup> with a Bruker IFS 48 spectrophotometer using KBr pellet technique. The total content of Mg, Al, S, Cl and P in the samples was determined by X-ray fluorescence (Oxford 2000) spectrometer.

## 4. Results and discussion

### 4.1 Temperature programmed desorption of ammonia

The aim for studying the acid properties for silica alumina and metal oxides supported on alumina (see chapter 4.2) is to find out if acid sites are responsible for the formation of specific products like MIPK in the MBOH test reaction. Therefore it is important to determine the amount of acidic sites in different samples for silica alumina solids and to study whether strong or weak acidic sites or even both are present on the catalysts surface. The answers to these questions allude to important points in this thesis because they will provide information according the mechanism of the formation of MIPK in the amphoteric pathway of the MBOH test reaction as will be discussed in this work in chapter 4.4.6.

On the other hand, measuring the amount of acidic sites in the investigated samples (silica-alumina solids and metal oxides supported on alumina) gives an objective correlation between the acidic concentration ( $\mu\text{mol/g}$ ) and the composition of different studied samples. For that, temperature programm desorption of ammonia stands as an important measurement in the present work.

*- Acid properties of the silica-alumina with different ratios.*

The  $\text{NH}_3$ -TPD profiles of samples with different Si/Al ratios calcined 3 h at 550 °C and at 900 °C are comparatively shown in figures 10 and 11, respectively. The results of  $\text{NH}_3$ -TPD show that the amount of interior alumina strongly influences the surface acidity of the presented catalysts. Applied method allows to determine relative strength and quantity of surface acidic centers (109).

The maximum desorption peaks of ammonia with different Si/Al ratios are reached at temperatures 228 °C, 223 °C, 205 °C, and 195 °C, for samples with the Si/Al ratios 5, 10, 20, and 40, respectively. Another but lower peak was observed for the sample containing 40 wt.%  $\text{SiO}_2$  at a higher temperature of 258 °C.

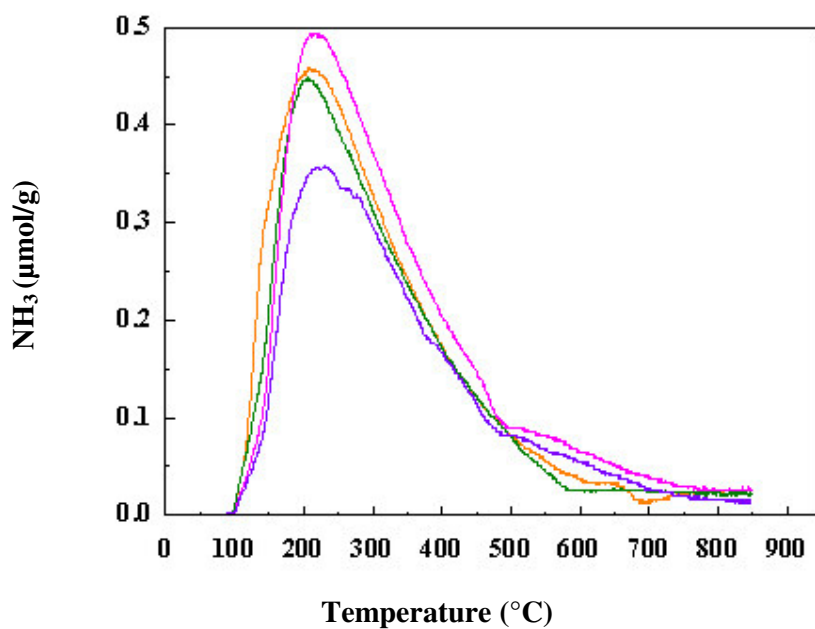


**Figure 10. Profiles of temperature programmed desorption of ammonia for silica alumina with different ratios (wt.%), calcined 3 h at 550 °C**

— Si/Al (5:95) — Si/Al (10:90) — Si/Al (20:80) — Si/Al (40:60)

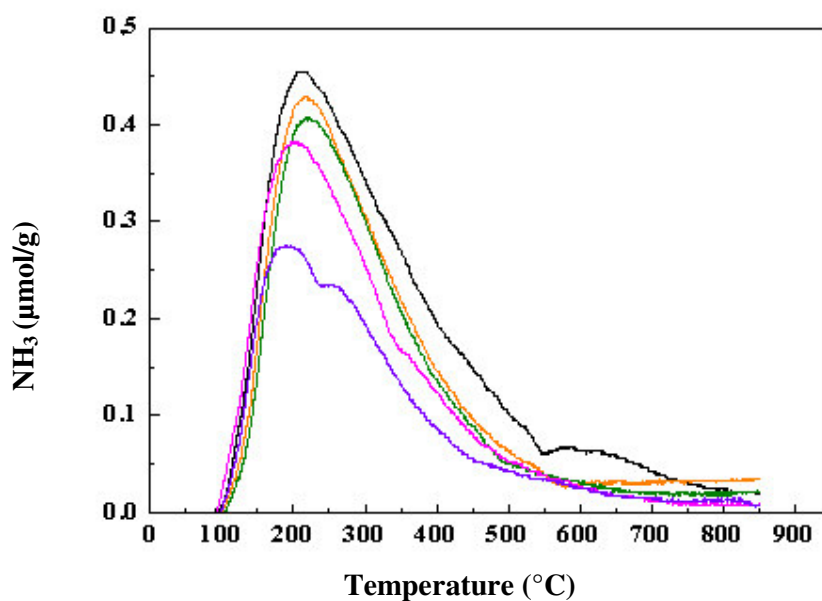


**Figure 11. Profiles of temperature programmed desorption of ammonia for silica-alumina with different ratios (wt.%), calcined 3 h at 900 °C**

— Pure alumina — Si/Al (5:95) — Si/Al (10:90) — Si/Al (20:80)  
— Si/Al (40:60)

From figure 11 it can be seen that the desorption of ammonia from the samples calcined at 900 °C reached its maximum at the temperatures 210 °C, 220 °C, 225 °C, 232 °C and 200 °C

for Si/Al ratios of pure alumina (calcined for 3h at 900 °C) 5, 10, 20, 40, respectively. A similarly asymmetric but lower peak, was detected for Si/Al 40 sample calcined 3 h at 900 °C and centered at a temperature of 260 °C. Somewhat lower quantity of NH<sub>3</sub> is desorbed from Si/Al samples calcined at 900 °C than from those calcined at 550 °C.

In table 9 the amounts of NH<sub>3</sub> that desorb from the calcined Si/Al samples are compared to the alumina content in the fresh samples. The samples calcined at the higher temperature showed desorption between 120 and 243 μmol/g and show therewith significantly lower variances compared to Si/Al calcined at 550 °C which amount of desorbed ammonia is in the range of 225 - 280 μmol/g.

The quantities of desorbed probe molecules are related to 1 g of sample. The order of the acidity of the investigated samples shows good correlation to the fraction amount of alumina: the higher alumina ratio in the sample, the higher amounts of desorbing ammonia.

Other scientists have also mentioned that the increase in Si/Al ratio corresponds to an decrease in the number of aluminium atoms with next-nearest neighbours and the strength of acid sites increases (114, 115).

**Table 9.** Comparison of total concentrations of acid sites and alumina content at different calcination temperatures

Sample	Calcination temperature at 550 °C (3h)		Calcination temperature at 900 °C (3h)	
	Acidity amount (μmol/g)	Al (wt.%)	Acidity amount (μmol/g)	Al (wt.%)
Pure alumina	-	-	260.6	100
Si/Al (5.95)	280.0	95.2	234.0	95.2
Si/Al (10.90)	257.2	89.9	223.1	89.9
Si/Al (20.80)	286.3	80.4	214.6	80.8
Si/Al (40:60)	225.4	61.3	120.1	60.8

Among the studied materials the highest amount of chemisorbed ammonia was measured for the sample which contains 5 wt.% SiO<sub>2</sub> prepared at lower treatment temperature of 550 °C. The relation of desorbed amount of ammonia from the above studied samples can be related to the content of alumina. Nevertheless, exhibit one exception in the acidity order for sample contains 20 SiO<sub>2</sub> wt.%. The reproducibility of the same sample calcined 3 h at 550 °C show the same maximum desorption peak as the first measurement and does not fit with the data

collected in table 9. This can be characterized by the presence of somewhat stronger acidic centers attributed to  $\text{Al}^{3+}$  cations placed in octahedral instead of tetrahedral sites throughout inaccuracy of the preparation method. Silica-aluminas calcined at the higher calcination temperature of 900 °C show a lower maximum desorption peak of ammonia than that ones calcined at lower calcination temperature. This can be attributed to dehydroxylation of hydroxyl groups at higher temperatures which leads to loss of active acid sites (OH).

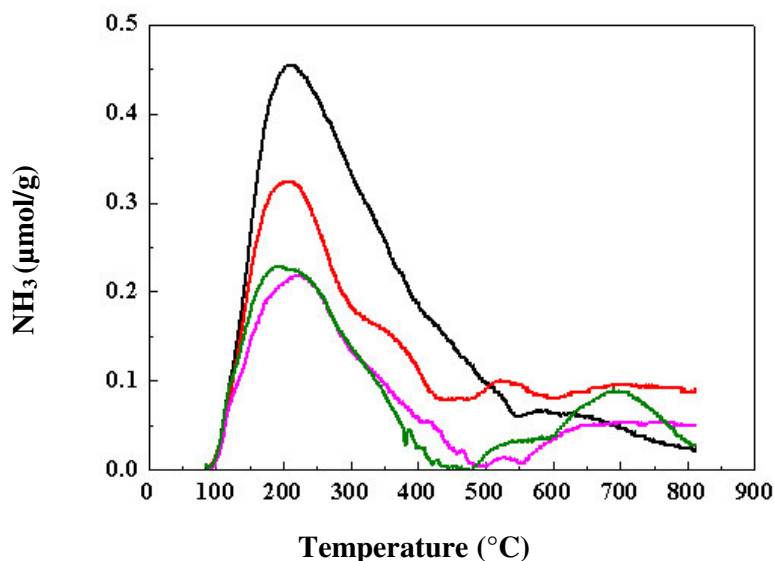
#### **4.2. Acid properties of the metal oxides supported on alumina**

Figure 12 presents ammonia TPD for three different metal oxides supported on alumina: zirconium oxide, hafnium oxide and titanium oxide. The sample was measured to calculate their capacity of desorbing ammonia (see table 10), and the results of  $\text{TiO}_2/\text{Al}_2\text{O}_3$  were higher than the ones of the other samples, which contained  $\text{ZrO}_2/\text{Al}_2\text{O}_3$  or  $\text{HfO}_2/\text{Al}_2\text{O}_3$ . The adsorption of ammonia for the three samples studied varies in reaching the maximum. The maximum of desorbing ammonia for pure alumina (pure alumina synthesized by Sasol Germany GmbH, calcined for 3h at 900 °C) is 200 °C, this point was observed for  $\text{TiO}_2/\text{Al}_2\text{O}_3$  at a temperature of 217 °C. A similar asymmetric but lower peak was found for the same sample of  $\text{TiO}_2/\text{Al}_2\text{O}_3$  at a higher temperature of 580 °C exhibiting strong acidic centres.

The maximum in the  $\text{NH}_3$ -TPD spectra for  $\text{ZrO}_2/\text{Al}_2\text{O}_3$  was obtained at 200 °C, while in the case of  $\text{HfO}_2$  sample, it is possible to distinguish two high peaks. The first one is detected at a temperature of 230 °C and the maximum of the second one is centered at 700 °C and is also high but less intensive than that observed at lower temperature. This temperature significantly shows strong acidic centers.

Figure 13 presents  $\text{NH}_3$ -TPD of hafnium oxide supported on alumina with different ratios. The experiment should prove the hypothesis that, when the higher the alumina content in the sample, the higher is the amount of desorbed ammonia. Looking at the desorption of ammonia from the samples with different  $\text{HfO}_2/\text{Al}_2\text{O}_3$  ratios, the highest point for all samples is reached at 200 °C.





**Figure 12. Profiles of temperature programmed desorption of ammonia for different metal oxides/alumina samples**

— Pure alumina —  $\text{TiO}_2$  —  $\text{HfO}_2$  —  $\text{ZrO}_2$

The sample containing 5 wt.% of hafnium oxide shows two high peaks at higher temperature whereas the second peak has its maximum around 700 °C, indicating strong acid sites. A straight correlation between the concentration of the acidic sites and the content of alumina in the catalyst can be proved by the data presented in table 10. The more is the content of alumina in the catalyst the higher is the maximum peak of ammonia and that is the same final result as obtained by ammonia desorption for solid silica-aluminas (chapter 4.1).

Because of the strong desorption of ammonia from the raw material used in the synthesis of the samples (pure alumina calcined 3h at 900 °C synthesized by Sasol GmbH) the results of  $\text{NH}_3$ -TPD for metal oxides supported on alumina are divided in two groups as shown in table 10. The first group shows the desorbed ammonia in temperature range between 100 °C and 500 °C which could be effected by alumina content. The second group presents the desorbed ammonia which could describe the acidity of the metal oxide and not of the alumina and that is in range temperatures between 500 °C and 900 °C.

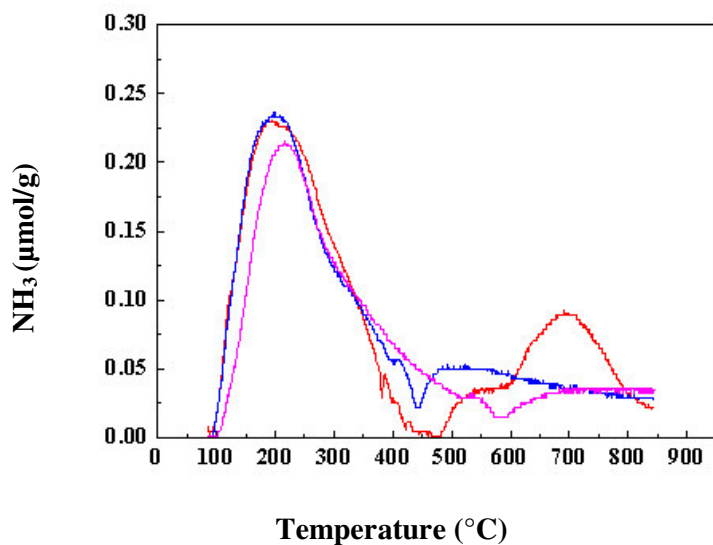


**Figure 13.** Profiles of temperature programmed desorption of ammonia for hafnium oxides supported on alumina with different ratios (wt. %)

— HfO<sub>2</sub>/Al<sub>2</sub>O<sub>3</sub> (5:95) wt.%, — HfO<sub>2</sub>/Al<sub>2</sub>O<sub>3</sub> (10:90) wt.%  
 — HfO<sub>2</sub>/Al<sub>2</sub>O<sub>3</sub> (15:85) wt.%

**Table 10.** Comparison of total concentrations of acidic sites and specific surface area for different pure rare earth metal oxides and oxides supported on alumina

*Fresh sample	*BET m <sup>2</sup> /g	*Fresh sample	Acidity amount in temp.range 100 °C – 500 °C (μmol/g)	Acidity amount in temp.range 500 °C – 900 °C (μmol/g)	Al <sub>2</sub> O <sub>3</sub> content wt.%	*BET m <sup>2</sup> /g
Pure Al <sub>2</sub> O <sub>3</sub>	197	-	260.6		100	-
TiO <sub>2</sub>	5.95	TiO <sub>2</sub> /Al <sub>2</sub> O <sub>3</sub>	239.0	74.2	95.0	129.6
ZrO <sub>2</sub>	8.25	ZrO <sub>2</sub> /Al <sub>2</sub> O <sub>3</sub>	168.6	62.1	95.0	108.3
HfO <sub>2</sub>	9.47	HfO <sub>2</sub> /Al <sub>2</sub> O <sub>3</sub>	175.2	52.6	95	100.1
-	-	HfO <sub>2</sub> /Al <sub>2</sub> O <sub>3</sub>	146.2	31.7	90	124.0
	-	HfO <sub>2</sub> /Al <sub>2</sub> O <sub>3</sub>	122.7	24.2	85	122.1

\* Surface area measured before the reaction

### 4.3. Acid-base properties of the hydrotalcite derived from mixed Mg-Al oxides

#### 4.3.1 Temperature programmed desorption of $\text{NH}_3$ and $\text{CO}_2$

The  $\text{NH}_3$ -TPD profiles of the calcined hydrotalcites are shown in figure 14. The desorption of ammonia from the cHT-TA sample begins at  $130^\circ\text{C}$  and after reaching maximum at  $200^\circ\text{C}$  slowly decreases. Similar asymmetric peak but significantly with lower intensity was detected for the cHT- $\text{SO}_4$  sample.  $\text{NH}_3$ -TPD spectra obtained for the cHT- $\text{HPO}_4$ , cHT-Cl and cHT- $\text{CO}_3$  samples are characterised by broad, asymmetric desorption patterns, spanned in the temperature range of  $140 - 630^\circ\text{C}$  with the maxima at about  $250 - 270^\circ\text{C}$ . The most intensive peak was detected for the cHT- $\text{CO}_3$  sample, significantly lower amount of ammonia desorbed from the calcined HT-Cl hydrotalcite, while the lowest maximum peak was observed for the cHT- $\text{HPO}_4$  one.

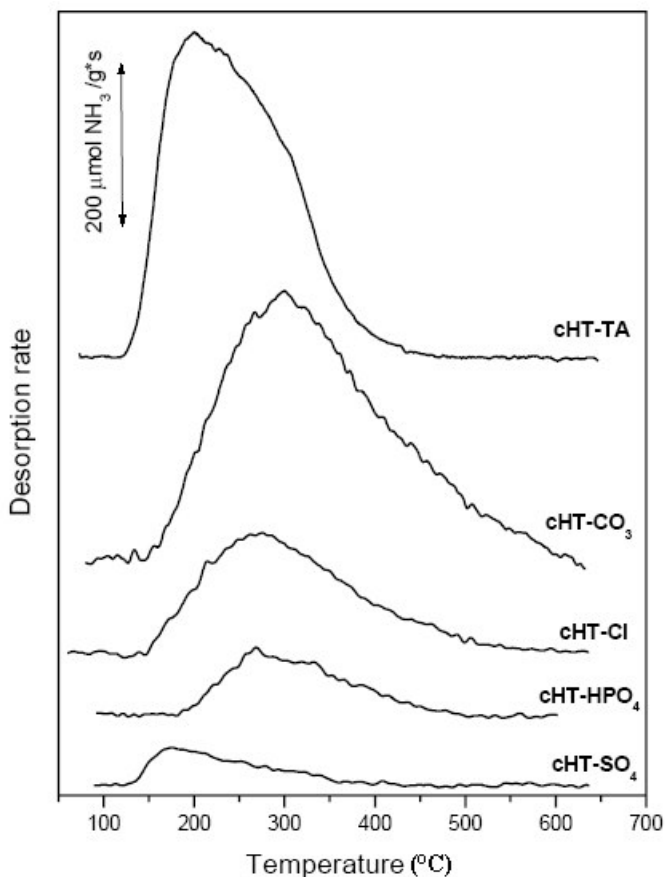


**Figure 14. Profiles of temperature programmed desorption of ammonia for the hydrotalcite derived samples (109)**

The CO<sub>2</sub>-TPD (figure 15) profiles of calcined hydrotalcites are comparatively shown in figure 14. The desorption of carbon dioxide from the cHT-TA sample reaches a maximum at 170 °C and decreases slowly. The CO<sub>2</sub>-TPD spectrum of the cHT-SO<sub>4</sub> calcined hydrotalcite consists of a sharp symmetric peak centred at 120 °C. The desorption from the HT-HPO<sub>4</sub> a maximum at 135 °C and the CO<sub>2</sub>-TPD pattern of HT-Cl calcined hydrotalcite is spanned in the temperature range of 140 – 480 °C and consists of two resolved maxima. The first peak is centred at 200 °C, while the maximum of the second one is at 380 °C.

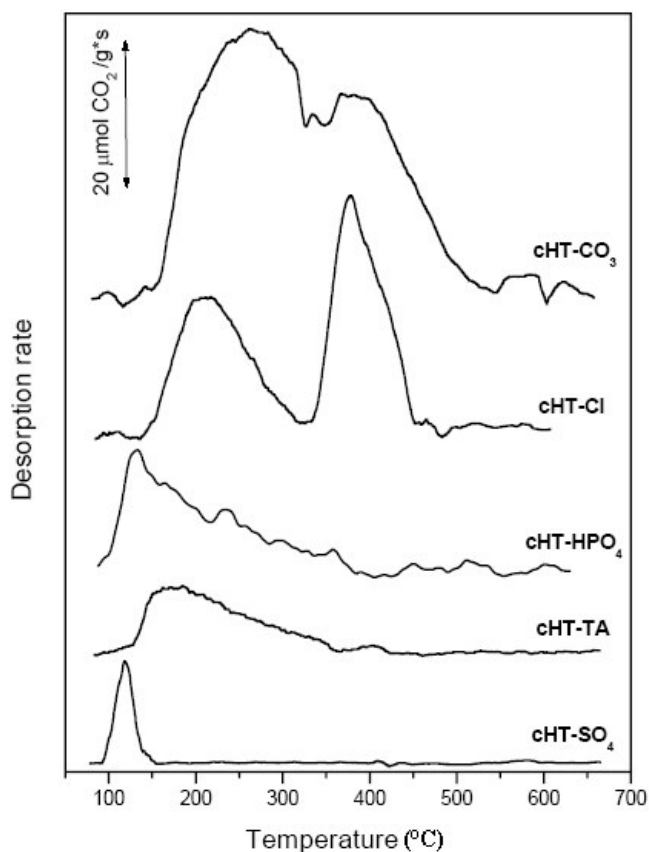


**Figure 15. Profiles of temperature programmed desorption of carbon dioxide for the hydrotalcite-derived samples (109)**

The highest amount of carbon dioxide was desorbed from the HT-CO<sub>3</sub> calcined hydrotalcite. The CO<sub>2</sub>-spectra recorded for this sample consists of at least two very broad and unresolved maxima. The first one is centred at 250 °C, and the second peak at 410 °C.

In table 11 the amounts of NH<sub>3</sub> and CO<sub>2</sub> desorbed from the calcined hydrotalcites are compared. The quantity of chemisorbed probe molecules are related to 1 g or 1 m<sup>2</sup> of a sample.

**Table 11.** Total concentrations of acidic and basic sites in the calcined samples

Sample	Desorbed NH <sub>3</sub>		Desorbed CO <sub>2</sub>	
	μmol/g	μmol/m <sup>2</sup>	μmol/g	μmol/m <sup>2</sup>
cHT-CO <sub>3</sub>	458.4	1.74	46.7	0.18
cHT-Cl	189.0	1.13	23.1	0.14
cHT-HPO <sub>4</sub>	78.6	0.60	6.5	0.05
cHT-SO <sub>4</sub>	41.9	1.90	1.8	0.08
cHT-TA	405.3	1.42	5.3	0.02

Among the studied materials the highest chemisorption of ammonia was measured for the calcined HT-CO<sub>3</sub> hydrotalcite, somewhat lower quantity of NH<sub>3</sub> desorbed from the cHT-TA sample, while the other mixed oxides were characterized by significantly lower amounts of desorbing ammonia. There are significantly lower differences in the concentrations of chemisorbed NH<sub>3</sub> related to the surface area of the samples which is in a range of 0.60 – 1.90 μmol NH<sub>3</sub>/m<sup>2</sup>. The calcined hydrotalcites chemisorbed considerably lower amounts of carbon dioxide than of ammonia. The highest quantity of CO<sub>2</sub> desorbed from the cHT-CO<sub>3</sub> sample. Over half as much chemisorbed carbon dioxide was measured for the calcined HT-Cl hydrotalcite, while the amounts of desorbing CO<sub>2</sub> for the other samples were significantly lower. Surface concentrations of chemisorbed carbon dioxide related to the surface area of the calcined hydrotalcites were also considerably higher for the cHT-CO<sub>3</sub> and cHT-Cl samples than for the other ones.

Applied method allows to determine relative strength and quantity of surface acidic and basic centres. The studied samples could be divided into two groups with regards to strength of acid sites. The results of NH<sub>3</sub>- and CO<sub>2</sub>-TPD experiments show that the kind of interlayer anions in the parent hydrotalcites strongly influences surface acidity and basicity of the obtained mixed metal oxides. The first group consists of the cHT-TA and cHT-SO<sub>4</sub> samples, which possess weaker acid surface centres, while the second one (cHT-CO<sub>3</sub>, cHT-Cl and cHT-HPO<sub>4</sub>) is characterized by stronger acid sites. However, for cHT-TA the asymmetry of desorption peak shows that this sample also has relatively strong acid surface sites. According to Shen *et al.* (116) mixed Mg-Al oxides contain Brønsted and Lewis acid sites. Brønsted sites, which are weaker than Lewis ones, are attributed to surface protons, whereas Lewis acid sites are assigned to Al-O-Mg species located within a MgO structure and containing Al<sup>3+</sup> cations predominantly in octahedral sites. It can explain the differences in surface density of acid centers in the studied samples. Nevertheless, diffusion effects due to very narrow pore size

distribution especially for the cHT-SO<sub>4</sub> sample cannot be excluded. The results of CO<sub>2</sub>-TPD seem to confirm rather the fact of inaccessibility of probe molecules to the inner part of the cHT-SO<sub>4</sub> particles.

The surface concentration of basic centres determined by the CO<sub>2</sub>-TPD measurements is significantly lower than the amount of acid sites. However, there is a great variety of different strength basic centres on the surface of the calcined hydrotalcites. Previously, on the basis of combined IR and TPD data Di Cosimo *et al.* (106) assigned CO<sub>2</sub> desorption peaks to species adsorbed on OH groups (low-temperature peak), Mg-O or Al-O pairs (intermediate-temperature peak), and O<sup>2-</sup> anions (high-temperature peak). Thus, the cHT-SO<sub>4</sub>, cHT-HPO<sub>4</sub> and cHT-TA samples possess weak OH basic centres in the majority. The asymmetry of desorption spectra of the calcined HT-HPO<sub>4</sub> hydrotalcite can be attributed to diffusion limitation and/or readsorption of CO<sub>2</sub> molecules. The cHT-TA sample is characterized by the presence of somewhat stronger basic centres attributed to M-O pairs. The highest amount and variety of basic sites are present on the surface of the calcined HT-CO<sub>3</sub> and HT-Cl hydrotalcites. In case of these samples it is possible to distinguish at least two types of basic sites assigned to Mg-O and Al-O pairs as well as O<sup>2-</sup> anions, which significantly differ in strength.

#### 4.3.2. X-ray diffraction (XRD)

The XRD patterns of all the as-synthesized samples are, as shown in figure 16, typical for layered double hydroxides structure (101) with sharp and symmetric basal reflections at low values of 2θ angles.

The XRD peaks observed at higher values of 2θ angles are broad and asymmetric, suggesting that the hydrotalcite phase is highly disordered. It is especially distinct for the HT-SO<sub>4</sub> and HT-HPO<sub>4</sub> samples.

The crystallographic parameters of the obtained hydrotalcites can be calculated for the hexagonal cell using the  $\bar{R}3m$  space group in rhombohedral symmetry. Unfortunately, the (110)-reflection, usually used for the calculation of the lattice parameter *a*, overlaps with the diffraction peak, and the precise estimation of the value of the parameter *a* was impossible (117). However, from the positions of the strongest (003)- and (006)-lines the basal spacings of the hydrotalcites were calculated and used to a determination of the lattice parameter *c*, which corresponds to 3 times the distance between adjacent hydroxide layers. As can be calculated from the data in figure 16, the values of the *c* parameter vary between 22.89 Å (for

HT-CO<sub>3</sub>) and 43.62 Å (HT-TA). Subtracting 4.8 Å for the thickness of the brucite-like layer gives the gallery heights of 2.83 Å (for HT-CO<sub>3</sub>), 3.04 Å (for HT-Cl), 4.06 Å (for HT-SO<sub>4</sub>), 5.84 Å (for HT-HPO<sub>4</sub>), and 9.74 Å (for HT-TA), which are in principle consistent with the size of the anions intercalated into the interlayer space (118). Nevertheless, it should be noticed that the gallery heights are lower than the corresponding free anions diameters due to a high content of Al<sup>3+</sup> in the studied hydrotalcites causing the strong interaction of the interlayer anions with the brucite-like sheets.

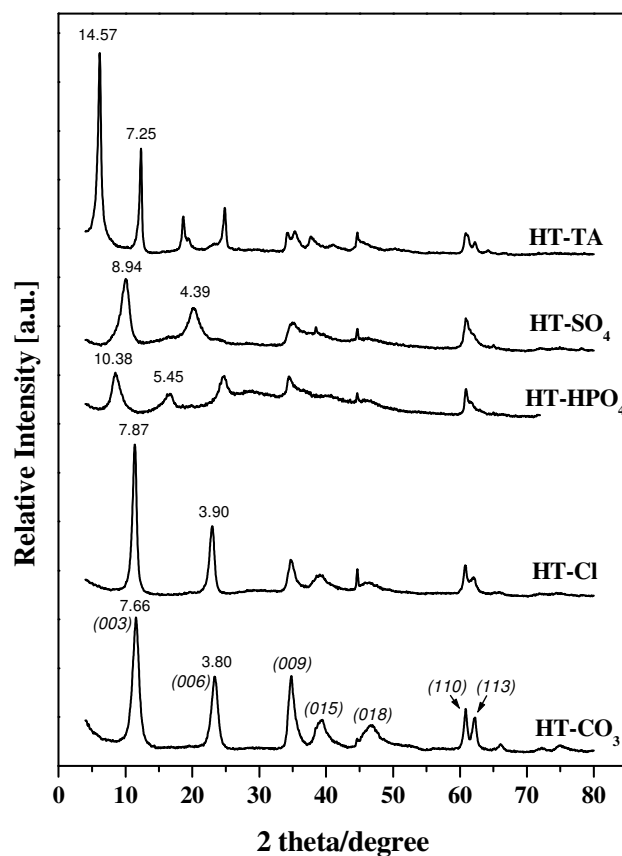


**Figure 16. Powder X-ray diffraction patterns of the as-synthesized samples (109)**

C numbers (Å): Lattice parameter which corresponds to 3 times the distance between adjacent hydroxide layers.

The analogous effect of the binding strength can be observed when we compare the gallery heights of HT-CO<sub>3</sub> and HT-Cl. The interaction of the divalent anions with the brucite-like layers is evidently stronger than that of the monovalent anions, and the lower peaks height is consequently found for HT-CO<sub>3</sub>.

The value of the basal spacing of the pillared TA-hydrotalcite (see figure 16) is in a good agreement with that calculated from a model assuming that the aromatic ring is perpendicular to the brucite-like sheets (113). It is assumed that the relatively sharp intense reflection at 7.25 Å can originate from the overlapping of two or even three different peaks (119). Obviously, it can represent reflections from interlayers containing carbonates anions (for HT-CO<sub>3</sub> the (003) peak was observed at 7.66 Å) and/or terephthalate anions oriented parallel to the Mg-Al hydroxide layers.

#### 4.3.3. Infrared spectroscopy (FTIR)

Three general types of IR-active vibrations of hydrotalcites can be distinguished: molecular vibrations of the hydroxyl groups, lattice vibrations of the octahedral layers and vibrations of the interlayer species (120). The FT-IR spectra of all the as-synthesized hydrotalcites, as presented in figure 17, show a very intense broad band at approximately 3450 cm<sup>-1</sup> corresponding to the  $\nu_{\text{OH}}$  stretching vibrations of the hydroxyl groups in the brucite-like sheets. As the samples were not dehydrated, this broad band can also demonstrate quantities of water. In the region of the spectra below 800 cm<sup>-1</sup> the lattice absorption bands are observed which can be assigned to the stretching modes of the oxygen in the brucite-like layers.

The bands around 550 and 750 cm<sup>-1</sup> correspond to the hydroxyl groups influenced mainly by Al<sup>3+</sup> cations, whereas the band around 640 cm<sup>-1</sup> is interpreted as representing the Mg-OH stretch mode. Two bands observed around 930 and 1020 cm<sup>-1</sup> can be assigned to the deformation modes of the hydroxyl groups. The absorption peak at about 1625 cm<sup>-1</sup> can be attributed to  $\delta_{\text{OH}}$  bending vibration of H<sub>2</sub>O molecules in the interlayer space (117 - 122).

The kind of anions introduced into the interlayer space of hydrotalcites can be identified by absorption bands observed below 1500 cm<sup>-1</sup>. The presence of carbonates is manifested by a band at about 1360 cm<sup>-1</sup> with a shoulder at around 1400 cm<sup>-1</sup> attributed to the  $\nu_3$  vibrations of CO<sub>3</sub><sup>2-</sup>. The appearance of the shoulder is a result of a lowering of the D<sub>3h</sub> symmetry of the interlayer carbonate anions. In the FTIR spectrum of the HT-CO<sub>3</sub> sample the  $\nu_4$  and  $\nu_2$  modes of carbonates are also observed at about 670 and 870 cm<sup>-1</sup> respectively. Moreover, a band observed at around 3000 cm<sup>-1</sup> can be interpreted as the CO<sub>3</sub><sup>2-</sup>-H<sub>2</sub>O bridging mode of carbonate and water in the interlayer (117, 121).



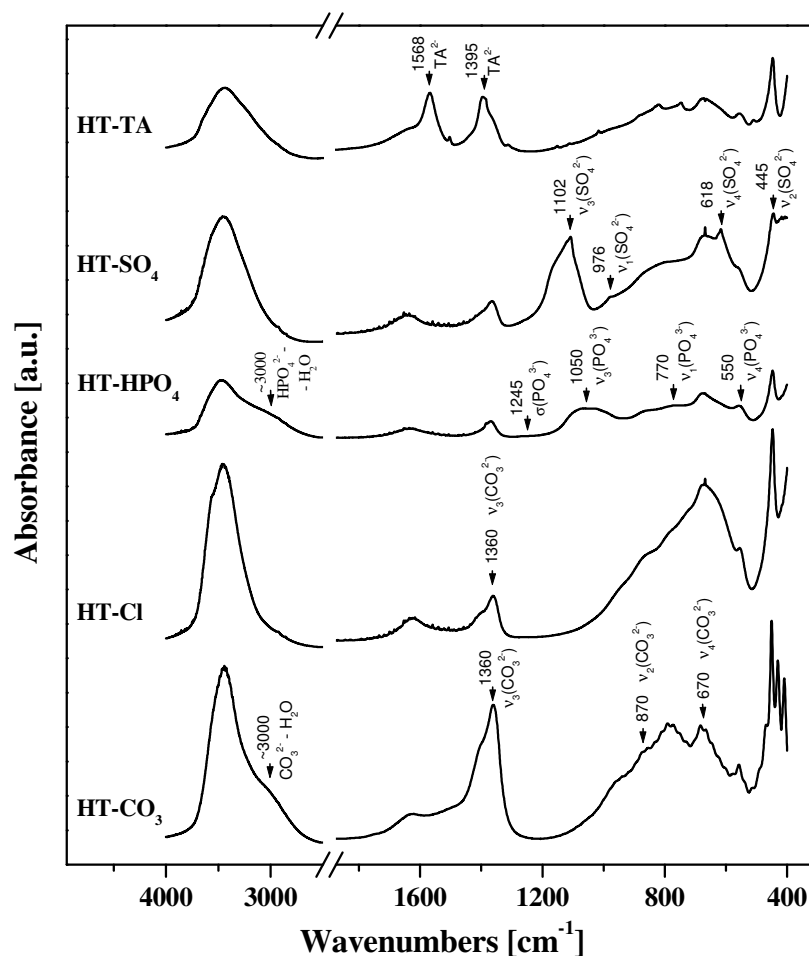


**Figure 17.** FTIR spectra of the as-synthesized samples

The FTIR spectrum of HT-SO<sub>4</sub> sample shows bands at 620 cm<sup>-1</sup> and 1102 cm<sup>-1</sup> associated with the  $\nu_4$  and  $\nu_3$  sulphate modes, respectively. Shoulders of the  $\nu_3$  vibration observed at higher frequencies (at about 1150 – 1180 cm<sup>-1</sup>) suggest the perturbation of the SO<sub>4</sub><sup>2-</sup> anions symmetry. The lowering of the symmetry results in the appearance of bands at approximately 976 cm<sup>-1</sup> and 445 cm<sup>-1</sup> that are related to the  $\nu_1$  and  $\nu_2$  modes, which are normally inactive under the T<sub>d</sub> symmetry (94, 123).

The evidences for the presence of phosphate anions in the HT-HPO<sub>4</sub> sample are found as the characteristic vibrations of  $\nu_1$ (P-O) at 770 cm<sup>-1</sup>,  $\nu_3$ (P-O) at 1050 cm<sup>-1</sup> and  $\nu_4$ (P-O) at 550 cm<sup>-1</sup>. The weak band attributed to the  $\delta$ (P-O) vibrations appears at approximately 1245 cm<sup>-1</sup> (117). The broad band observed at about 3000 cm<sup>-1</sup> in the FTIR spectrum of the HT-HPO<sub>4</sub> sample can be attributed to hydrogen bonds between the phosphate anions and the water molecules in the interlayer space.

For the HT-TA sample the characteristic doublet formed by two strong bands at 1395 and 1568  $\text{cm}^{-1}$  is due to the terephthalate dianion (122). The  $\nu_{\text{OH}}$  band centered at 3431  $\text{cm}^{-1}$  is broader than that in other hydrotalcites, probably due to many different hydrogen-bonded hydroxyl groups, with participation of the carboxylic groups of the terephthalate anion. The absence of an absorption close to 1700  $\text{cm}^{-1}$ , characteristic of the presence of free acid, confirms that only the anion form was built into the interlayer of the hydrotalcite.

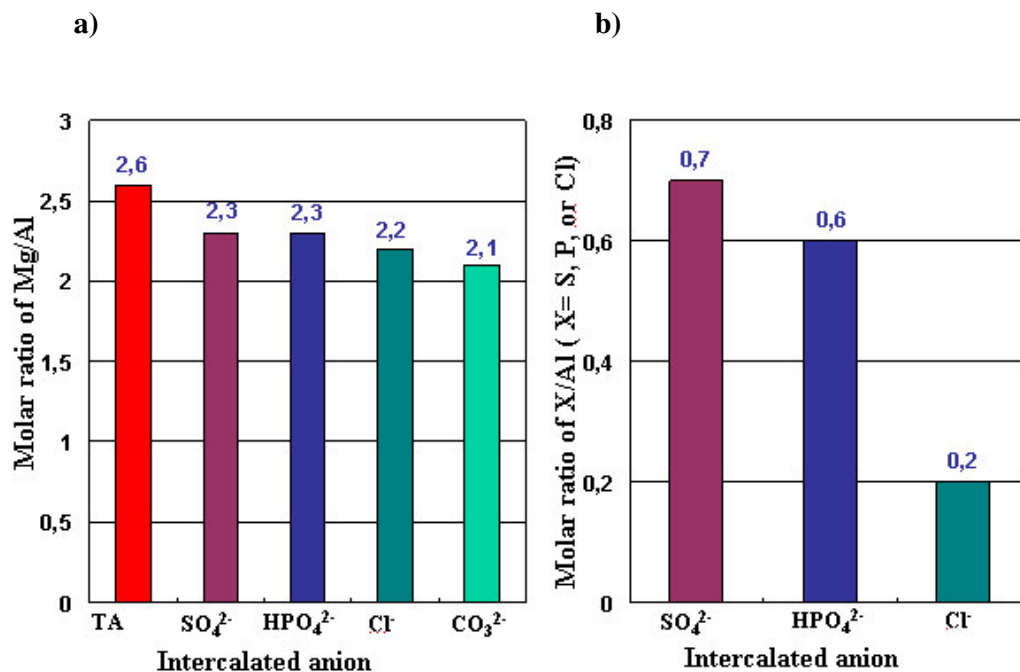
Thus, it should be pointed that the used coprecipitation and ion-exchange methods allowed to prepare Mg-Al hydrotalcites containing the intended counterbalancing anions -  $\text{CO}_3^{2-}$ ,  $\text{SO}_4^{2-}$ ,  $\text{Cl}^-$ ,  $\text{HPO}_4^{2-}$  or terephthalates. Nevertheless, in spite of precautions, the interlayer gallery and external surface of all the synthesized LDHs were contaminated by  $\text{CO}_2$  adsorbed from the atmosphere.

#### 4.3.4. Structural and chemical composition of the mixed Mg-Al oxides

The content of metals as well as P, S, and Cl in the samples calcined at 600 °C was determined by X-ray fluorescence. The obtained results as molar ratios of Mg/Al, S/Al, P/Al, and Cl/Al, are presented in scheme 10. The measured molar ratio of Mg/Al in the samples is essentially in accordance with intended one. Slight excess in Mg content in relation to Al can be caused by the high level of pH (10.0) used during the synthesis of hydrotalcites. Probably, in such basic conditions a part of aluminum was dissolved. However, even in the cHT-TA sample with the lowest content of Al, shortage of aluminum does not exceed 30 %.

Assuming the relation of  $[\text{A}^{x-}] = \frac{1}{x} \cdot [\text{Al}^{3+}]$  and total compensation of positive charge of the brucite-like sheets by the supposed  $\text{A}^{x-}$ , the molar ratios of S/Al (for HT- $\text{SO}_4$ ), P/Al (for HT- $\text{HPO}_4$ ) and Cl/Al (for HT-Cl) should be equal to 0.5, 0.5 and 1.0, respectively. On the other hand, thermal treatment of hydrotalcites leads to dehydration, followed by dehydroxylation and decomposition of anions localized in the interlayer gallery (124). The XRF results show that phosphorus and sulfur remain in the hydrotalcites upon heating as opposed to chlorine leaving the material.

**Scheme10. (10 a) Molar ratio of Mg/Al in the samples, (10 b) molar ratios of S/Al, P/Al, and Cl/Al**



#### 4.3.5 X-ray diffraction (XRD) after calcination at 600 °C

During calcination the decomposition of hydrotalcites occurs resulting in formation of mixed oxides phases. This fact is confirmed by the XRD patterns of the samples calcined at 600 °C, which are shown in figure 18.

For all the samples the reflections observed at around 43 and 63° 2 $\theta$  correspond to a MgO-like phase (periclase) or rather magnesia-alumina solid solution (94, 125, 126). It is especially noteworthy that the intensities of these peaks are higher for cHT-Cl indicating the presence of well-crystallized MgO in this sample. For cHT- $\text{SO}_4$  and cHT- $\text{HPO}_4$  the broaden peak, which appeared in a 2 $\theta$ -range of 20 – 35°, can suggest that traces of S and P-containing amorphous phases are present in these samples.

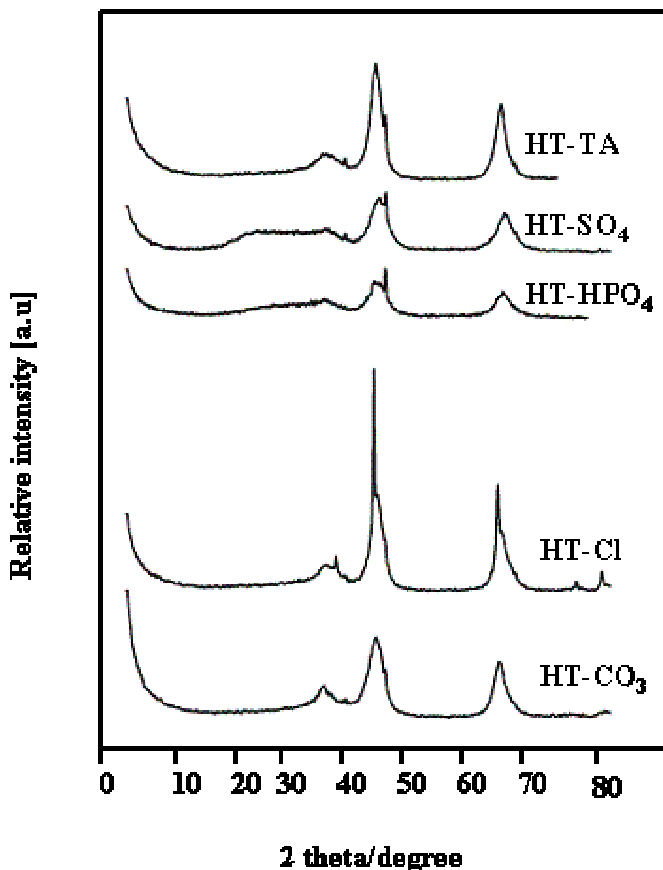


**Figure 18. Powder X-ray diffraction patterns of the samples calcined at 600 °C for 16 h in air**

#### 4.3.6. BET measurements

The mixed Mg-Al oxides showed a low-temperature N<sub>2</sub> adsorption isotherm (figure 19) of type IV in the classification of IUPAC, which is characteristic for a mesoporous solid. Moreover, the hystereses in desorption branches can be found in the BET isotherms.

The type H1, according to the IUPAC classification, is observed for the cHT-CO<sub>3</sub>, cHT-Cl, cHT-HPO<sub>4</sub> and cHT-TA samples, which is characteristic for solids consisting of cylindrical pores of uniform size and shape as dominant, whereas the type H3 of the hysteresis has been recognized for the cHT-SO<sub>4</sub> sample.

Evidently, a large majority of pores present in HT-SO<sub>4</sub> can be classified as nonuniform size, slit-shaped channels. It should be supposed that gaseous products evolved upon the thermal decomposition of the interlayer anions developed a porous system of the calcined samples.

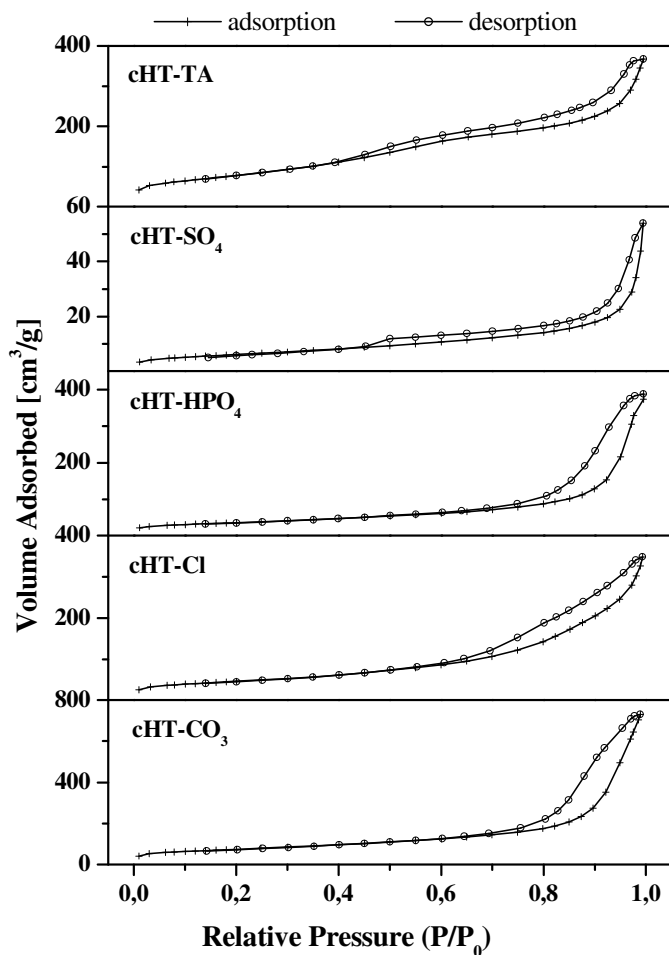


**Figure 19.** Low temperature  $N_2$  sorption isotherms for the calcined samples

As suggested by Reichle *et al.* (125),  $CO_2$  formed during the evolution of  $CO_3^{2-}$ , escapes from the material through holes in the crystal surface, which then appear as small, fairly regularly spaced craters. Such mechanism of decomposition, known as a cratering, explains the presence of cylindrical channels in the calcined samples, which prior to the thermal treatment consisted of considerable amounts of  $CO_3^{2-}$  introduced as the compensating anions into the HT- $CO_3$  hydrotalcite or impurities to the other synthesized LDHs. It should not be surprising that also other gases evolved on heating the hydrotalcites containing particularly  $Cl^-$  or terephthalate anions can leave the material passing by the brucite-like layers and forming the cylindrical pores. The pore-size distribution curves obtaining from the adsorption pore volume are shown in figure 20.

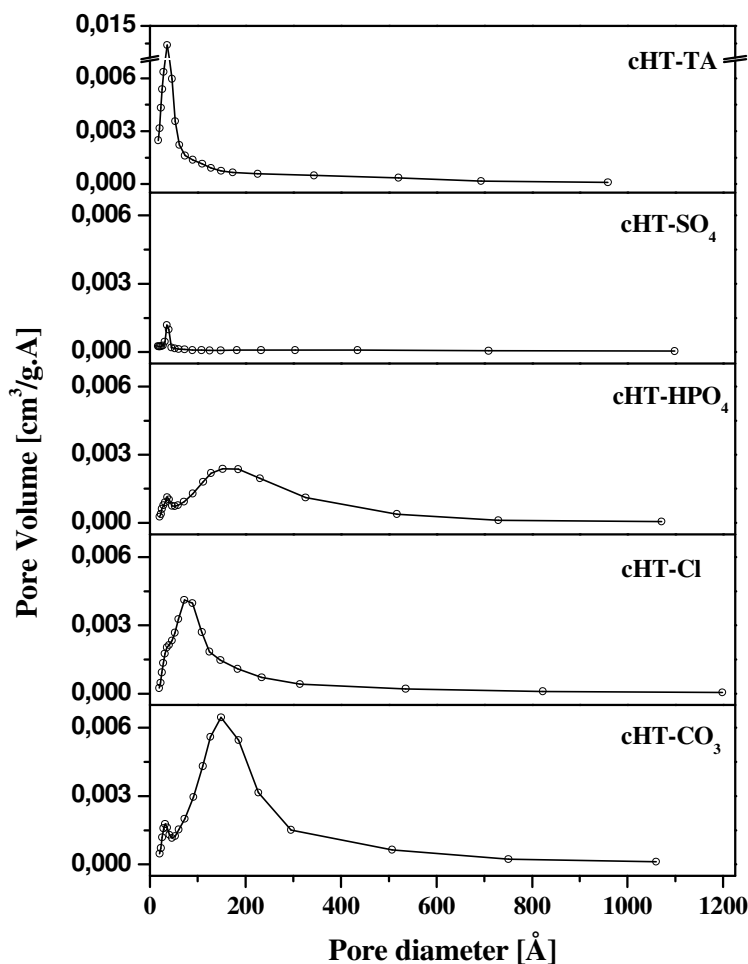


**Figure 20. Pore size distribution profiles of the calcined samples**

It is evident that all the mixed Mg-Al oxides possess pores in the range of 20 - 40 Å, which were most likely formed owing to the escape of evolved gaseous products during the decomposition of the interlayer anions. Taking into account that the cratering mechanism of hydroxalcite decomposition results in an appearance of small pores in a calcined material (125), it should be noticed that the highest effect of porous system development is found for the cHT-TA sample. The pore-size distribution profiles of the HT-Cl, HT-CO<sub>3</sub> and HT-HPO<sub>4</sub> samples show additionally a wide maximum centered at around 90 Å, 150 Å and 190 Å, respectively.

The BET surface area of the calcined hydroxalcites varies in the range from 22 m<sup>2</sup>/g to 285 m<sup>2</sup>/g, (see table 12). Among the studied samples the calcined HT-SO<sub>4</sub> hydroxalcite is characterized by the lowest surface area (22 m<sup>2</sup>/g) and total pore volume (0.04 cm<sup>3</sup>/g). It is most likely that sulfur remaining in the sample on the calcination blocks up the channels and

causes a decrease in porosity. Constantino and Pinnavaia (94) found that sulfate groups show a tendency towards grafting with brucite-like layers resulting in inaccessibility of the internal surface of material. On contrary to cHT-SO<sub>4</sub> the total pore volume of the other samples is relatively high ranging from 0.43 cm<sup>3</sup>/g (for cHT-Cl) to 0.94 cm<sup>3</sup>/g (for cHT-CO<sub>3</sub>). The high porosity of cHT-CO<sub>3</sub> larger twice than cHT-Cl, cHT-HPO<sub>4</sub> or HT-TA should be explained by the presence of considerable amount of pores having a width in a range of 50 – 300 Å, see figure 20.

**Table 12** Surface area, chemical composition and textural properties of the mixed Mg-Al oxides

Sample	Molar ratio				BET surface area (m <sup>2</sup> /g)	Total pore volume (cm <sup>3</sup> /g)
	Mg/Al	S/Al	P/Al	Cl/Al		
cHT-CO <sub>3</sub>	2.1	-	-	-	264.0	0.94
cHT-Cl	2.2	-	-	0.2	167.0	0.43
cHT-HPO <sub>4</sub>	2.3	-	0.6	-	130.0	0.47
cHT-SO <sub>4</sub>	2.3	0.7	-	-	22.0	0.04
cHT-TA	2.6	-	-	-	285.0	0.45

#### 4.4. MBOH conversion on silica-aluminas with different Si/Al ratios

##### 4.4.1 Catalytic activity of methyl butynol over different Si/Al ratios at different reaction temperatures 120 °C, 180 °C.

The conversion of methyl butynol (MBOH) was utilized as test reaction for different catalysts which were already described in chapter 3.1. Taking into account the temperature dependence of the catalytic activity, the MBOH conversion was studied at different reaction temperatures, i.e. 120 °C and 180 °C.

Performing the conversion of MBOH on silica-aluminas mainly MBYNE and Prenal are detected as products and both are products of the acid pathway of the conversion of methyl butynol. This indicates that silica-aluminas are acid catalysts what has also been shown by NH<sub>3</sub>-TPD, see chapter 4.1. Before the selectivities of the products should be discussed in detail, the conversions on different catalysts and at different temperatures are presented.

Figures 21 and 22 show the activity of catalysts with different Si/Al ratios calcined for 3h at 550 °C towards decomposition of methyl butynol at a reaction temperatures of 120 °C and 180 °C, respectively.

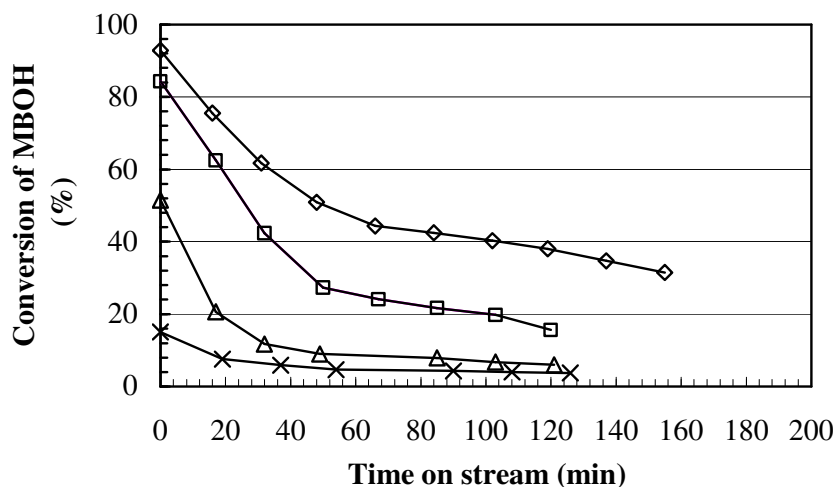


**Figure 21. Conversion of MBOH over different Si/Al ratios calcined 3 h at 550 °C, reaction temperature 120 °C**

× Si/Al 5    △ Si/Al 10    □ Si/Al 20    ◇ Si/Al 40

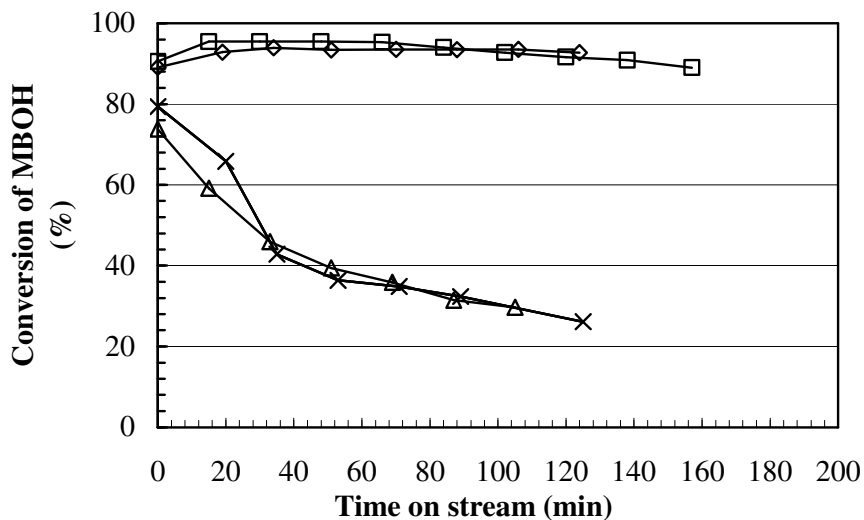


**Figure 22. Conversion of MBOH over different Si/Al ratios calcined 3 h at 550 °C, reaction temperature 180 °C**

× Si/Al 5    △ Si/Al 10    □ Si/Al 20    ◇ Si/Al 40

The figures show that at a reaction temperature of 120 °C the differences in the activities are limpid and methyl butynol conversion increases proportionally upon the loading amount of silica to the alumina. So catalysts which contain less SiO<sub>2</sub> show lower catalytic activity,



because they contain a lower amount of acid sites which is due to the fact that acid sites exist there where  $\text{AlO}_4^-$  and  $\text{SiO}_4$  are next to each other. The activities markedly increase at the reaction temperature of 180 °C. At the lower reaction temperature of 120 °C the activities decline with reaction time for all tested catalysts. At 180 °C the activities only decrease for Si/Al 5 and Si/Al 10. These observations lead to the conclusion that deactivation of the catalysts is linked to the strength of the acid sites and is caused by strong adsorption of the products on the acid sites. At lower temperature all acid sites adsorb products irreversibly, but at the higher reaction temperature only Si/Al 5 and Si/Al 10, which have fewer but therefore stronger acid sites than Si/Al 20 and 40, show deactivation.

Figures 23 and 24 present the MBOH conversion as a function of time for catalyst samples calcined for 3 h at a temperature of 900 °C. They show a higher conversion of methylbutynol than those calcined at 550 °C. This can better be seen over SA 5 and 10 at the higher temperature reaction of 180 °C after 20 minutes from starting the reaction. The decrease in the activities for all samples with reaction time appears to be more clear at lower reaction temperature.

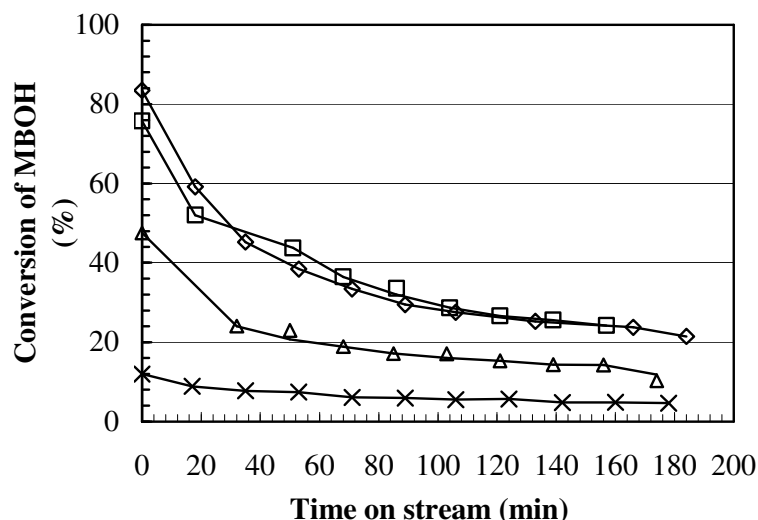


**Figure 23. Conversion of MBOH over different Si/Al ratios calcined 3 h at 900 °C, reaction temperature 120 °C**

× Si/Al 5    △ Si/Al 10    □ Si/Al 20    ◇ Si/Al 40

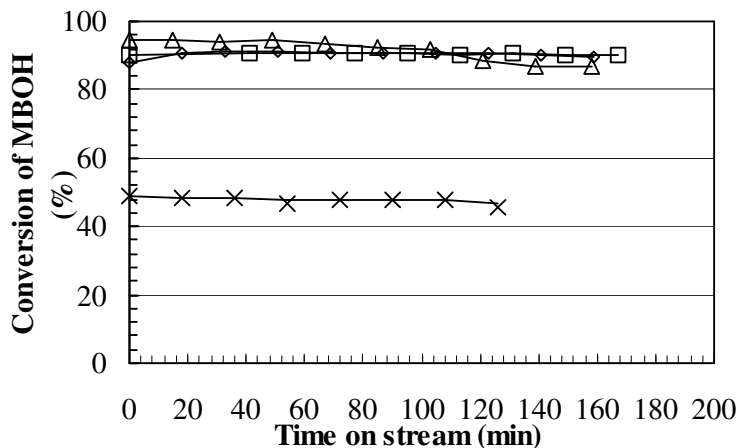


**Figure 24. Conversion of MBOH over different Si/Al ratios, calcined 3 h at 900 °C, reaction temperature 180 °C**

× Si/Al 5    △ Si/Al 10    □ Si/Al 20    ◇ Si/Al 40

Doping alumina with silica does not only influence the conversion but also the physical properties of the catalysts like specific surface area. The specific surface area increases continuously the more silica is added to the alumina and the higher is the treatment temperature (see table 13). A straight correlation between the conversion of MBOH after 120 min time on stream and the surface area after the reaction can be seen for all investigated Si/Al ratios and for both reaction temperatures (i.e. 120 °C and 180 °C).

T <sub>reaction</sub>	Si/Al wt. %	Calcined samples at 550 °C			Calcined samples at 900 °C			
		X <sub>after 120 min</sub> %	BET <sub>used</sub> m <sup>2</sup> /g	X/BET	Si/Al wt. %	X <sub>after 120 min</sub> %	BET <sub>used</sub> m <sup>2</sup> /g	X/BET
120 °C	5	3.7	115.8	0.032	5	5.7	161.2	0.035
	10	5.9	134.8	0.044	10	15.3	189.4	0.081
	20	15.6	183.2	0.085	20	26.6	210.2	0.126
	40	38.0	199.6	0.191	40	27.5	212.6	0.129
180 °C	5	26.0	201.0	0.130	5	45.0	221.4	0.203
	10	29.6	215.1	0.134	10	88.5	241.1	0.367
	20	91.5	292.2	0.313	20	90.5	248.2	0.364
	40	93.5	259.1	0.360	40	90.4	247.4	0.365

The increase in conversion with growing Si/Al ratio is not only caused by the higher surface area. The ratio X/BET shows that the conversion per square meter increases, because the amount of active sites, means acid sites, increases per area unit. At higher reaction temperature the converted amount of MBOH is higher per square meter what could be simply explained by the higher reaction rate.

Interestingly, the BET surface area is smaller for the catalysts which were used in the reaction at 120 °C than for the catalysts used at 180 °C. This is caused by the adsorption of products on the acid sites. This process takes place especially at the lower reaction temperature as shown on the previous pages.

Additionally the surface area after the reaction of the samples calcined at 550 °C is smaller than the one of the samples pre-treated at 900 °C. Again this can be explained with a higher adsorption of products during the reaction. For example, comparison of figures 22 and 24 shows that deactivation takes places on the catalysts calcined at 550 °C but not on those which were pre-treated at the higher temperature of 900 °C.

#### 4.4.2 Influence of reaction temperature and pretreatment conditions of the sample on the reaction behavior

Figures 25 (a) and 25 (b) depict the selectivities over Si/Al 5 catalyst calcined 3 h at 550 °C for reaction temperatures of 120 °C and 180 °C, respectively.

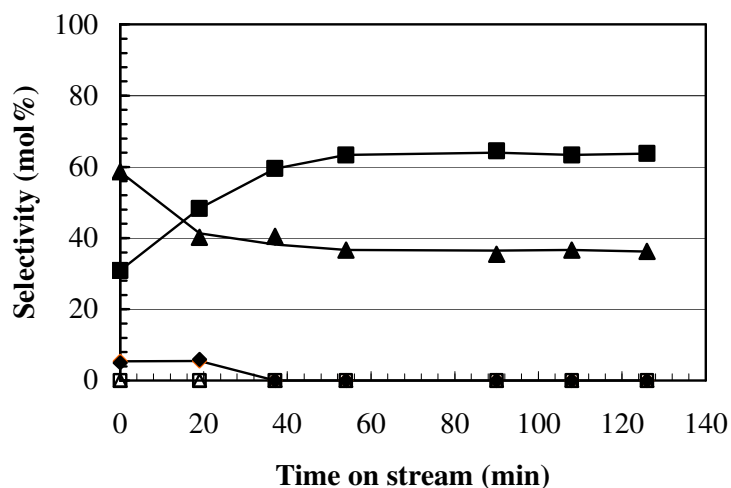
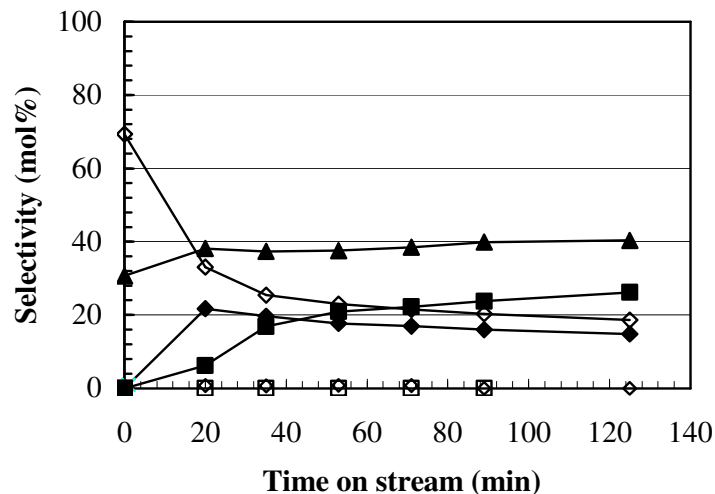


Figure 25 a. Selectivity of the products over Si/Al 5, calcined 3 h at 550 °C, reaction temperature 120 °C

◇ Acetylene   ◆ Acetone   ▲ MBYNE   △ Prenal   ■ MIPK   □ HMB



**Figure 25 b. Selectivity of the products over Si/Al 5 calcined 3 h at 550 °C, reaction temperature 180 °C**

◇ Acetylene    ♦ Acetone    ▲ MBYNE    △ Prenal    ■ MIPK    □ HMB

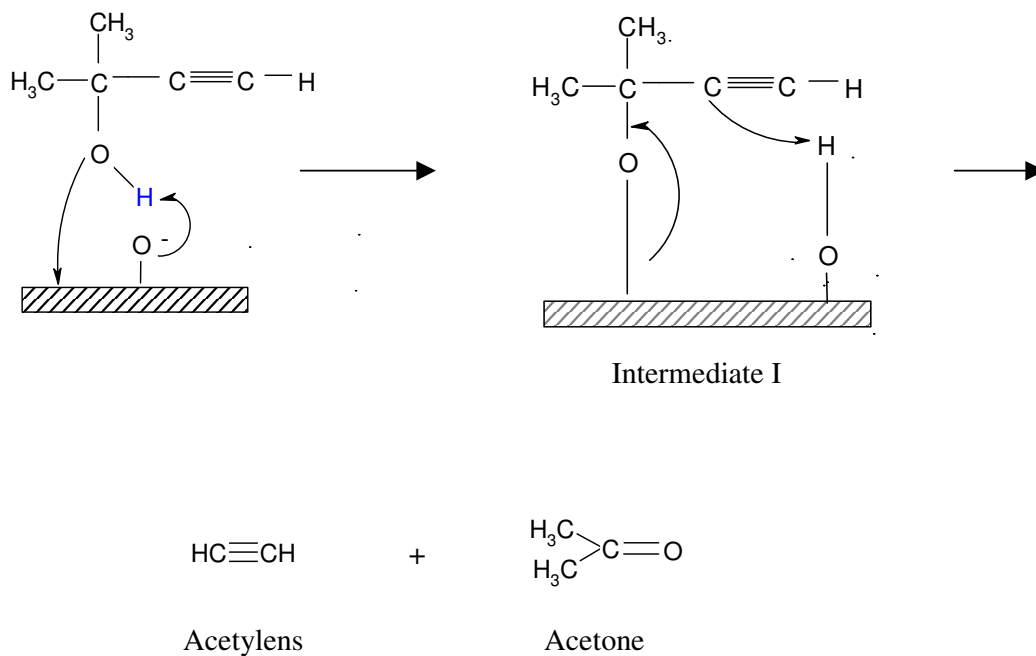
As observed from figure 25 (a) at a reaction temperature of 120 °C it is clearly observed that the selectivity of MBYNE increases within 40 min on time on stream from 25 to 40 mol% while the selectivity of MIPK decreases from 60 to 40 mol%. Selectivities for both products became constant after 40 min time on stream at about 60 and 38 mol% for MBYNE and MIPK, respectively. Other products like acetone are only observed at the initial of the reaction (up to 20 min t.o.s.) then disappeared. Increasing the reaction temperature (see figure 25 b), effects the selectivities of the products MBYNE and MIPK by a decrease about the half compared to the reaction temperature of 120 °C. This decrease in the selectivity is accompanied with the appearance of two new products, which are acetylene and acetone with selectivities of about 25 mol%. Scheme 11 shows the mechanism of the formation of acetylene and acetone through conversion of MBOH. The surface oxide ions attract to the alcoholic hydrogen (OH) to form the intermediate I.

The scission of the C-C-bond and the rearrangement of the C-O bond leads to the formation of acetone and acetylene, respectively. The chemical nature of the active site is not affected at the end of the process.

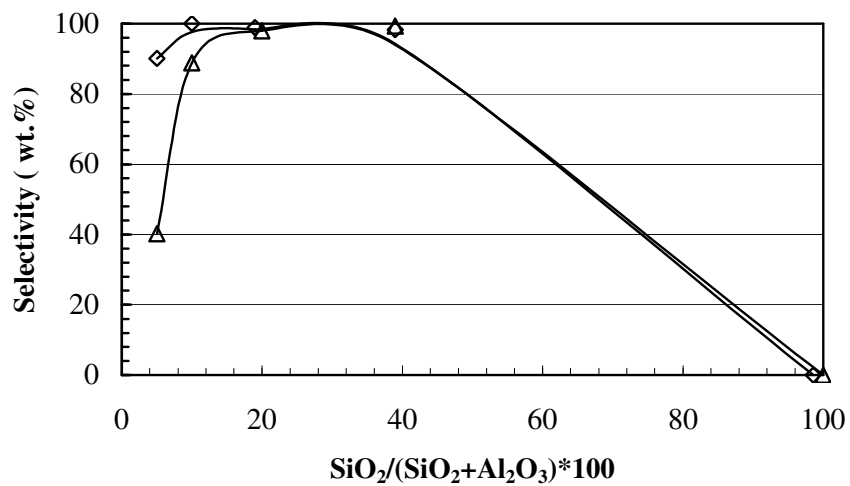
It is noteworthy that the ratio between acetylene to acetone over studied samples is close but not equal to one. This is discussed in detail later for a strong basic catalyst (chapter 4.2).

Hence it can be concluded that the selectivities of the products are influenced by the reaction temperature

**Scheme 11.** Transformation of methyl butynol to acetylene and acetone



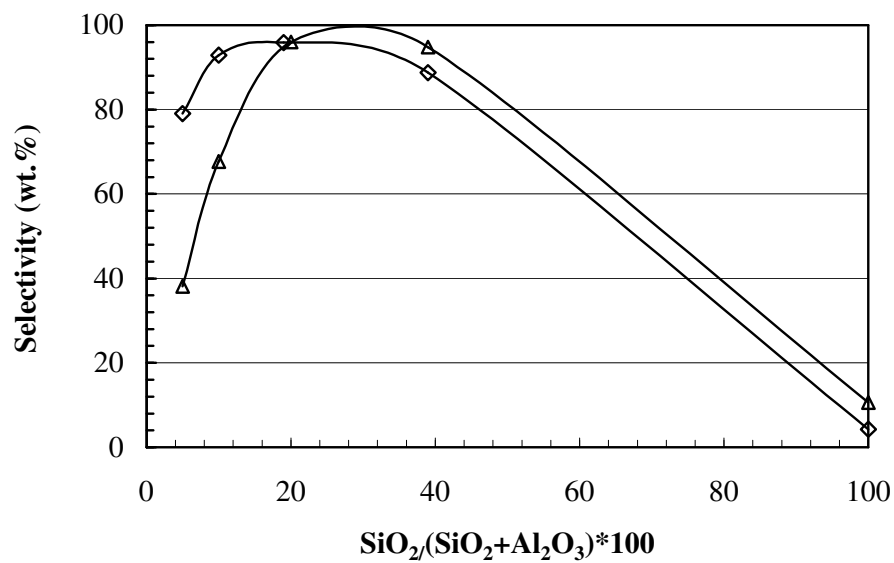
This conclusion is built up not only for one sample but was also controlled for the other silica-alumina solids and is shown only for Si/Al 5 because almost all products were observed. However, the selectivities admit the importance not only of acid sites in the alcohol dehydration, but also of basic centers. The results revealed the change in catalytic activity and product distribution with the Si/Al ratio. Since acetone and acetylene are produced over basic sites, while MBYNE and Prenal are produced over acidic sites, then the yield of acetylene and acetone can be estimated by measuring the basicity. In order to visualize the influence of the Si/Al ratio on the one hand, and the effect of the pre-treatment conditions on acid/base function on the other hand, the selectivities of MBYNE and acetone were plotted against the silica to alumina ratio at different reaction temperatures: 120 °C and 180 °C for both calcined groups (figures 26, 27, and 28).



**Figure 26. Selectivity of MBYNE (acid function)**

**reaction temperature 120 °C, t.o.s = 30 min**

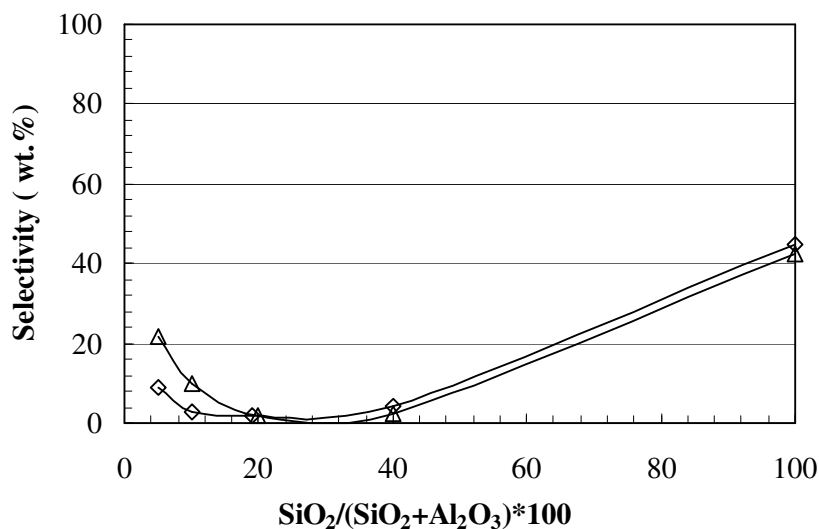
△ calcined at 550 °C    ◇ calcined at 900 °C



**Figure 27. Selectivity of MBYNE (acid function)**

**reaction temperature 180 °C, t.o.s = 30 min**

△ calcined at 550 °C    ◇ calcined at 900 °C

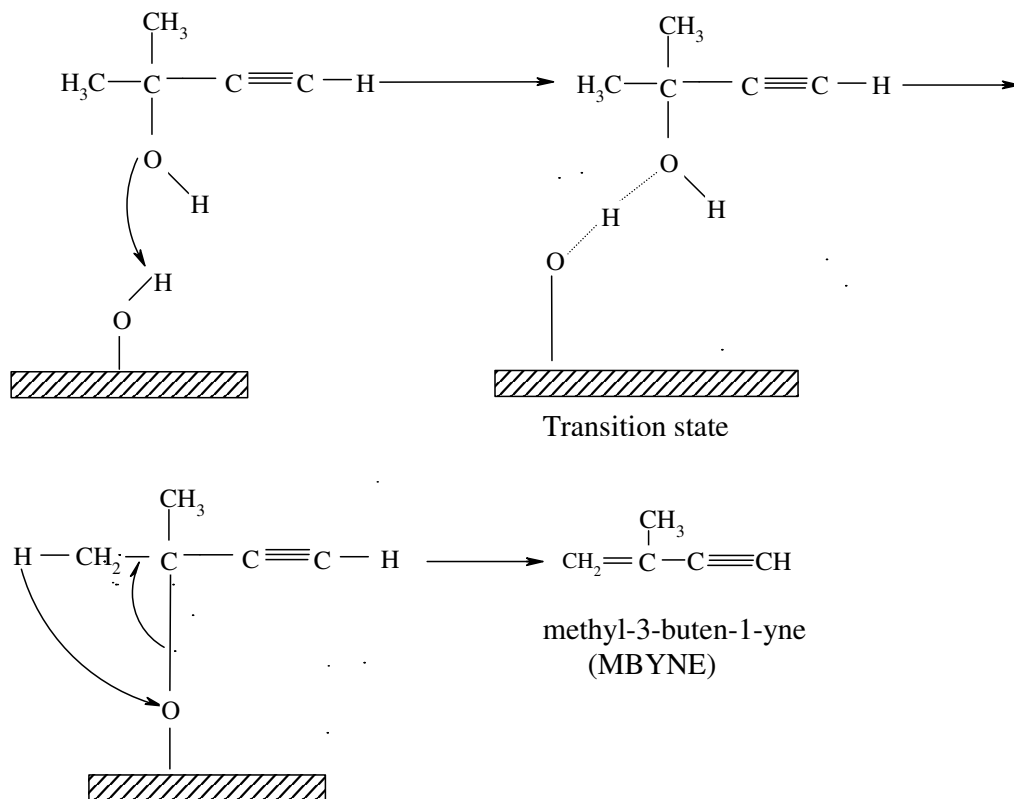


**Figure 28. Selectivity of acetone (basic function)**  
**reaction temperature 120 °C, t.o.s = 30 min**  
 △ calcined at 550 °C   ◇ calcined at 900 °C

As can be observed from figures 26 and 27, the higher the loaded amount of silica to alumina, the higher is the acidity (MBYNE) independent of pretreatment or reaction temperature. The acidity obtained by MBOH test reaction shows an inversely correlation to the results obtained by temperature programmed desorption of ammonia (see table 9), where the acidity assigned by NH<sub>3</sub>-TPD shows, that the higher the alumina content in the silica-alumina solids the higher is the desorbed amount of ammonia.

The obtained selectivity of MBYNE is a significantly high merge between 80 to 99 mol%. It is further noticed that Prenal is always a product and its amount ranges between 0.5 – 0.9 mol%. The mechanism of the transformation from methyl butynol to 3-methyl-3-buten-1-yne (MBYNE) or 3-methyl-2-buten-1-al (Prenal) can be explained by scheme 12, route a and route b, respectively.

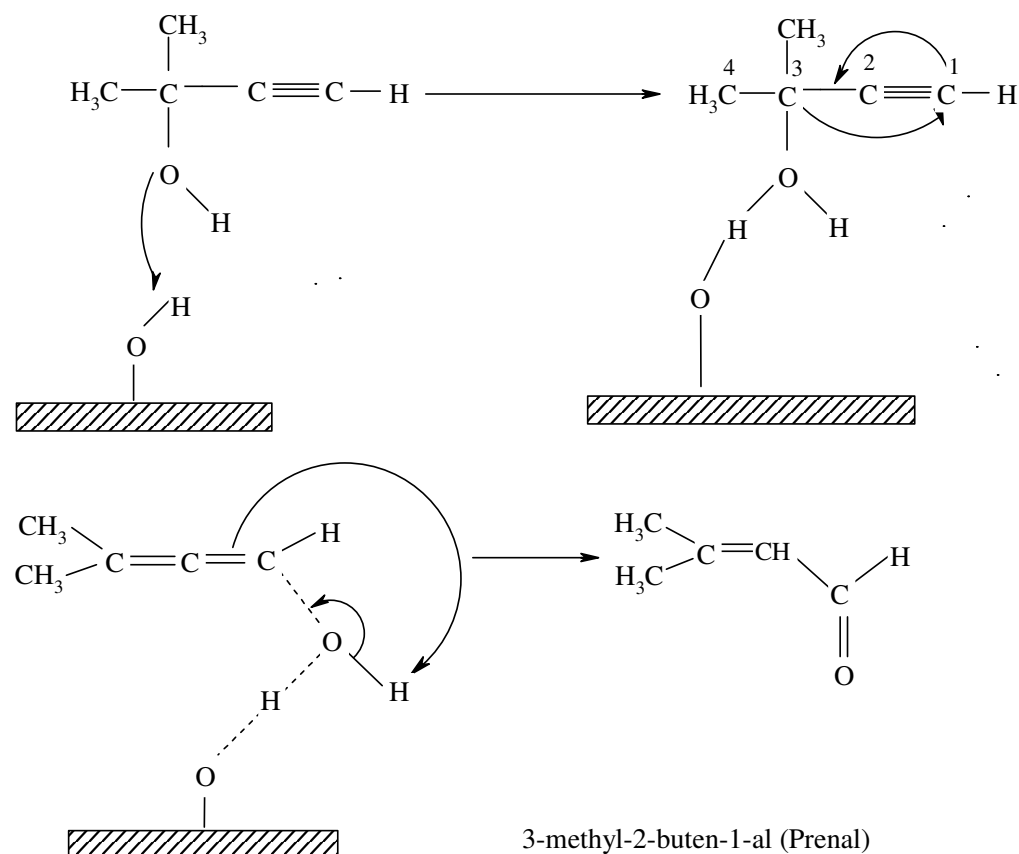
Additionally, figure 28 shows that the basicity of the catalysts decreases with decreasing amount of alumina in the catalyst.

**Scheme 12.** Route a: Transformation of methyl butynol to 3-methyl-3-buten-1-yne (MBYNE)

The acidic OH groups form a transition state in which the alcoholic oxygen is attached to the acidic hydrogen of the surface. After elimination of water the acid site is rebuilt in one step which leads to the formation of 3-methyl-3-buten-1-yne (MBYNE).

For the formation of Prenal, the first step is identical to the mechanism explained above (scheme route 12 a). The next step is shifting the C-O bond from C<sub>3</sub> to C<sub>1</sub> while forming two double bonds leads to an intermediate which undergoes a keto-enol-shift and this rearrangement of a H atom gives the ketone Prenal.



**Scheme 12.** Route b: Transformation of methyl butynol to 3-methyl-2-buten-1-al (Prenal)

#### 4.4.3 Influence of the deactivation on the catalytic activity

Deactivation in MBOH conversion was observed with increasing time-on stream at a lower reaction temperature of 120 °C. The decrease in the activity could be caused by strong adsorption of the products on the solids surface. With the aim of getting more information about the deactivation process, than previously given in figures 21 to 24, conversion of methyl butynol was normalised to the conversion after 125 min from starting the reaction, because at this time the conversion was constant. This was performed by normalising the conversion for each measurement after 125 min on stream.

Normalised methyl butynol conversion after 125 min on stream for applied samples calcined at 550 °C and 900 °C at both reaction temperatures of 120 °C and 180 °C are shown in figures 29 to 32.

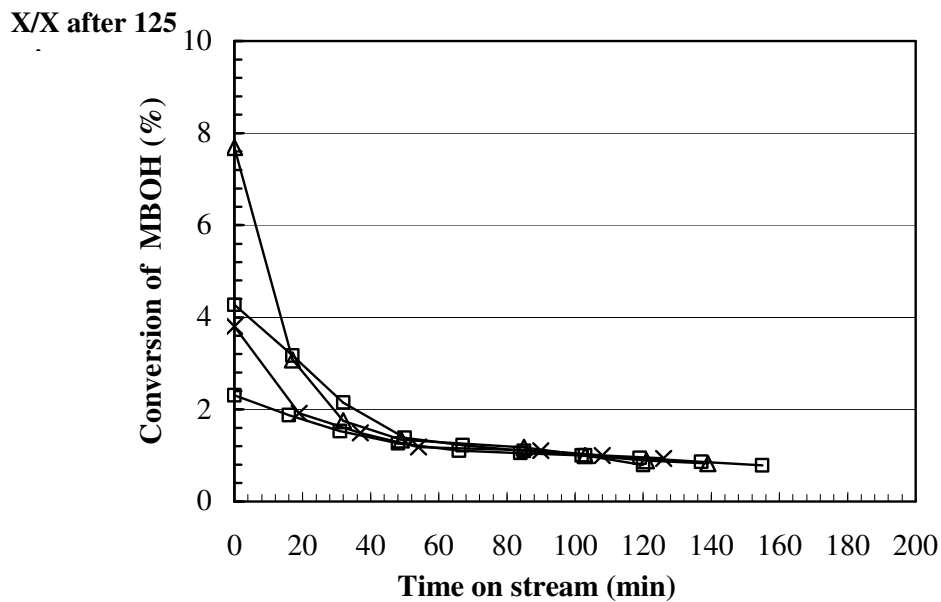


**Figure 29. Normalised conversion of MBOH over different Si/Al ratios, calcined 3 h at 550 °C, reaction temperature 120 °C**

× Si/Al 5    △ Si/Al 10    □ Si/Al 20    ◇ Si/Al 40

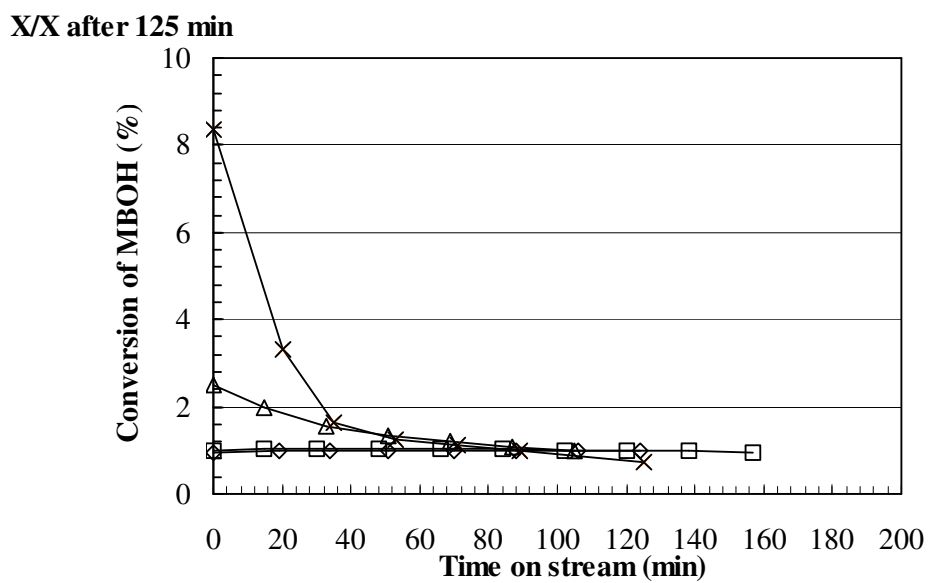


**Figure 30. Normalised conversion of MBOH over different Si/Al ratios, calcined 3 h at 550 °C, reaction temperature 180 °C**

× Si/Al 5    △ Si/Al 10    □ Si/Al 20    ◇ Si/Al 40

X/X after 125 min

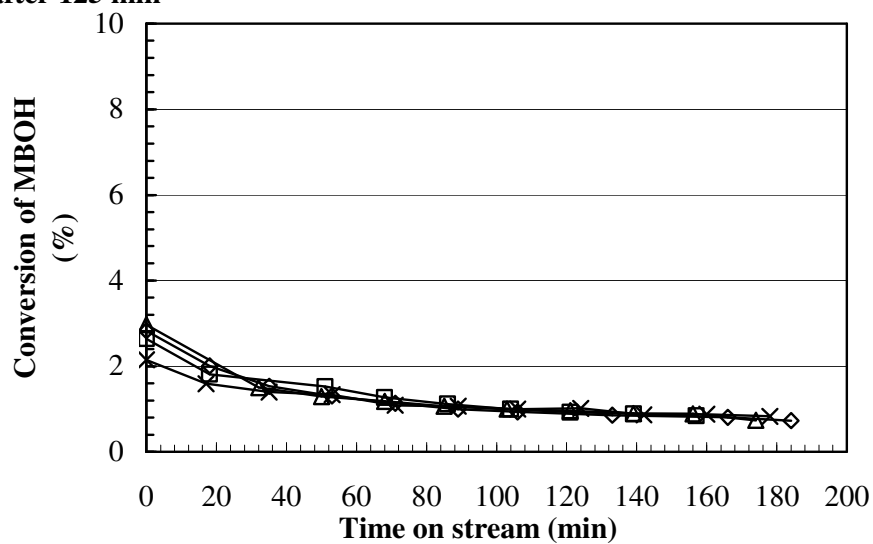


**Figure 31. Normalised conversion of MBOH over different Si/Al ratios, calcined 3 h at 900 °C, reaction temperature 120 °C**

× Si/Al 5    △ Si/Al 10    □ Si/Al 20    ◇ Si/Al 40

X/X after 125 min

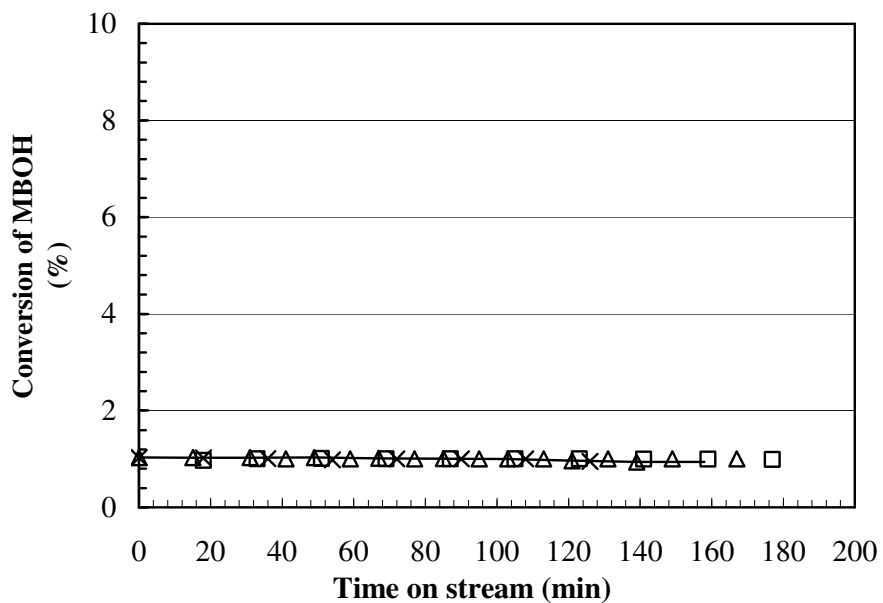


**Figure 32. Normalised conversion of MBOH over different Si/Al ratios, calcined 3 h at 900 °C, reaction temperature 180 °C**

× Si/Al 5    △ Si/Al 10    □ Si/Al 20    ◇ Si/Al 40

The results in figures 29 to 32 show that deactivation takes place if the reaction conditions allow firm interaction between the organic molecules and the catalyst. Adequate conditions for strong interaction are low temperature and strong attracting forces, which can be provided by strong acid sites. If both premises are fulfilled – reaction temperature of 120 °C and catalyst pretreated at 550 °C only – all catalyst samples show deactivation, see figure 29. If both premises are not fulfilled – reaction temperature of 180 °C and catalyst pretreated at 900 °C what causes loss of acid sites – all catalyst samples show a constant activity with time on stream, see figure 32. It can not be also excluded a deactivation by water, formed during reaction which molecules are strongly adsorbed.

Moreover, and studying the effect of calcinations temperature on the studied catalysts for the same reaction temperature of 180 °C (e.g. figures 30 and 32, respectively) it can be derived that, the MBOH conversion is diminished at the higher pre-treatment temperature of 900 °C.

#### 4.4.4 The dependency of the selectivity of MBYNE as a function of the conversion over different Si/Al ratios

The dependency of the selectivity of MBYNE as a function of the conversion over silica-aluminas calcined 3 h at 550 °C, with different SiO<sub>2</sub> content at reaction temperatures of 120 °C and 180 °C is shown by the figures 33 and 34.

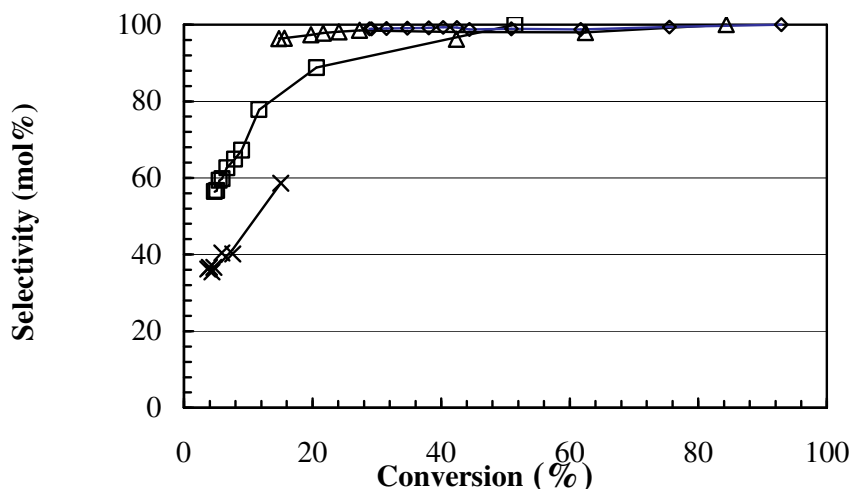


**Figure 33. Selectivity of MBYNE depending on the conversion over different Si/Al ratios calcined 3 h at 550 °C, reaction temperature 120**

× Si/Al 5      △ Si/Al 10      □ Si/Al 20      ◇ Si/Al 40

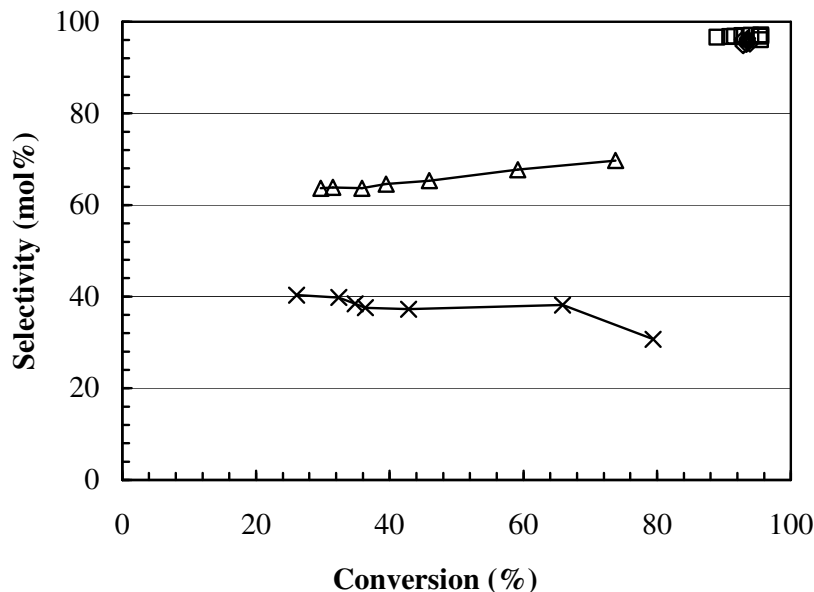


**Figure 34. Selectivity of MBYNE depending on the conversion over different Si/Al ratios calcined 3h at 550 °C, reaction temperature 180 °C**  
 × Si/Al 5    △ Si/Al 10    □ Si/Al 20    ◇ Si/Al 40

The selectivity of MBYNE shows a proportional dependence on the methyl butynol decomposition. This can be better seen at the lower reaction temperature of 120°C over Si/Al 5 and Si/Al 10. The selectivity of MBYNE monotonously increases with increasing conversion. At higher treatment preparations i.e. 900 °C a high selectivity of MBYNE between 70 – 95 mol% is obtained.

In general, a high Si/Al ratio causes a lower electron density on the structure oxygens, thus the protons will be more loosely bonded to these oxygens and therefore the acid strength increases (128). Another explanation for the strong acidity at high ratios of SiO<sub>2</sub> is that weak bonds between alcohol oxygen and the structure alumina cations are formed. Therefore, the electron pair acceptance power of these cations increases, hence acidity increases.

#### 4.4.5 The formation of MIPK as a function of the conversion over different Si/Al ratios

Figures 35 and 36 show the selectivity of MIPK as a function of the conversion over silica-aluminas calcined 3 h at 550 °C with different SiO<sub>2</sub> content at reaction temperatures of 120 °C and 180 °C, respectively.

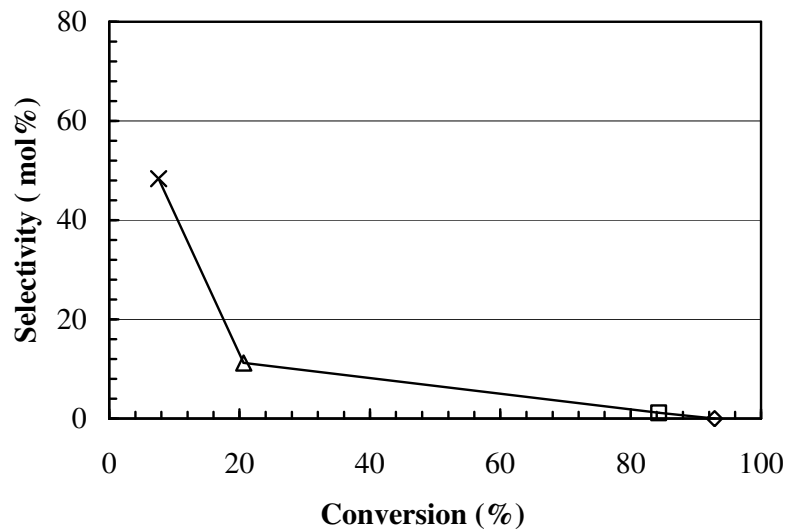


**Figure 35.** Selectivity of MIPK depending on the SiO<sub>2</sub> content over different Si/Al ratios calcined 3 h at 550 °C, reaction temperature 120 °C, t.o.s. = 20 min

× Si/Al 5    △ Si/Al 10    □ Si/Al 20    ◇ Si/Al 40

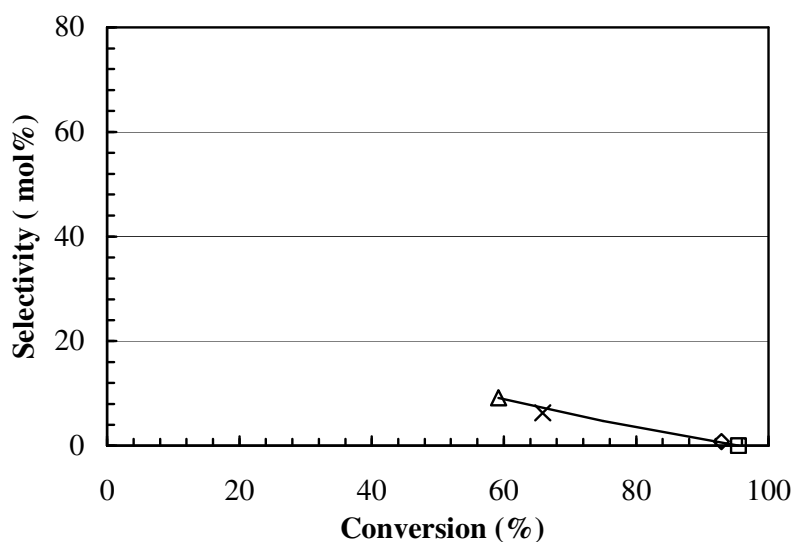


**Figure 36.** Selectivity of MIPK depending on the SiO<sub>2</sub> content over different Si/Al ratios calcined 3 h at 550 °C, reaction temperature 180 °C, t.o.s. = 20 min

× Si/Al 5    △ Si/Al 10    □ Si/Al 20    ◇ Si/Al 40

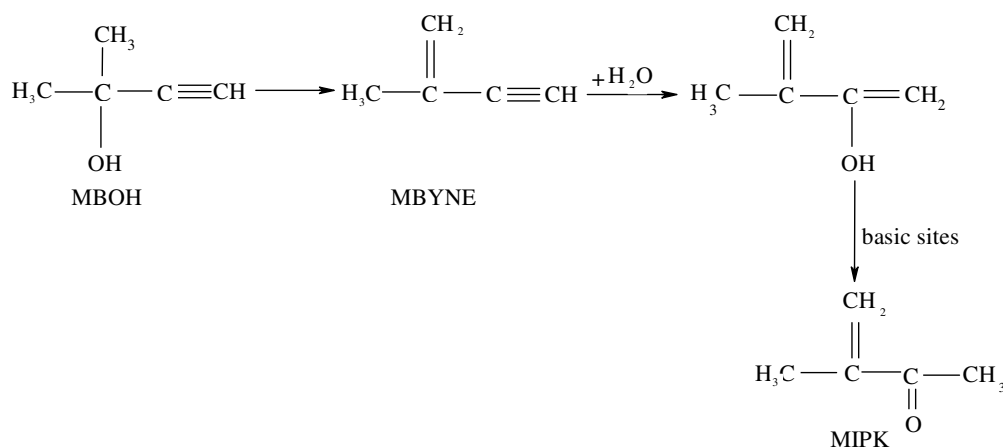
The amphoteric product MIPK was detected in a range of 30 mol% over the sample Si/Al 5 for the group calcined 3 h at 550 °C at lower reaction temperature of 120 °C. The selectivity of MIPK decreases with decreasing alumina content in the catalysts. At the higher reaction

temperature of 180 °C MIPK was also noticed as a product of the decomposition of methylbutynol but only over Si/Al 5 and Si/Al 10.

#### 4.4.6 Correlations and formation of MIPK as primary product over Si/Al solids

Since Lauron Pernot suggested that the formation of MIPK requires both acid and basic sites Aramendia (8) proposed the reaction mechanism which describes the appearance of MIPK as a secondary product by both sites acidic and basic, see scheme 13.

**Scheme 13.** Possible formation of MIPK as a secondary product on basic sites according to Aramendia et.al (8).



However, results obtained by NH<sub>3</sub>-TPD in this study show that the desorption of ammonia depends on the Si/Al ratio in the catalyst. Decreasing framework aluminium content is associated with a decrease in the number of acidic OH groups, but generally the strength of the remaining sites initially increases (129, 130). The solids silica alumina studied temperature program desorption of ammonia can be arranged according to the maximum of ammonia desorption peak (equation 15) and number of acidic sites (equation 16), as follows (see table 9):

Maximum desorption peak: Si/Al 40 < Si/Al 20 < Si/Al 10 < Si/Al 5 equation (15)

Number of acid sites: Si/Al 5 < Si/Al 10 < Si/Al 20 < Si/Al 40 equation (16)

The presence of Brönsted acid sites (proton donor) is required for the formation of MIPK (128). Since in the present study only silica alumina containing 95 wt.% and 90 wt.% of alumina have formed MIPK from methyl butynol, the mechanism proposed in scheme 13 for the formation of MIPK can be excluded because all samples have strong acidic sites as shown from NH<sub>3</sub>-TPD measurements (chapter 4.1). Another evidence that MIPK formation does not exclusively require strong acid sites is, that MIPK has not been detected in the MBOH reaction over other strong acid solids like zeolites, see table 14.

**Table 14.** Conversion of MBOH and selectivities over different types of zeolites

Catalyst	Si/Al ratio	X <sub>MBOH</sub> t.o.s=90 min	C <sub>2</sub> H <sub>2</sub> mol%	C <sub>3</sub> H <sub>6</sub> O mol%	MBYNE mol%	Prenal mol%	MIPK mol%
H-ZM5	45	46.9	0.0	0.0	90.4	9.6	0.0
H-Beta	25	9.6	0.0	0.0	95.8	4.2	0.0
Y-Si/Al	5.5	4.9	0.0	0.0	95.5	4.5	0.0

In addition, researchers (131) studied the aluminosilicate phase versus silica encapsulation for different Si/Al ratios (silica range: 1.5 - 90 wt.%) by FTIR spectroscopy and they observed for Si/Al (silica range: 10 – 20 wt.%) three surface phases:

(i) The formation of an aluminosilicate phase, co-ordinately unsaturated Al<sup>3+</sup><sub>(TET)</sub> ions are detected exposed on the surface, and sites with enhanced Brönsted acidity, attributed to bridged OH groups on the exposed aluminosilicate. (ii) A second phase showing only silica phase. (iii) The third surface phases is a mixed aluminomsilicate. Figure 37 shows the model proposed by Knözinger *et al* (134) depicting different surface compositions for pure alumina and different Si/Al ratios. On the basis of the model proposed by Knözinger *et al* (134), it can be suggested that formation of MIPK over silica-alumina (Si/Al 5, Si/Al 10) takes place when their surface structure phases is a mixture of aluminomsilicate, see figure 37, e.g. (C). The reaction starts with converting the triple bond of methyl butynol to a double bond by attack of an proton resulting from the aluminosilicate phase to form a strong bond. Then isomerization occurs to form a carbenium intermediate and proton abstraction leads finally to the ketone of MIPK, see scheme 14.



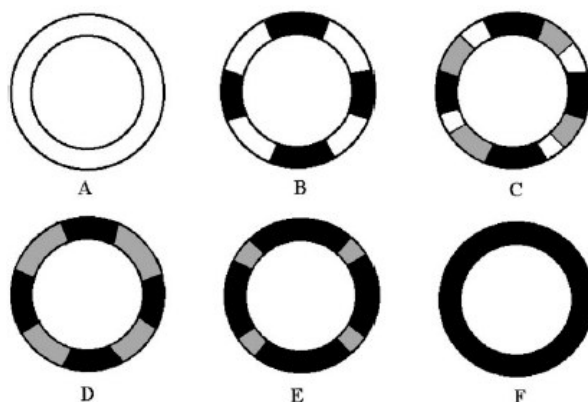


**Figure 37. Model depicting the surface composition of pure alumina, pural SB (A)**

SIRALS 1.5-5 (B), SIRALS 10-20 (C), SIRALS 30-40 (D) SIRALS 60-80 (E),  
SIRALS 90-100 (F)

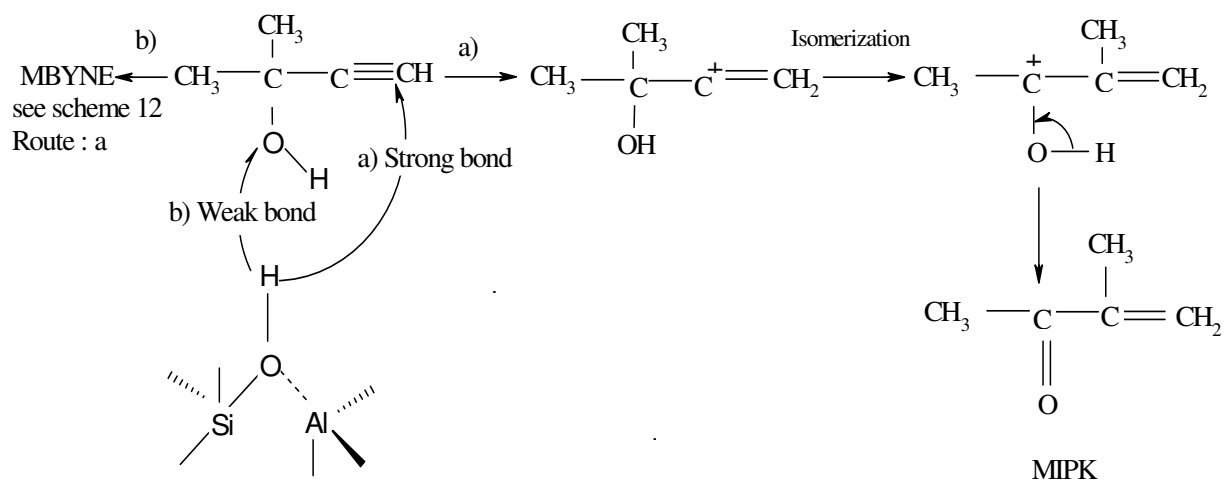
□  $\text{Al}_2\text{O}_3$

■ Al-Si Oxide

■  $\text{SiO}_2$

The second pathway possibility for the reaction, is the attack of a proton resulting from the aluminosilicate phase to an oxygen to form a weak bond, scheme 14 (pathway direction b), and this leads to MBYNE.

**Scheme 14.** Possible formation of MIPK from decomposition of methyl butynol over Si/Al



A correlation between the results from MBOH conversion on silica-alumina samples at

a reaction temperature of 120 °C with the mechanism proposed in the present work (scheme 14) exists and is explained in more details for the formation of MBYNE (scheme 12 route/ a) in chapter (4.4.5) and for route (b) in chapter (4.4.6). It can be observed that Si/Al 5 and Si/Al 10 permit both pathways presented in scheme 14: route (a) to MBYNE and route (b) to MIPK, while Si/Al 20 and Si/Al 40 favor only route (a) because MIPK is not observed.

The interpretation for the above behavior of silica alumina samples becomes clear when we check the amount of the acidity for silica alumina and that is characterized by the NH<sub>3</sub>-TPD measurements (see table 9). It has been observed that samples which contain more alumina like Si/Al 5 and Si/Al 10 show a higher acidic amount than Si/Al 20 and Si/Al 40. These samples (i.e. Si/Al 5 and Si/Al 10) favor both routes a, and b (see scheme 14). This can be effected by the strong acidity of the catalyst which is able to produce MBYNE and MIPK in the MBOH conversion. Therefore the direction of route a in scheme 14 is inscribed as strong bond relating to strong acidic catalysts (i.e. Si/Al 5 and Si/Al 10).

Continuously, the amount of the acidic sites for silica alumina samples like Si/Al 20 and Si/Al 40 is lower than for Si/Al 5 and Si/Al 10, and the reaction is favored to form MBYNE (see scheme 14 route b) and the formation of MIPK is excluded for these samples (Si/Al 20 and Si/Al 40).

Moreover, the reason for the observation that at higher reaction temperatures (i.e. 180 °C) or higher treatment temperatures (i.e. 900 °C) the selectivity of MIPK decreases for Si/Al 5 and is not longer a product for the other solids (Si/Al 10, 20, and 40) can be ascribed to dehydroxylation of hydroxyl groups which leads to loss of active acid sites (OH).

But the strength of the acid sites seems not be the only criteria if MIPK is formed or not. Interestingly MIPK is formed on the silica-alumina samples Si/Al 5 and Si/Al 10 synthesized by Sasol Germany GmbH but not on solids which have also strong acid sites like zeolites (see table 14).

To express a summary for this chapter, a mechanism is proposed for the formation of MIPK as a primary product (scheme 14) which explains the effects of the nature of the catalyst (i.e. Si/Al 5 and Si/Al 10) and which shows that only the stronger acidic sites are involved in the formation of MIPK from MBOH with the alumino phase structures resulted by the attribution of OH groups between silica. Depending on the structure for the aluminophase in silica-alumina samples, the MBOH conversion can show two possible pathways:

Through the first possibility the investigated silica-alumina is only able to form MBYNE. This requires acidic sites (see scheme 14 route b) which are present at all investigated silica-alumina samples in high amounts, what was already presented by NH<sub>3</sub>-TPD (see table 9). But,

this is not enough to form MIPK in the MBOH conversion because only two of the silica-alumina samples in the present study show a formation of MIPK. It seems to require additionally a specific structure of aluminosilica phase. Knözinger (134) presented a model depicting different surface compositions of aluminosilicates (see scheme 37). From that, it can be suggested that some types of aluminophase structures facilitate the attack of strong protons to the triple bond of methyl butynol and the formation of MIPK can occur, see scheme 14 route a. Premises for this aluminosilicate structure seem to be a high ratio of alumina and the availability of silica. Since a sample with a high alumina content provides most likely tetrahedral and octahedral coordinated aluminum cations, the ratio between  $\text{Al}^{3+}_{(\text{TET})}$  and  $\text{Al}^{3+}_{(\text{OCT})}$  may play an important role.

In the literature (48) it is described that MIPK formation increases with addition of water to MBOH. Therefore the addition of water to MBOH has been considered in the present work in a separate in the following chapter 4.5.

#### **4.5 Effect of water on the conversion of MBOH**

In the literature (48) it is explained and from scheme 13 it can be seen, that the formation of MIPK is affected by the amount of water which is present during the reaction. To study if this hypothesis is correct for the different types of solids investigated in the present thesis this matter was considered.

##### **4.5.1 Varying the concentration of MBOH passed over the investigated catalysts**

Figure 38 shows a comparison of the MBOH concentrations before and after addition of water over empty reactor at an oven temperature of 180 °C. To keep the GHSV of MBOH constant the nitrogen flow was reduced to 11 ml/min in case of addition of 2 wt.% water.

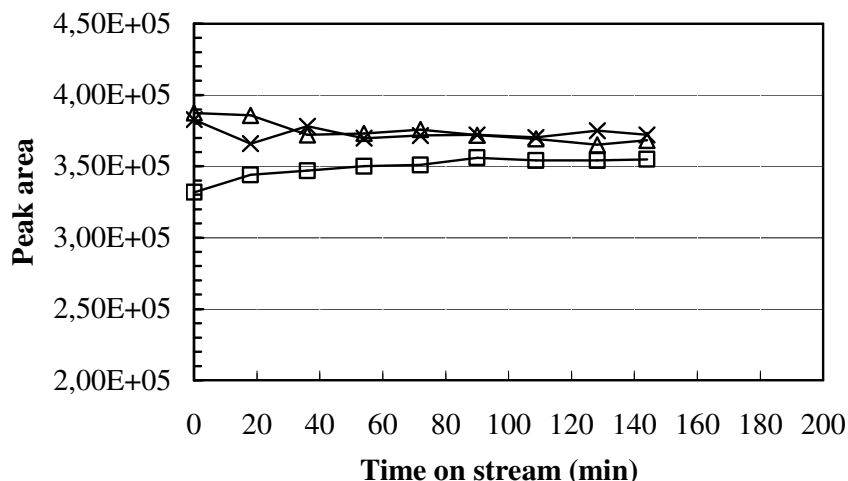


**Figure 38. Comparison of MBOH concentration over empty reactor before and after addition of 2 wt.% water, oven temperature 180 °C**

△ MBOH peak area before addition of H<sub>2</sub>O 2 wt.%, N<sub>2</sub> flow=13 ml/min

□ MBOH peak area after addition of H<sub>2</sub>O 2 wt.%, N<sub>2</sub> flow=13 ml/min

× MBOH peak area after addition of H<sub>2</sub>O 2 wt.%, N<sub>2</sub> flow = 11 ml/min

#### 4.5.2 Hydrotalcites Puralex MG 70, zeolites, silica–alumina with different ratios

Conversion of MBOH on catalysts such as hydrotalcites Puralex MG 70, zeolites, pure alumina or Si/Al with different ratios have not been affected by addition of water to MBOH and show no changes in the results comparing to those obtained by MBOH test reaction (substrate: 95 wt.% MBOH and 5 wt.% n-hexane). It can be concluded that the formation of MIPK or HMB in the conversion of MBOH on the investigated solids (hydrotalcites Puralex MG 70, zeolites, pure alumina or Si/Al with different ratios) is not effected by the addition of water to MBOH. This is another evidence for the mechanism presented in scheme 14.

#### 4.5.3 Bulk metal oxides: ZrO<sub>2</sub>, TiO<sub>2</sub>, HfO<sub>2</sub>, Zr(OH)<sub>4</sub>

Figure 39 presents the catalytic activity for the bulk metal oxides ZrO<sub>2</sub>, TiO<sub>2</sub> and HfO<sub>2</sub> against time on stream. An increase in the conversion affected by the addition of water to MBOH was observed on zirconium hydroxide Zr(OH)<sub>4</sub> (as-synthesized, see chapter 3.1.3), where MBOH conversion was more than twice higher than conversion observed in case of substrate A (95 wt.% MBOH, 5 wt.% n-hexane). In case of TiO<sub>2</sub> and HfO<sub>2</sub> the conversion was a little

higher with water. Changes in the conversion over other investigated catalysts like  $ZrO_2$  or calcined  $Zr(OH)_4$  have not been observed.

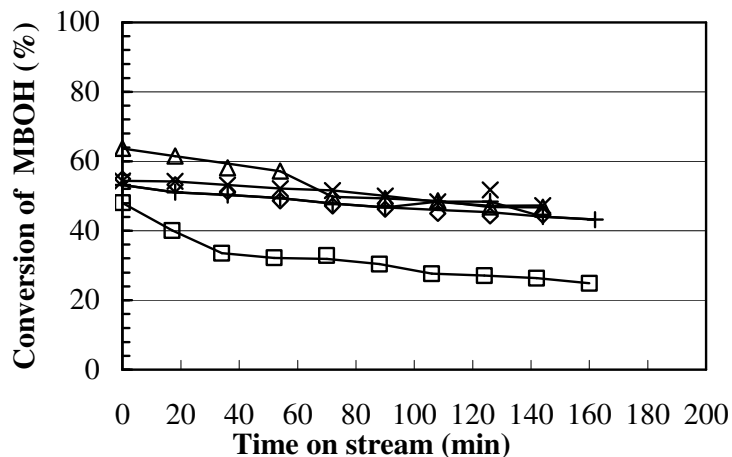


**Figure 39. Conversion of MBOH over different rare earth metal oxides supported on alumina, reaction temperature 180 °C**

**substrate: MBOH + 2 wt.% H<sub>2</sub>O**

× HfO<sub>2</sub>/Al<sub>2</sub>O<sub>3</sub> (5:95)    △ HfO<sub>2</sub>/Al<sub>2</sub>O<sub>3</sub> (10:90)    ◇ HfO<sub>2</sub>/Al<sub>2</sub>O<sub>3</sub> (15:85)

+ TiO<sub>2</sub>/Al<sub>2</sub>O<sub>3</sub> (5:95)    □ ZrO<sub>2</sub>/Al<sub>2</sub>O<sub>3</sub> (5:95)

Table 15 presents a comparison of the conversions and selectivities of the products before and after addition of 2 wt.% water to methyl butynol at 18 min time on stream. The selectivities of the formed products were compared using the substrate 95 wt.% methyl butynol mixed with 5 wt.% n-hexane on the one hand, and using the second substrate methyl butynol mixed with 2 wt.% water on the other hand after 18 min time on stream.

**Table 15.** Comparison of the conversions and selectivities of the products before and after addition of 2 wt.% water to methyl butynol at 18 min time on stream

Catalyst	Conversion		Acetylene mol%		Acetone mol%		MBYNE mol%		MIPK mol%		HMB mol%	
	X <sub>A</sub>	X <sub>B</sub>	A	B	A	B	A	B	A	B	A	B
ZrO <sub>2</sub>	97.3	97.4	0.2	0.1	0.1	0.1	0	0	99.6	98.9	0.0	1.0
TiO <sub>2</sub>	17.3	19.8	26.6	29.8	12.1	25.6	49.5	27.8	3.8	2.7	8.0	14.2
HfO <sub>2</sub>	11.6	15.9	44.2	29.6	37.3	26.1	8.4	2.5	0.0	3.1	10.0	38.7
Zr(OH) <sub>4</sub>	16.7	37.5	27.0	24.2	11.7	22.1	0	0	3.9	1.0	6.5	52.8

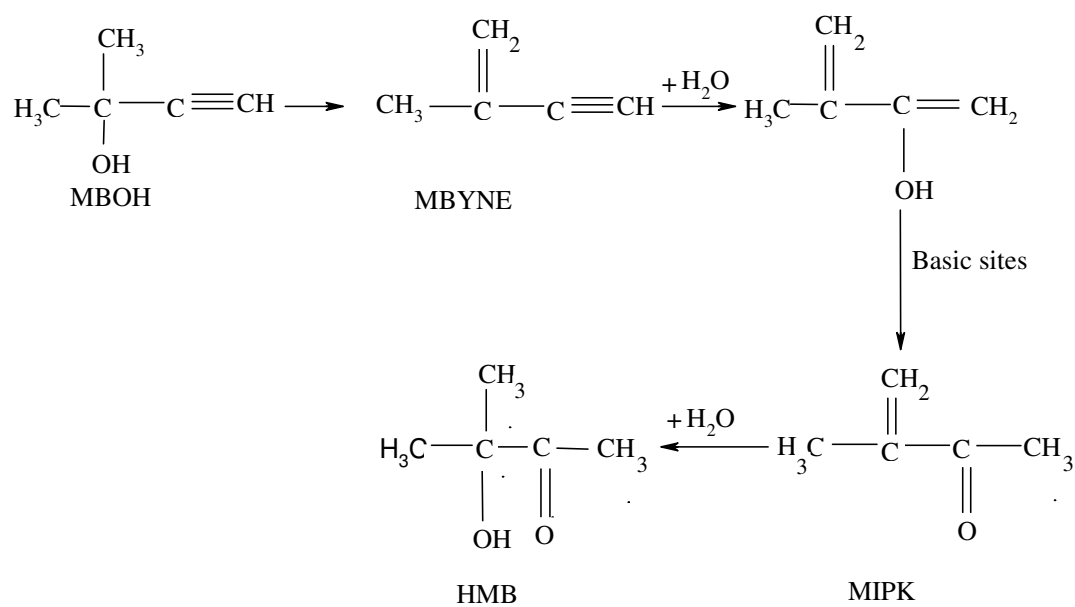
Composition A: 95 wt.% MBOH + 5 wt.% n-hexane

Composition B: MBOH + 2 wt.% H<sub>2</sub>O

Obtained results show an intensive increase in the selectivity of HMB on zirconium hydroxide, or zirconia when water was added to MBOH. This increase is accompanied with a decrease in amount of acetylene and acetone.

An explanation for the appearance of MIPK in case of  $\text{ZrO}_2$  could be that additional water reacts with MBYNE which provides to MIPK as presented by Aramendia in scheme 13, chapter 4.5. The product HMB was observed over hafnium oxide and titanium oxide (see table 18). Scheme 15 shows the possible pathways for the formation of HMB by addition of water to MBOH.

**Scheme 15.** Possible formation of HMB from decomposition of methyl butynol over bulk metal oxides with addition of 2 wt.%  $\text{H}_2\text{O}$  to MBOH.



#### 4.5.4 Metal oxides supported on alumina: ( $\text{ZrO}_2$ , $\text{TiO}_2$ , $\text{HfO}_2$ )/ $\text{Al}_2\text{O}_3$

Table 16 depicts the conversions after 100 min time on stream, surface areas after the reaction and the correlation between the conversion and the surface areas for bulk metal oxides ( $\text{ZrO}_2$ ,  $\text{TiO}_2$ ,  $\text{HfO}_2$ )/ $\text{Al}_2\text{O}_3$  catalysts before and after the addition of water to MBOH.

With the exception of  $\text{ZrO}_2$  a clear increase of the MBOH conversion is observed when water is added. The increase in the MBOH conversion can be significantly improved with the

samples hafnium oxide doped with alumina, where with  $\text{HfO}_2/\text{Al}_2\text{O}_3$  (10:90) the conversion raised from 40 to 50 % by addition of water.

**Table 16.** Conversion and surface area of used samples of the synthesized solids

Sample (wt.%)	$X_{\text{MBOH, t.o.s}=100 \text{ min}}$ %		BET surface area $\text{m}^2/\text{g}$			$X_{\text{MBOH, t.o.s}=100 \text{ min}}/\text{BET}$	
	$X_A$	$X_B$	As-synthesized	$\text{BET}_A$	$\text{BET}_B$	$X_A/\text{BET}_A$	$X_B/\text{BET}_B$
$\text{ZrO}_2/\text{Al}_2\text{O}_3$ (5:95)	23.7	27.6	108	110	108	0.2	0.3
$\text{TiO}_2/\text{Al}_2\text{O}_3$ (5:95)	21.8	48.4	129	114	97	0.2	0.5
$\text{HfO}_2/\text{Al}_2\text{O}_3$ (5:95)	22.7	48.3	122	110	101	0.2	0.5
$\text{HfO}_2/\text{Al}_2\text{O}_3$ (10:95)	42.0	48.6	130	125	109	0.3	0.4
$\text{HfO}_2/\text{Al}_2\text{O}_3$ (15:85)	31.1	45.0	135	122	108	0.3	0.4

In addition the difference in the conversion calculated by using the ratio of internal standard and the yield of the products is found to be in a small amount and reaches 1 %. In addition, a comparison between the conversion related to the surface area before and after water addition to MBOH shows only small changes in a range of 1 – 2 %. Figure 40 presents the affect of addition of water on the yield of MIPK.

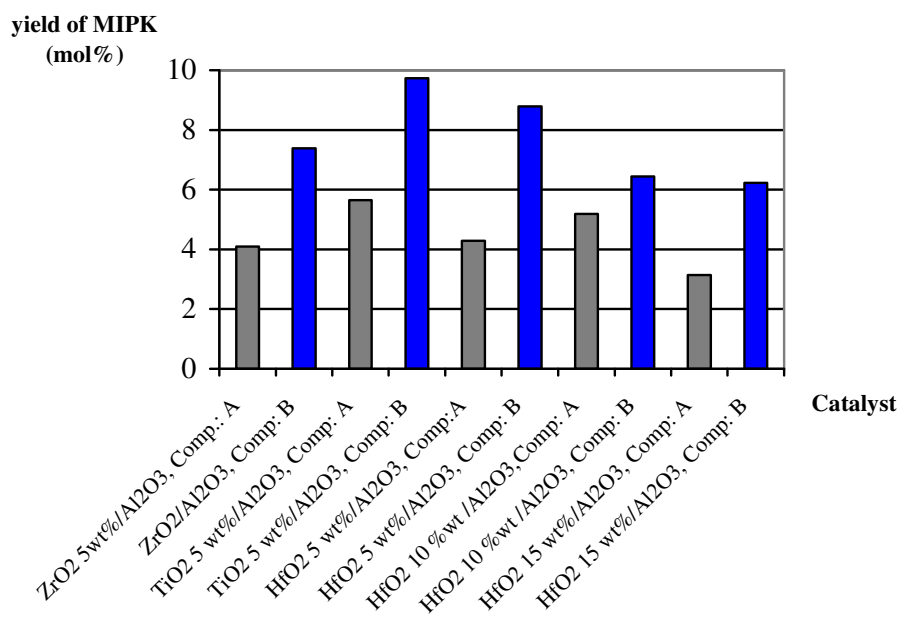
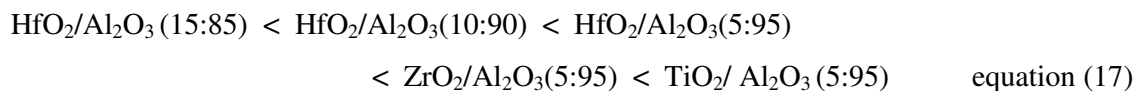


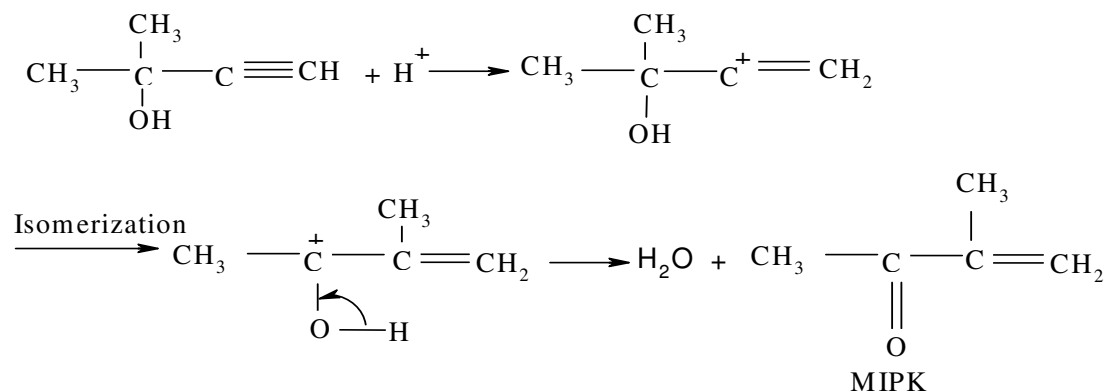
**Figure 40.** Comparison of the yielded MIPK product after 108 min time on stream

Addition of 2 wt.% water to methyl butynol causes a remarkably increase in the selectivity of MIPK on  $\text{ZrO}_2/\text{Al}_2\text{O}_3$  (5:95 wt.%) of about 10 %. Aramendia (48) tested the effect of addition of water to MBOH on pure  $\text{ZrO}_2$  and explained the increase of the yield of MIPK by the proton attack resulting from water dissociation on the sites of catalyst, followed by the conversion of the triple bond to a double bond and isomerization, see scheme 13. On the other hand, increasing the content of hafnium oxide in the catalyst causes a decrease in the MIPK product, as can be seen in the comparison shown in figure 40 between the samples  $\text{HfO}_2/\text{Al}_2\text{O}_3$  (5:95 wt.%) and sample  $\text{HfO}_2/\text{Al}_2\text{O}_3$  (15:85 wt.%). This can be explained because increasing the fraction of hafnium oxide in the catalyst decreases also the acidic centers (OH) of alumina which is needed to attack the triple bond of methyl butynol as proposed in the mechanism in scheme 14. Moreover,  $\text{NH}_3$ -TPD (high desorption peak of ammonia), and the results presented in table 10 show that the acidity of metal oxides supported on alumina takes the following sequence as in equation (17).



It was suggested that the formation of MIPK in the present study is not resulted exclusively from the proton attack by water dissociation as proposed by Aramendia (48) in scheme 16, but it could be more feasible that the formation of MIPK results from solids containing strong acidic sites (i.e.  $\text{TiO}_2/\text{Al}_2\text{O}_3$  (5:95 wt.%) or  $\text{ZrO}_2/\text{Al}_2\text{O}_3$  (5:95 wt.%) and that the proton coming from water dissociation is only a promoter to these sites.

**Scheme 16.** Possible formation of MIPK from decomposition of methyl butynol over metal oxides supported on alumina with addition of 2 wt.%  $\text{H}_2\text{O}$  to MBOH.





#### 4.6 Determination of activation energies in the MBOH test reaction

From an Arrhenius diagram, the rate constant of the conversion of MBOH was calculated as well as the apparent activation energies for the three pathways of the MBOH reaction.

To calculate the reaction rate constant a reaction order of one relating to MBOH was assumed which can be described with the rate law equation 18.

$$p_i = p_0 \cdot e^{-kt} \quad \text{equation (18)}$$

After resolving for k, equation 19 is obtained, in which the partial pressure of methyl butynol is 100 at time zero and  $(100 - X_{\text{MBOH}})$  for time i. The contact time t is the reciprocal value of the GHSV.

$$k = \frac{-\ln\left(\frac{p_i}{p_0}\right)}{t} = \frac{-\ln\left(\frac{100 - X_{\text{MBOH}}}{100}\right)}{t} \quad \text{equation (19)}$$

The Arrhenius-Equation (equation 20) describes the dependency of the reaction rate constant from the temperature.

$$k = A \cdot e^{-\frac{E_A}{R \cdot T}} \quad \text{equation (20)}$$

A: pre-exponential factor     $E_A$ : activation energy    R: general gas constant

After logarithmic calculus of the Arrhenius-Equation equation 21 is obtained. If the natural logarithm of k is plotted against the reciprocal value of the absolute temperature, a straight line with the slope  $-E_A/R$  is obtained. From the slope the apparent activation energy  $E_A$  of the reaction can be calculated (132, 133).

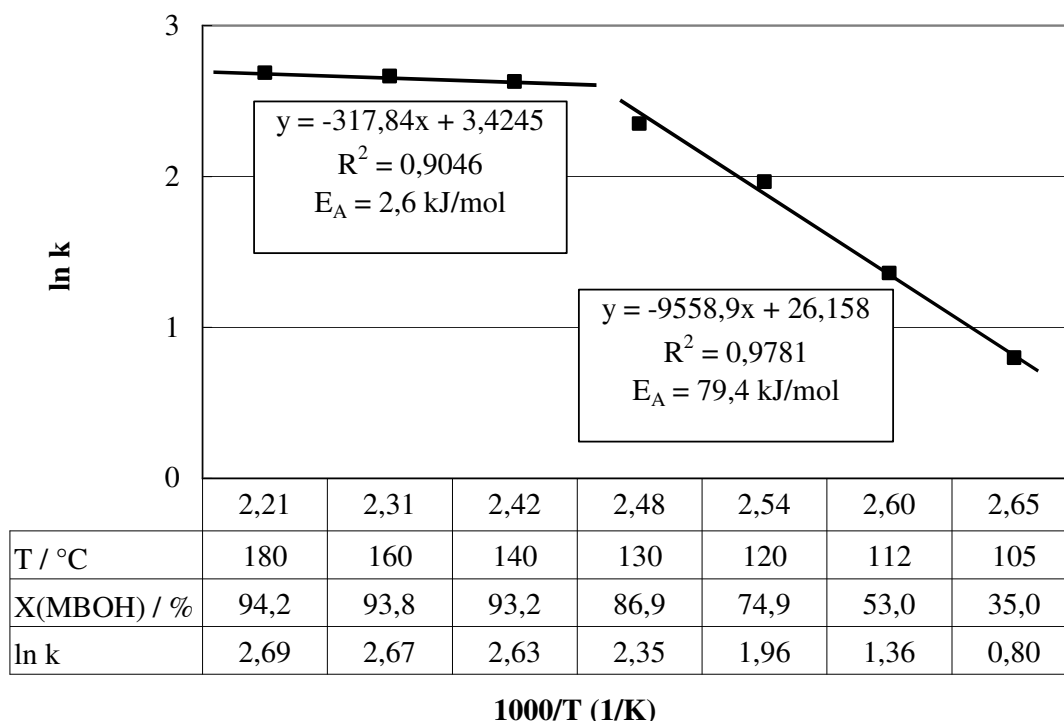
$$\ln k = \ln A - \frac{E_A}{R} \cdot \frac{1}{T} \quad \text{equation (21)}$$

A study of the activation energies was performed for the three different pathways of the MBOH test reaction: basic over Puralox MG 70, acidic over Siralox 30 and amphoteric over zirconia by varying the reaction temperature. Changing the temperatures alters the rate of the reaction by changing the rate constant and the amount of these changes depends on the activation energy. Table 15 presents reaction temperatures and initial MBOH conversions for different catalysts for the three pathways of the MBOH test reaction (basic, acidic, and amphoteric). The data presented in table 15 does not give a direct correlation between the three pathways of MBOH conversion because the activation energy does also depend on the type of catalyst.

**Table 19.** Values of MBOH conversions at different reaction temperatures for three pathways of the MBOH test reaction (basic, acidic, and amphoteric )

Reaction path	Reaction temperature °C	MBOH conversion $X$ after 20 min on stream %
Basic over Puralox MG 70	105	35.0
	112	53.2
	120	74.0
	130	86.2
	140	93.1
	160	93.8
	180	94.2
Acidic over Siralox 30	120	33.0
	140	58.4
	160	81.2
	180	92.3
Amphoteric over zirconia	117	10.1
	140	25.2
	160	45.2
	180	60.0
	240	96.2

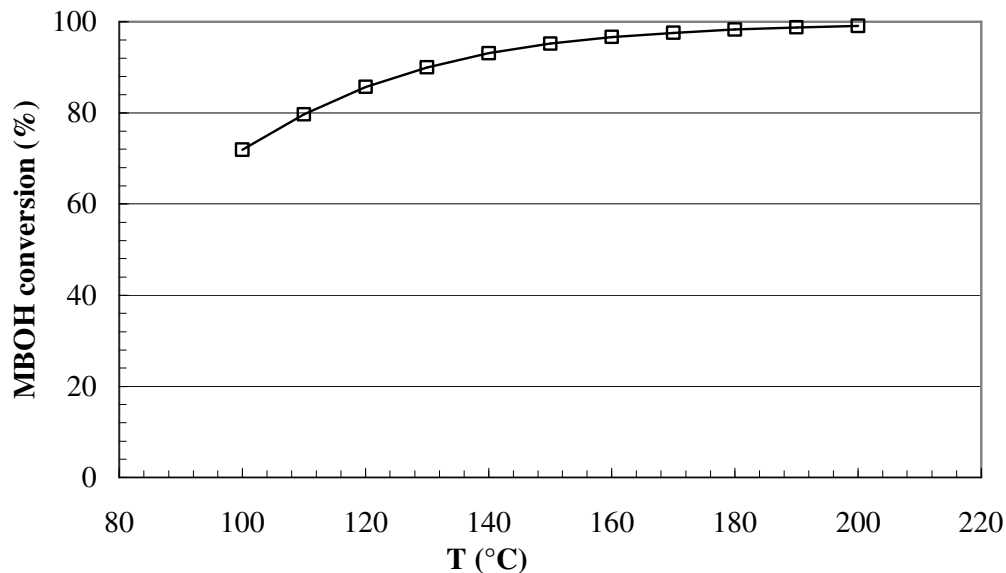
Figure 41 shows two ranges of temperatures with two different slopes, i.e. two different values of activation energy. The first value indicates that the reaction needs an activation energy of  $E_a = 79.4$  kJ/mol in the temperature range from 105 °C – 130 °C what means at this range of reaction temperatures, the reaction is kinetically limited.



**Figure 41. Arrhenius diagram for basic pathway of the MBOH test reaction over**

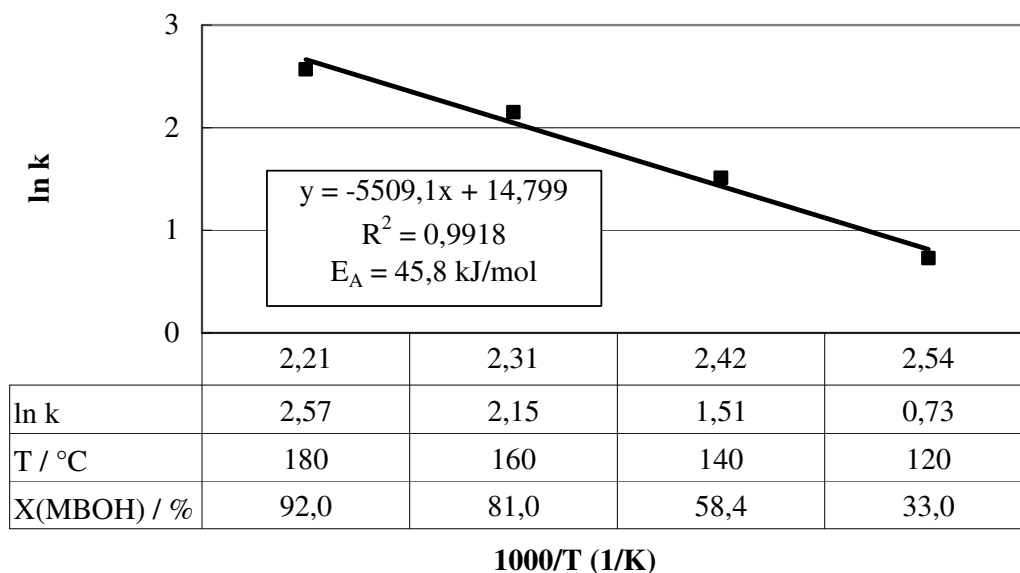
The second activation energy obtained for the basic pathway reaction shows that the activation energy in the temperature range of 140 °C – 180 °C is very low and counts  $E_a = 2.6$  kJ/mol, because the conversion in this range is near the thermodynamic equilibrium. This was proved by the calculation of the thermodynamic equilibrium (135) of the basic pathway of the MBOH test reaction (see appendix point 7.4).

Figure 42 shows the thermodynamic equilibrium of the conversion of MBOH to acetone and acetylene according the basic pathway of the MBOH test reaction. It can be seen, that the MBOH conversion is around 70 % for 100 °C and increases with reaction temperature to become close to 100 % at 200 °C.



**Figure 42. Thermodynamic equilibrium of the basic pathway for MBOH test reaction**

Figure 43 shows the Arrhenius diagram for the acidic pathway of the MBOH test reaction over Siralox 30 (i.e. 30 wt.% silica).



**Figure 43. Arrhenius diagram for the acidic pathway of the MBOH test reaction over Siralox 30**

In the second pathway of the test reaction (i.e. acidic) MBOH was converted over pure acidic catalyst in order to determine the activation energy in a temperature range of 120 °C – 180 °C with a value of  $E_a = 45.8$  kJ/ mol and that is characterization for a kinetic control.

Lauron Pernot (136) measured the activation energy for only the acidic pathway of MBOH conversion on metal nitrides ( $W_2N$ , NbN and  $Mo_2N$ ) passivated by oxygen after synthesis and found a similar global activation energy for MBYNE of about  $E_a = 24.7$  KJ/ mol and for Prenal of about  $E_a = 22.1$  KJ/ mol. Lauron Pernot (136) interpreted the similar global activation energy in terms of acidic hydroxyl and metal-oxo groups, linked to the same surface transition metal atom. Continuously, dehydration occurs on Brönsted acid sites, whereas isomerisation occurs on metals-oxo ones. Kinetic coupling of two catalytic cycles, linked by the same elementary step (MBOH chemisorption), leads to the saturation of all surface active sites by the reactant.

Figure 43 shows the Arrhenius diagram for the amphoteric pathway of the MBOH test reaction.

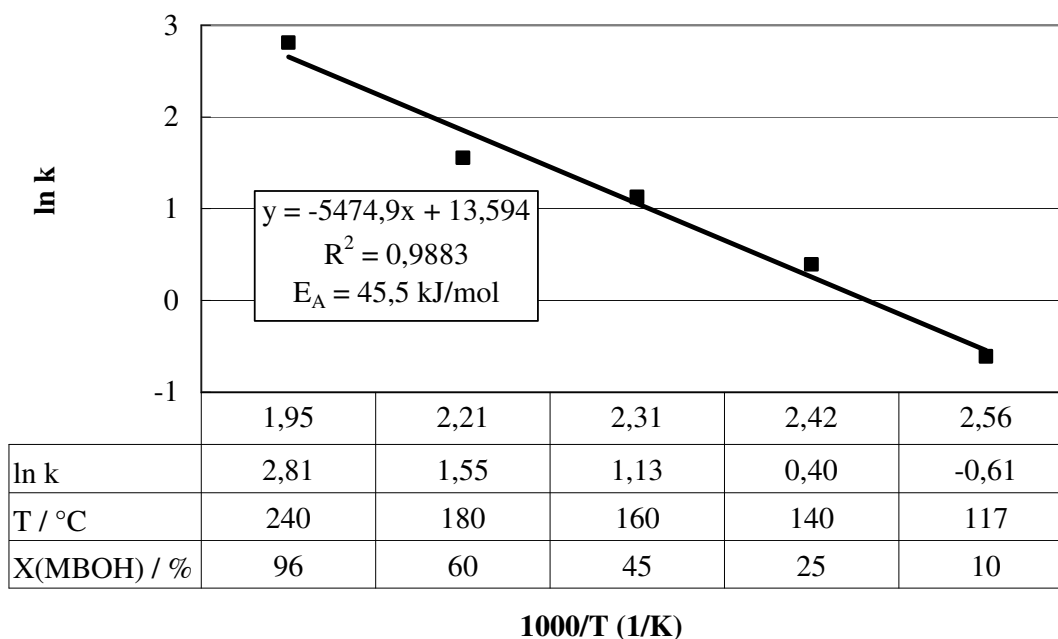


**Figure 44. Arrhenius diagram for amphoteric pathway of the MBOH test reaction**

From the presented diagram it can be seen that the activation energy occurring for this reaction is about  $E_a = 45.5$  kJ/ mol for the temperature range of 117 °C - 240 °C.

The similar kinetic data in the present study for acidic and amphoteric pathways of the MBOH conversion (45 kJ/mol) permit to propose that the rate determining step in the acidic and amphoteric pathway is the same.

#### 4.7 Basicity of hydrotalcites derived from mixed Mg-Al oxides studied by MBOH test reaction

The catalytic performance of the hydrotalcites derived from mixed Mg-Al oxides was studied at 120 °C (figure 45) and 160 °C (figure 46).

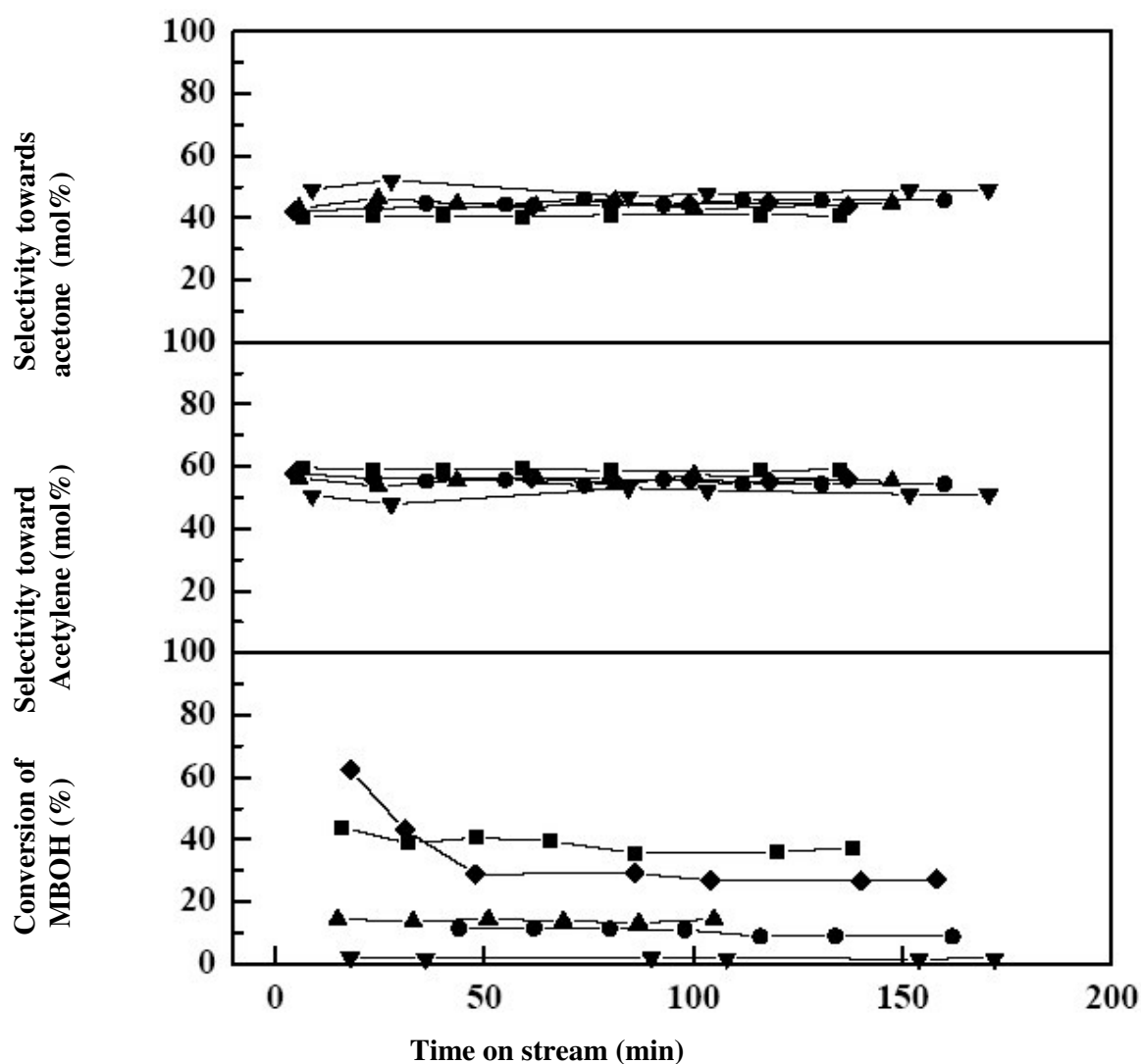
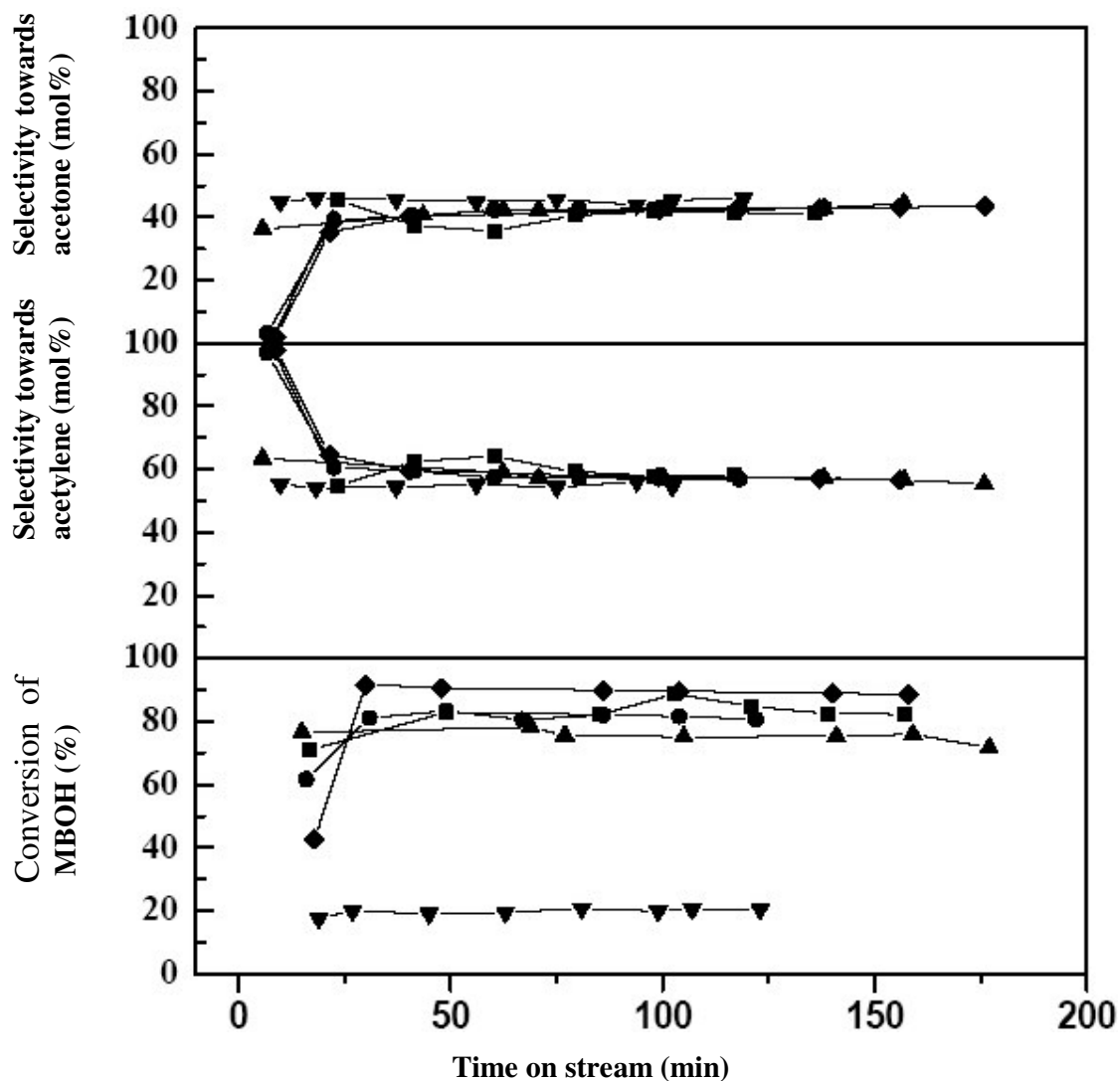


Figure 45. Conversion of MBOH and selectivities towards the products at 120 °C on hydrotalcites intercalated different anions

■ cHT-CO<sub>3</sub> ● cHT-Cl ▲ cHT-HPO<sub>4</sub> ▼ cHT-SO<sub>4</sub> ◆ cHT-TA



**Figure 46. Conversion of MBOH and selectivities towards the products conversion at 160 °C on hydrotalcites intercalated different anions**  
 ■ cHT-CO<sub>3</sub> ● cHT-Cl ▲ cHT-HPO<sub>4</sub> ▼ cHT-SO<sub>4</sub> ◆ cHT-TA

Raising the temperature to 160 °C the activity for all catalysts increases (figure 46). The differences are more pronounced. Furthermore, an induction period for cHT-Cl and cHT-TA can be identified. Here, only acetylene was detected. The consumption of acetone can be explained by reactions via a combined aldol condensation and Michael addition according to the mechanism proposed by Armendia et al (8). All this products are strongly adsorbed on the

catalytic sites because no additional peaks were detected. Over all examined mixed Mg-Al oxides the conversion of MBOH proceeds only via a base-catalyzed pathway to yield acetylene and acetone as the major products with a selectivity higher than 99 %, i.e. all catalysts have only basic centers. Additionally, a third compound was detected (< 0.9 wt.%) which could not be identified.

The amount of carbon deposits on the catalyst can be estimated by calculation of the conversion by two methods (figure 47): (i) by using the ratio internal standard to MBOH and (ii) by using the yield of the products. If coke formation would take place, both values should be different. However, it is evident that both values are identically in frame of the accuracy of the experimental error. Nevertheless, the catalysts were slightly brown colored.

Except for cHT-TA all catalysts have a constant activity at 120 °C for about 150 min. After 50 min the activity follows the sequence:

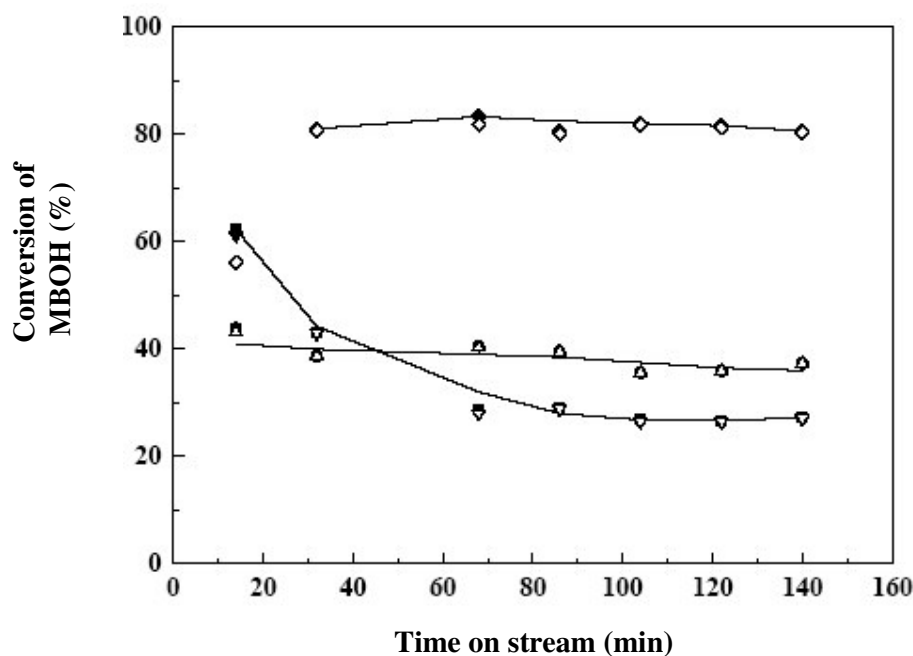


**Figure 47. Comparison of the MBOH conversion of at 120 °C calculated on the base of yields of products (P) and on base of internal standard (I):**  
 ■ cHT-TA (I), ▽ cHT-TA (P), ● cHT-CO<sub>3</sub> (I), △ cHT-CO<sub>3</sub> (P),  
 ◆ cHT-Cl (I, 160°C), ◇ cHT-Cl (P, 160 °C)



It is especially noteworthy that a molar ratio of acetone to acetylene is close but not equal to one, and an excess of acetylene appears in relation to acetone (55...60 to 40...45 %) among the products. Taking into account the data from figure 47, the slight deviation could be explained by the experimental accuracy of gas chromatographic determination of the response factors.

On contrary to this observation Zadrozna et al. (137) showed that over  $\text{Cr}^{3+}$  containing  $\text{AlPO}_4\text{-5}$ , which is a more acidic material, a rapid deactivation connected with a higher yield of acetone in comparison to acetylene was observed. It can be suggested that in case of acid solids a polymerisation process of acetylene occurs on the surface leading to coking and deactivation of the catalyst.

## 4.8 Conversion of isopropanol

### 4.8.1 Determination of basic properties by isopropanol test reaction

In order to compare the results obtained by MBOH test reaction with isopropanol decomposition, the experiments of isopropanol were performed as described in chapter 3.1 on  $\text{SiO}_2/\text{Al}_2\text{O}_3$  with different ratios, calcined for 3 h at 550 °C and 900 °C and on Puralox HT MG 70 (see table 5, 6), for a reaction temperature of 180 °C.

Results show on the one hand that isopropanol is favourably converted over Si/Al (synthesized by Sasol Germany GmbH, see table 7) in a range of 77 – 96 mol% for a reaction temperature of 180 °C, and on the other hand, the reaction shows only the ability to describe the acidity by dehydration of isopropanol to propene. The dehydrogenation process to acetone was not observed independent on pretreatment temperature. Acetone is not formed as product in the isopropanol test reaction despite increasing the reaction temperature up to 250 °C.

In contrast MBOH decomposition occurs on Si/Al solids under the used reaction conditions (chapter 3.1) where basicity decreases with decreasing amount of alumina (see figure 28).

Notwithstanding, acetone and acetylene were detected with high selectivities in case of pure silica (see figure 28) but this result is not representative for the basic properties, because MBOH conversion is very low over pure silica and does not exceed 2 %.

Table 20 shows a comparison in the selectivities for acetylene and acetone between MBOH and isopropanol test reactions on pure alumina, Si/Al 5 calcined for 3 h at 550 °C, and hydrotalcite Puralox HT MG 70.

**Table 20.** Comparison of isopropanol and methyl butynol conversion at 180 °C

T <sub>reac</sub> = 180 °C	Isopropanol			MBOH		
Sample	X <sub>t.o.s= 18 min</sub> (mol%)	Sel <sub>acetone</sub> (mol%)	Sel <sub>propene</sub> (mol%)	X <sub>t.o.s= 18 min</sub> T <sub>reac</sub> = 180 °C	Sel <sub>acetone</sub> (mol%)	Sel <sub>acetylene</sub> (mol%)
Si/Al (5:95 wt.%) cal. 3 h at 550 °C	78.2	0	100	65.8 <sup>(*)</sup>	21.78	33.1
Pural SBA 150	70.5	0	100	60.0 <sup>(**)</sup>	29.73	36.25
Puralox MG HT 70	10.1	13.3	86.7	81.77	45.7	55.6

<sup>(\*)</sup> Presence of : MBYNE = 38.2 mol%, Prenal = 0.7 and MIPK = 6.3 mol%, <sup>(\*\*)</sup> Presence of : MBYNE = 15.3 mol%, Prenal = 0.0 and MIPK = 19.1 mol%

In the literature, the strength of the basic sites for isopropanol test reaction is still a matter of discussion (138, 139). Lahousse (51) studied different oxides included MgO, ZnO and the corresponding aluminates. It was observed that isopropanol decomposition only occurs on ZnO and Zn aluminates, and was not observed on MgO and Mg aluminates, well known as basic oxide. Because ZnO exhibits redox ability, it facilitates the abstraction of protons from isopropanol what leads to the formation of acetone.

For instance, one notes that introduction of a small amount of a redox component such as Fe and Cr oxides (137) is necessary to reveal the basicity of the catalysts (51). This can be the reason for dehydrogenation of isopropanol on Puralox HT MG 70 to acetone since this catalyst contains 48 ppm of iron<sup>\*</sup>, which could be enough to affect the reaction.

However, Corma (5) found while investigating the conversion of isopropanol on hydrotalcites that acetone is not the only product, but condensation products of acetone or isopropanol were formed. Since acetone is formed and consumed in reactions other than the dehydrogenation of isopropanol, the concentration of acetone cannot be taken as a measure of the dehydrogenation reaction.

Comparing the isopropanol and MBOH test reaction it can be concluded that the results attained over silica alumina solids do not characterize the same surface properties. The disadvantage of the isopropanol reaction is, that only one product can be found at the investigated systems. This can be explained by the un existence of the redox ability of silica alumina solids. Because of that it is not possible with isopropanol test reaction to get more detailed information about the basicity of the catalysts. This results are supported by Lauron-

\* measured by Sasol fabric GmbH

Pernot and Lahousse (51) who are the only ones who did identically statements in a large spectrum of studies.

#### 4.8.2 Determination of activation energy of the isopropanol test reaction

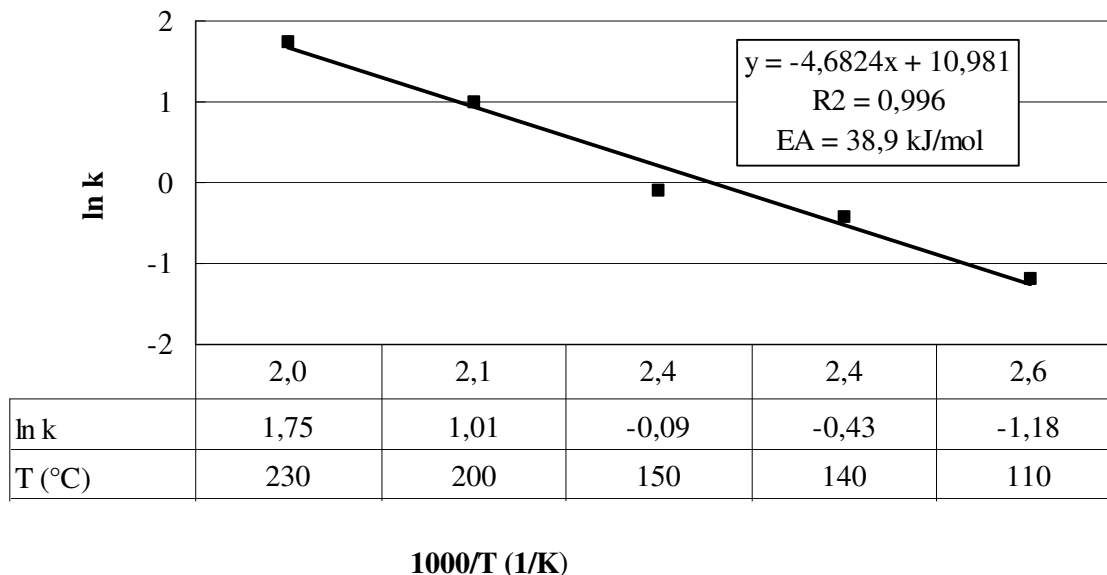
A study of the activation energy of the isopropanol test reaction was performed for the two pathways: basic and acidic at different reaction temperatures. Basic over hydrotalcite with double layer alumina intercalated with  $Zn^{2+}$  (HT Zn/Al<sub>2</sub>O<sub>3</sub>) prepared by Schwieger et. al., acidic over SiO<sub>2</sub>/Al<sub>2</sub>O<sub>3</sub> (40:60 wt.%), both for residence time  $\tau = 0.1$  s.

Table 21 presents initial isopropanol conversions, for the two pathways of the isopropanol test reaction (basic, acidic).

**Table 21.** Initial conversion of isopropanol over different catalysts

Reaction path	Reaction temperature °C	C <sub>3</sub> H <sub>8</sub> O conversion X <sub>15 min</sub> / mol %
Basic over HT- Zn/Al <sub>2</sub> O <sub>3</sub>	110	3.22
	140	6.68
	150	9.22
	200	25.28
	230	45.86
Acidic over Si/Al 40 calcined 3 h at 900 °C	120	69.06
	130	93.12
	140	97.39
	160	99.60
	180	99.64
	200	99.90

Figure 48 presents the Arrhenius diagram for the basic pathway of isopropanol test reaction.



**Figure 48. Arrhenius diagram for basic pathway of the isopropanol test reaction over HT Zn/Al<sub>2</sub>O<sub>3</sub>**

The above diagram shows that an activation energy of  $E_A = 38,9$  kJ/mol is obtained in the temperature range of 110 °C - 230 °C, which means that the reaction is kinetically limited.

The second pathway of the isopropanol test reaction was performed over only acidic catalyst to calculate the apparent activation energy. Two temperature ranges with different activation energies were found (figure 49). The first value of the apparent activation energy is  $E_A = 76.8$  kJ/mol between reaction temperatures of 120 °C and 140 °C and that is characteristic for a kinetic control. The second activation energy for this pathway reaction is observed at reaction temperatures in a range of 160 °C - 200 °C and has a value of  $E_A = 9.6$  kJ/mol where the reaction is near the complete conversion of isopropanol and therewith near the thermodynamic equilibrium (see table 12).

Thus, a controversy correlation was found between the conversion of isopropanol and the apparent activation energies, since the reaction with the lower value of  $E_A$  shows the lower conversion. This can be caused by the dependency of the reaction to the relative concentration of surface active sites and the properties of the catalysts. Since the apparent activation energy which was measured in these experiments does not indicate an activation barrier but presents a general parameter for the temperature dependence of a reaction, it is clear that the reaction with the higher apparent activation energy increases faster with increasing temperature.

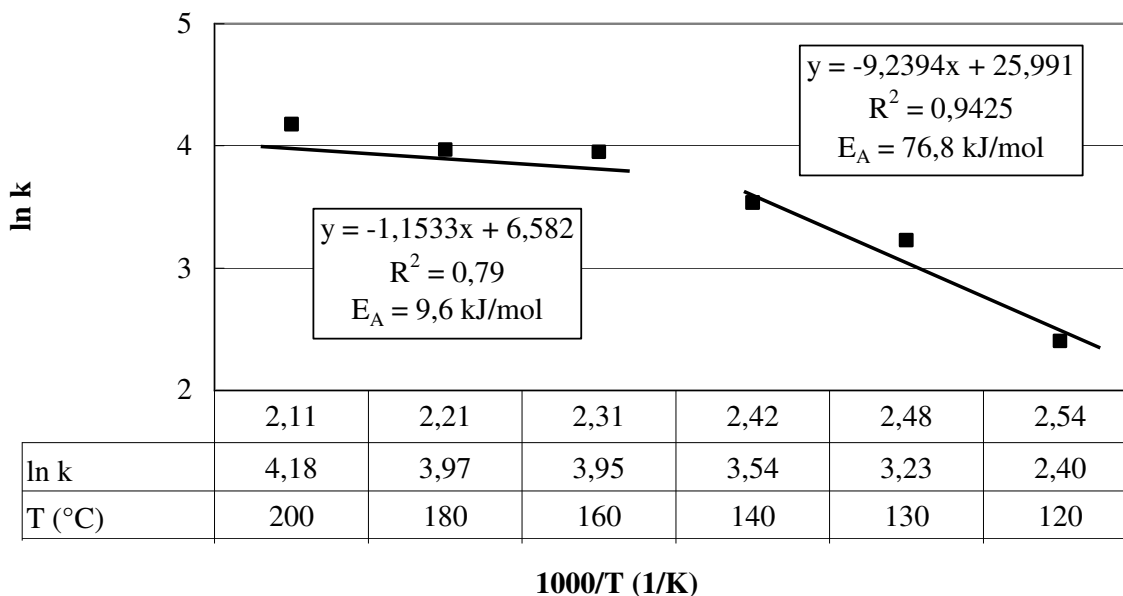


**Figure 49. Arrhenius diagram for the acidic pathway of the isopropanol test reaction over Si/Al 40**

In addition, the activation energy for the basic pathway of isopropanol conversion to acetone was found to be lower than the activation energy for acidic pathway to propylene. A reason can be that the formation of isopropanol on Zn/Al<sub>2</sub>O<sub>3</sub> to acetone is probably associated with the formation of an intermediate product like 2-propoxid and the role of basic centers on its formation is limited. Díez (140) measured the activation energy for acetone formation on MgO, Li/MgO and Cs/MgO samples in the temperature range 240 °C - 280 °C in order to confirm that acetone formation occurs on strong basic sites. It is observed that the  $E_A$  value decreases with increasing relative concentration of high-strength base sites. The highest activation energy was measured on Li/MgO (119 kJ/mol), which presents the lowest average basic strength.

#### 4.9 Knoevenagel condensation

The dependency of the malonitrile conversion on reaction time over different types of silica alumina and hydrotalcites (see table 7, 8) is depicted in figure 50.

The conversion was normalized to the maximum value of the stoichiometry of limiting compounds (i.e. benzaldehyde). As blind probe, is denoted a sample without catalyst. (see experimental part, chapter 3.4).

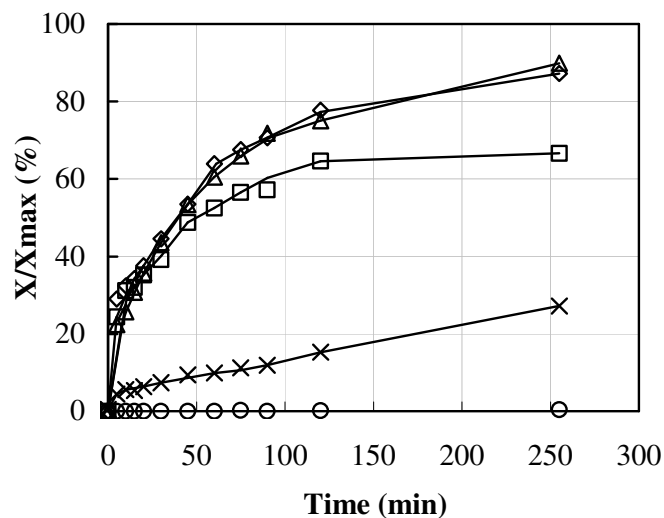


**Figure 50. The normalised conversion of malononitrile over different types of Puralox**

amount of the catalyst: 0.2 g, malononitrile: 47.5 mmol, benzaldehyde: 15.8 mmol  
 △ Puralox SBA 200 ◇ Puralox SBA 150 □ Puralox Mg 30 × Puralox MG 70  
 ○ blind probe

Benzylidenmalononitrile was detected over studied samples as the only product. The highest conversion of malononitrile was reached over Puralox SBA 200 and Puralox SBA 150. On the other hand, Puralox containing different amounts of MgO (Puralox MG 30 and Puralox MG 70) show lower conversion of malononitrile. The smaller the quantity of MgO in the catalyst, the higher is the conversion. In the present study the conversion in Knoevenagel condensation can be only related to the alumina content, and that the yield of benzylidenmalononitrile for Puralox MG 30 is higher than of Puralox MG 70. Because only one product (benzylidenmalononitrile) could be detected, the conversion is considered to be dependent of the yield of benzylidenmalononitrile and takes the following sequence:

Alumina: Puralox SBA 150  $\cong$  Puralox SBA 200 equation (22)

Puralox Puralox Mg HT 70 < Puralox Mg HT 30 equation (23)

A correlation of the basic strength (yield of benzylidenmalononitrile) found at Knoevenagel condensation to the basic strength found at the MBOH test reaction seems to be conformed on alumina SBA 200 and 150 while basicity for Puralox Mg 70 and Puralox Mg 30 in the

Knoevenagel reaction shows a controversy correlation to that observed in MBOH reaction. This can be ascribed to the contents of MgO in the catalyst.

Skarzewski and Zon (143) reported on the oxidative coupling of dimethyl malonate of tetramethyl ethene-1,1,2,2-tetracarboxylate using a cerium ammonium nitrate/magnesium oxide catalyst. The reaction does not take place in the absence of MgO towards Knoevenagel condensation. Other researches (144) observed by condensation of phenyl sulfonylacetonitrile and benzaldehyde on MgO-Al<sub>2</sub>O<sub>3</sub> mixed oxides derived from hydrotalcite an increase in basicity when introducing Al<sub>2</sub>O<sub>3</sub> in the MgO structure.

#### **4.9.2 Knoevenagel condensation over layer double hydroxaltes (LDHs)**

Figure 51 presents the possible maximum conversion of malononitrile over calcined hydroxaltes intercalated with different anions (CO<sub>3</sub><sup>2-</sup>, SO<sub>4</sub><sup>2-</sup>, Cl<sup>-</sup>, HPO<sub>4</sub><sup>2-</sup> or terephthalate)

The yield of the product benzylidenmalononitrile increases with time over hydroxaltes intercalated different anions. LDHs possess basic sites and give arise to a smoothly condensation, because no other products (such as benzoic acid) were detected in the reaction medium. Additionally, the yield of benzylidenmalononitrile shows proportional dependence on reaction time and the maximum yield observed after 4 hours was high over the catalysts cHT-CO<sub>3</sub>, cHT-HPO<sub>4</sub>, and cHT-Cl respectively, while cHT-TA and cHT-SO<sub>4</sub> show lower yields, what can be ascribed to weaker basic centers. LHDs catalysts show good activity to convert malononitrile. Activity depends on the chemical composition and on the interlayer anion.

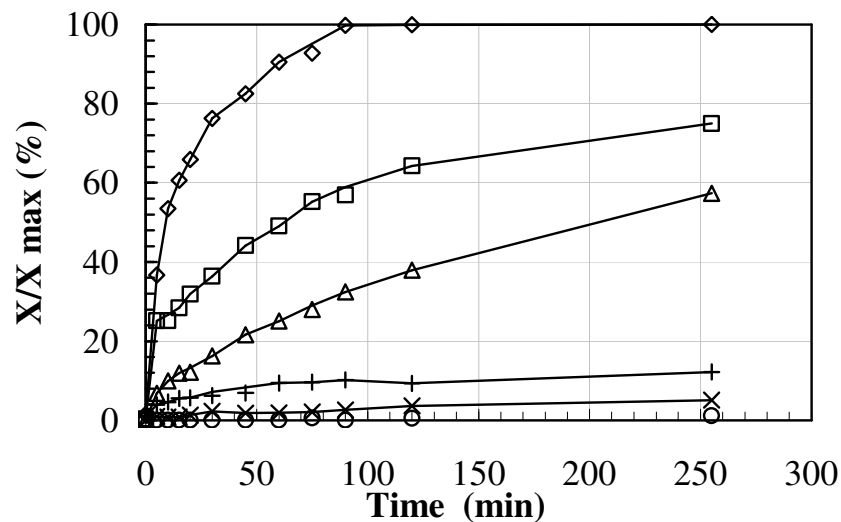


**Figure 51. Normalized conversion of malononitrile over hydrotalcites intercalated different anions**

amount of the catalyst: 0.2 g, malononitrile: 47.5 mmol,

benzaldehyde: 15.8 mmol

◇cHT-CO<sub>3</sub> □ cHT-HPO<sub>4</sub> △ cHT-Cl + cHT-TA × cHT-SO<sub>4</sub> ○ blind probe

A straight correlation between the normalised conversion of benzylidenmalononitrile and the surface areas of the as-synthesized samples of hydrotalcites intercalated with different anions and with desorbed amount of CO<sub>2</sub> is presented in table 22.

When the normalised conversion is correlated to the basicity ( $\mu\text{mol CO}_2/\text{m}^2$ ), the investigated samples can be classified into two groups (see table 22), regarding to their basic strength, strong and weak. To the strong group belong samples like cHT-HPO<sub>4</sub>, cHT-CO<sub>3</sub>, and cHT-Cl while to the weak group cHT-SO<sub>4</sub> and c-HT-TA are belonging



**Table 22.** Surface areas and desorbed amount of CO<sub>2</sub> for hydrotalcites (as-synthesized) intercalated with different anions correlated to the normalized conversion of benzylidenmalononitrile (X<sub>n</sub>) after 50 min

Sample	X <sub>n</sub>	BET surface area	Desorbed amount of CO <sub>2</sub>	X <sub>n</sub> / BET surface area	X <sub>n</sub> / desorbed amount of CO <sub>2</sub>
	%	area (m <sup>2</sup> /g)	μmol/g		μmol/g
cHT-CO <sub>3</sub>	82.5	264.0	46.7	0.31	1.76
cHT-Cl	30.1	167.0	23.1	0.14	1.1
cHT-HPO <sub>4</sub>	44.1	130.0	6.5	0.34	6.7
cHT-SO <sub>4</sub>	1.9	22.0	1.8	0.08	1.0
cHT-TA	4.4	285.0	5.3	0.01	0.8

#### 4.9.3 Basicity of calcined silica-aluminas

To characterize the basicity of silica-alumina catalysts with varying ratios, the catalysts were used in Knoevenagel condensation.

Figures 52, 53, respectively, illustrate the maximum conversion of malononitrile in dependency of reaction time over different SiO<sub>2</sub>/Al<sub>2</sub>O<sub>3</sub> ratios calcined at 550 °C and 900 °C.

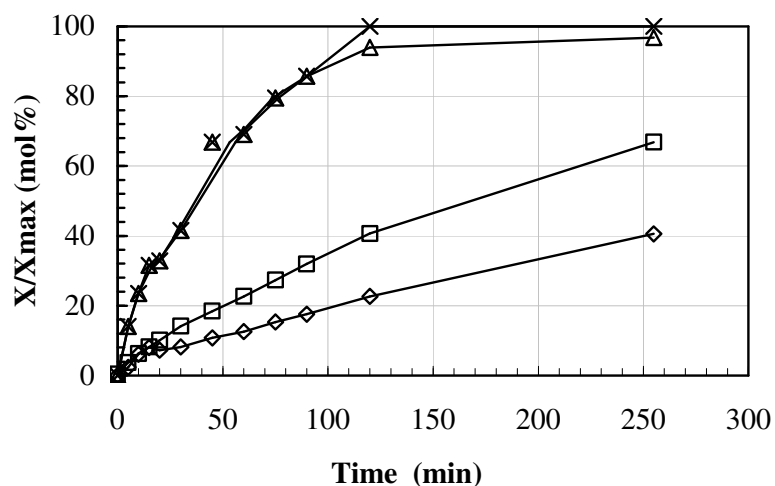


**Figure 52.** The possible maximal conversion of malononitrile over different Si/Al ratios calcined 3 h at 550 °C

amount of the catalyst: 0.2 g, malononitrile: 47.5 mmol, benzaldehyde: 15.8 mmol

× Si/Al 5    Δ Si/Al 10    □ Si/Al 20    ◇ Si/Al 40

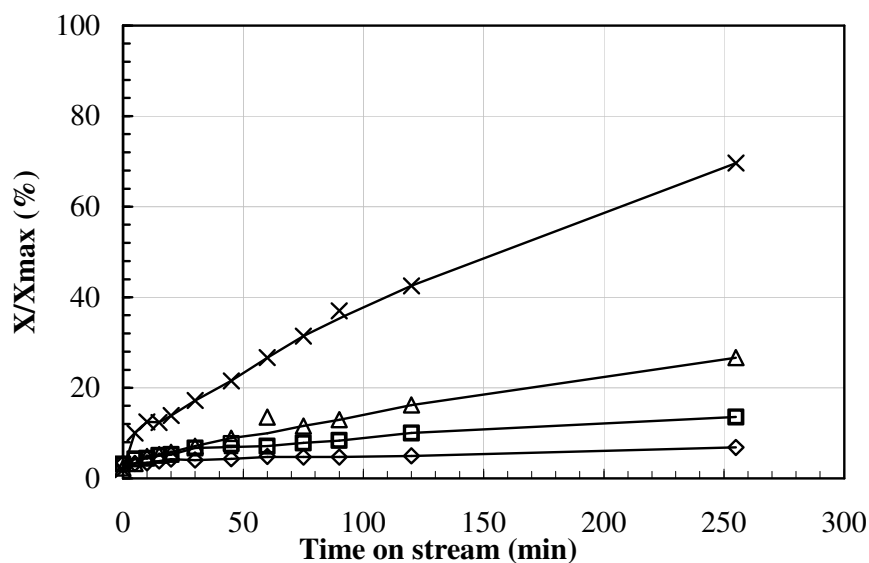


**Figure 53. The possible maximal conversion of malononitrile over different Si/Al ratios calcined 3 h at 900 °C**

amount of the catalyst: 0.2 g, malononitrile: 47.5 mmol,

benzaldehyde: 15.8 mmol

× Si/Al 5    △ Si/Al 10    □ Si/Al 20    ◇ Si/Al 40

It has been observed that the conversion of malononitrile is higher if the catalyst contains small percent quota of SiO<sub>2</sub> (Si/Al 5) independently of the preparation temperature.

In addition, a relation of malononitrile conversion to the calcination temperature exists as Si/Al calcined at 550°C shows higher catalytic activity than the one calcined at 900 °C. The percent content of SiO<sub>2</sub> and the basicity increases in the series:

$$\text{Si/Al 40} < \text{Si/Al 20} < \text{Si/A 10} < \text{Si/Al 5} \quad \text{equation (24)}$$

On the other hand, a correlation of the basic strength of Si/Al catalysts determined with MBOH test reaction and Knoevenagel condensation is presented by figure 54a, and 54b for the group of catalysts calcined for 3 h at 900 °C.

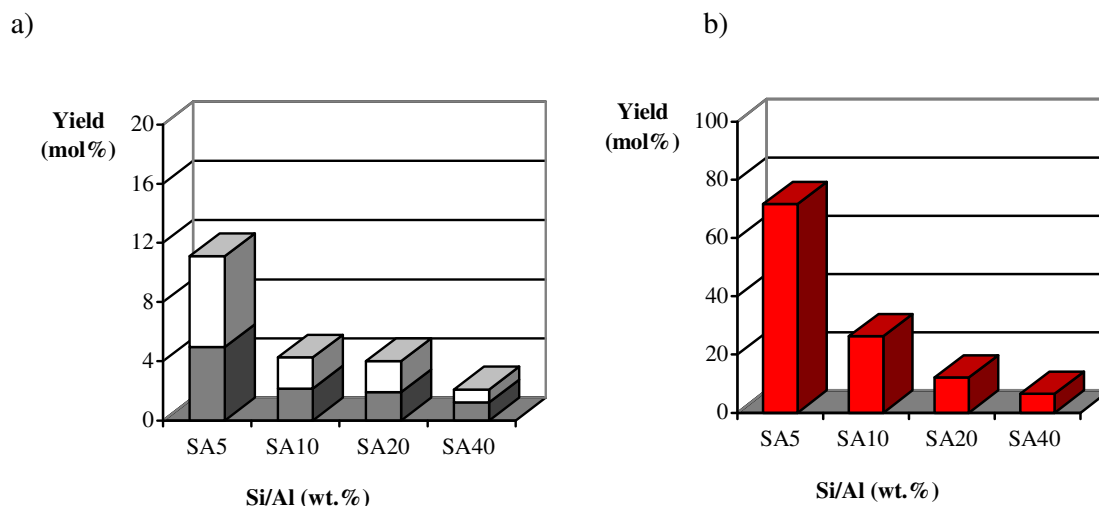


**Figure 54. Correlating the basic strength over different Si/Al ratios calcined 3 h at 900 °C by**

a) MBOH test reaction

Catalyst: 0.2 g, time on stream: 125 min, reaction temperature: 180 °C

□ acetylene                      ■ acetone

b) Knoevenagel condensation

■ benzylidenmalononitrile

amount of the catalyst: 0.2 g, malononitrile: 47.5 mmol

benzaldehyde: 15.8 mmol, time reaction: 130 min

reaction temperature: 97 °C

The results show that the MBOH and Knoevenagel condensation test reactions used in the present study seem to characterize the same basic properties, and with both reactions the same sequence of basic activity of the Si/Al catalysts is achieved.

In addition Knoevenagel condensation shows advantages like the easy separation of the catalyst by simple filtration and from above diagram (figure 54) it is clear that Knoevenagel condensation presents better visibility of differences in basic strength than the MBOH test reaction for the studied silica-alumina solids, because the yield in Knoevenagel condensation is 5 times higher than in MBOH test reaction for the samples Si/Al 10 and Si/Al 20, see figure 54 a and 54 b.

## 5. Conclusions

In the present thesis, three test reactions were performed to verify their suitability for characterization of acidic and basic properties of solid catalysts. The test reactions investigated were methyl butynol and isopropanol conversion in gas phase and Knoevenagel condensation in liquid phase.

To evaluate the test reactions for the classification of catalysts, the catalytic characteristics obtained of MBOH test reaction in the gas phase were correlated with the results of other characterisation methods applied to the surface like BET surface measurement, temperature programmed desorption of ammonia (NH<sub>3</sub>-TPD) and carbon dioxide (CO<sub>2</sub>-TPD). Other characteristic methods like FTIR spectroscopy or XRD have been taken into account. In addition, results obtained for Knoevenagel condensation in liquid phase were correlated with temperature program desorption of carbon dioxide.

Looking at the conversion of methyl butynol on silica-alumina with different Si/Al ratios and prepared with different calcination temperatures (550 °C and 900 °C) MBYNE was found to be the major product, independent of the reaction temperature. The selectivity of MBYNE is proportional to the reaction temperature and to the content of silica. This presents that MBYNE formation is an indication for acidic sites in the investigated solids.

The product of the amphoteric reaction - MIPK - was detected in range upto 30 mol% over silica-alumina 5 calcined at 550 °C at a reaction temperature of 120 °C. The selectivity of MIPK decreases with loading more silica to the catalysts. At the higher reaction temperature of 180 °C MIPK was also noticed as a product of the decomposition of methyl butynol but only over silica-alumina 5, and silica-alumina 10. Plotting the selectivity of MIPK to the initial conversion of methyl butynol MIPK is proved to be a primary product of MBOH conversion. This is in contrast with literature's opinion which always described the formation of MIPK as a secondary product. The primary formation can be explained by direct proton attack to the triple bond of MBOH. The criterias for the proceeding of this attack is not only the strength or amount of the acid sites but also the presence of a specific aluminosilicate phase. This conclusion can be drawn from the observation, that all silica-aluminas show a high amount of acid sites in the NH<sub>3</sub>-TPD whether they are able to form MIPK or not. Additionally MIPK is formed on the silica alumina samples (i.e. Si/Al 5 and Si/ Al 10)

synthesized by Sasol Germany GmbH and not on solids which have also strong acid sites like zeolites (see table 14).

The proposed specific aluminosilicate phase is in line with considerations of Knözinger (134), who presented a model depicting different surface compositions of aluminosilicates for different types of aluminophase structures (see scheme 37).

Moreover, the influence of the addition of water of MIPK product for the conversion of MBOH was taken into account. In the literature (48) explained that MIPK formation is affected by adding water to MBOH. Therefore, the effect of water on the conversion of MBOH was studied in the present work on catalysts such as hydrotalcites Puralox MG 70, zeolites, pure alumina and silica-aluminas with different ratios.

The study with these catalysts shows no changes in the results compared to those obtained by MBOH test reaction without additional water, while in case of bulk metal oxides supported on alumina the selectivities of MIPK and HMB increased after addition of water. What can be concluded from this observation is that, the formation of MIPK or HMB is not resulted exclusively in the proton attack by water dissociation as proposed in the literature (48) but strongly depends on the catalysts structure. Then, an attack of the triple bond of methylbutynol by strong acid protons to form MIPK is more feasible as proposed in this thesis for the mechanism on silica-alumina (see scheme 12 route a). Additionally, in this thesis the mechanisms for the basic and acidic pathways for methylbutynol conversion are explained in detail (chapter 4.5.3 and 4.5.4, respectively).

Acetone and acetylene were found to be the products of the basic pathway of the conversion of MBOH. During basic reactions, deactivation of the catalyst was observed with time on stream at a lower reaction temperature of 120 °C for all catalysts. When the reaction temperature raised to 180 °C no deactivation was observed for silica-alumina samples, which are the less acid ones.

The decrease in the activity at lower reaction temperature can be explained by a strong adsorption of the products, namely acetone, on the solids surface. Carbon deposit can be estimated by a comparison of the conversion calculated by using the yield of the products with the conversion calculated by using the ratio of the internal standard. If carbon deposition takes place, a difference between both conversions should be observed. However, it was found a deviation for silica alumina catalysts about 4 % at the lower reaction temperature of 120 °C only and that for both calcination temperatures (i.e. 550 °C and 900 °C). This again

supports the idea that carbon deposition could be responsible for the decrease in the surface area over silica alumina samples, while a lower deviation of about 0.5% was found at higher reaction temperature of 180 °C while the decrease of surface area was lower for this samples. As another conclusion it can be extracted, that the deactivation is strongly dependent from the reaction temperature, but the amount of silica loaded to the catalyst affects the adsorption of the products only slightly.

Beside silica-aluminas other groups of catalysts were examined by conversion of methyl butynol: hydrotalcites intercalated with different anions and metal oxides. For hydrotalcites intercalated with different anions it can be concluded that the nature of the interlayer anions strongly influence surface acidity and basicity of the obtained mixed metal oxides and the pore diameter is also influenced by the interlayer anions present in the hydrotalcite-like precursor. Finally the excess of acetylene in comparison to the expected stoichiometry value (acetylene/ acetone = 1) indicates coke formation.

Measuring the apparent activation energy for basic pathway of the MBOH test reaction results in a value of approximately  $E_A = 80$  kJ/mol aside the thermodynamic equilibrium. The apparent activation energy for the conversion of MBOH at acid and amphoteric sites was calculated and found as about 35 kJ/mol lower than at basic sites.

The second gas phase test reaction in this thesis was the conversion of isopropanol. The obtained activation energy for the basic pathway reaction is approximately  $E_A = 40$  kJ/mol in the region of kinetic limitation. In the acidic pathway the apparent activation energy was determined with  $E_A = 77$  kJ/ mol aside complete conversion.

Comparing the isopropanol and MBOH test reaction it can be concluded that the results attained over silica-alumina solids do not characterize the same surface properties. In the conversion of isopropanol propene was found as the only product over the investigated systems like hydrotalcites or silica-aluminas. This can be explained by the un existence of redox ability of silica-alumina solids and hydrotalcites like Puralox MG 70. Over samples containing redox compounds with alumina ( $Zn/Al_2O_3$ ) acetone was detected as main product. Due to the fact that only one product is formed it is not possible with isopropanol test reaction to get more detailed information about the basicity of the catalysts.

In this study the Knoevenagel condensation of benzaldehyde and malononitrile was taken to characterize the basicity of silica-alumina solids in liquid phase. The results show that MBOH and Knoevenagel test reactions characterize the same basic properties, since with both reactions the same sequence of basic activity of the silica-alumina catalysts is achieved.

Furthermore, Knoevenagel condensation shows advantages like the easy separation of the catalyst by simple filtration and additionally Knoevenagel condensation generates better visibility of differences in basic strength of studied silica alumina solids than MBOH test reaction, because the yield in Knoevenagel condensation is up to 5 times higher than in MBOH test reaction (see figure 54 a and 54 b).

Besides the comparison of different test reactions, in this work correlations between characteristics derived from MBOH test reaction with physical and chemical properties of the studied solids are presented.

For silica alumina solids, doping alumina with silica does increase the specific surface area continuously the more silica is added. Characterization with  $\text{NH}_3$ -TPD shows that the maximum adsorption of ammonia at the investigated solids is proportional to the content of alumina. Thereby the sequence of catalysts in activity for acid catalyzed reaction is the same regardless whether determined by MBOH test reaction or by  $\text{NH}_3$ -TPD. The same conclusion can be drawn for a correlation of  $\text{NH}_3$ -TPD results with the acidity of bulk metal oxides supported on alumina in MBOH test reaction.

On the other hand, the correlation of the conversion over hydrotalcites intercalated different anions in the liquid phase and  $\text{CO}_2$ -TPD spectra was performed in this work. TPD spectra of carbon dioxide allow to discriminate between weak and strong basic sites. With this results the investigated samples can be classified into two groups, regarding to their basic strength, into strong and weak. To the strong group belong samples like cHT- $\text{HPO}_4$ , cHT- $\text{CO}_3$ , and cHT-Cl while cHT- $\text{SO}_4$  and c-HT-TA belong to the weak group.

Again, the test reaction leads to the same conclusion as the physical method, proving the explanatory power of the test reaction. Altogether it may be said, that test reactions like MBOH conversion and Knoevenagel condensation are valuable and adequate tools for characterization of basic solid catalysts.

## 6. References

- (1) L. John, A. James, *J. Catal.* 2 (1983) 141.
- (2) G. Zhang, H. Hattori, K. Tanabe, *Appl. Catal.* (1988) 36, 189.
- (3) J. Dwyer, *Appl. Catal. A: general* 136 (1996) 303, 321.
- (4) D. Barthomeuf in B. Imelik et al. (eds.): *Catal. in zeolites,*” *Stud. Surf. Sci. Catal.* 5 (1980) 55.
- (5) A. Corma Frones, V. Martin-Aranda, *J. Catal.* 134 (1992) 58.
- (6) L. Pernot, H. Luck, F. Popa, J. M. *Appl. Catal.* 78 (1991) 213.
- (7) A. M. Audry, *J. Catal.* 168 (1997) 471.
- (8) M. Aramendia, A. Borau, V. Garcia, I. M. Jimenez, C. Marrinas, A. Marinas, J. M. Porras, A. Urbano, *Appl. Catal.* 184 (1999) 115.
- (9) A. Tench, J. Pott, G. T. *Chem. Phys. Lett.* 26 (1974) 590.
- (10) R. A. Sheldon, *Chem. Tech*, 3 (1994) 38.
- (11) M. Thomas, T. Maschmeyer, B.F.G. Johnson, D.S. Shephard, *J. Mol. Catal. A:* 141 (1999) 139.
- (12) M. Otake. *Chem. Tech*, 9 (1995) 36.
- (13) S. Ratton, *Chimica Oggi, Catal. Today*, 9 (1998) 33.
- (14) R. Prins, *J. Catal.* 37 (1997) 103.
- (15) A. Martin, B. Lücke, *Stud. Surf. Sci. Catal.* 168 (1994) 1965.
- (16) F. Figueras, D. Tichit, M. Bennani Naciri, R. Ruiz, F.E. Herkes, *Catalysis of Organic Reactions*, Marcel Dekker, New York, (1998) 37.
- (17) M. Utiyama, H. Hattori, K. Tanabe, *J. Catal.* 4 (1978) 237.
- (18) R. L. Nelson, J. Hale, *W. Disc. Faraday Soc.* 52 (1958) 77.
- (19) A. Zechina, M. Lofthouse, F.S.G. Stone, *J. Chem. Soc. Faraday Trans. 1* (1957) 71.
- (20) R. J. Kokes, *Proceedings of the 5<sup>th</sup> International Congress of Catalysis; Miami Beach, FL* (1972) 1
- (21) B. Choudary, M. Kantam, M.L. Reddy, C.R.V.; Rao, K.K., F. Figueras, *J. Mol. Catal. A: Chemical* 146 (1999) 279.
- (22) S. Velu, C.S. Swamy, *Appl. Catal. A: General.* 145 (1996) 225.
- (23) Y. Watanabe, T. Tatsumi, *Mesopor. Mater.* 22 (1998) 399.
- (24) B.F. Sels, D. E. De Vos, P.A Jacobs, *Catal. Rev.* 43 (2001) 443.
- (25) L.M. Bull, A. Cheetham. T. Anupold, Reinhold, A. Samoson, A. Sauer, J. Bussemer, B. Lee, Y. Gann, S. Shore, J. Pines, A. Dupree, *R. J. Am. Chem. Soc.* 120 (1999) 160.



- (26) L.P. Hammett, *Physical Organic Chemistry*, McGraw-Hill, New York 56 (1940) 231.
- (27) J.H. Clark, D. Cork, G. Robertson, *Chem. Lett.* (1983) 1145.
- (28) H. Tsuji, F. Yagi, H. Hattori, H. Kita, In *New Frontiers in Catalysis: Proceedings of the 10th International Congress on Catalysis, 1992, Budapest, Hungary*; Guzzi, L.; Solymosi, F.; Tétényi, P., Ed.; Elsevier (Amsterdam)-Akadémia Kiadó (Budapest), *Stud. Surf. Sci. Catal.*, 75 (1993) 1171
- (29) H. Hattori, *Chem. Rev.* 95 (1995) 537.
- (30) R. Prins, *Catal. Today*, 37 (1997) 103.
- (31) H. Tsuji, F. Yagi, H. Hattori and H. Kita, *Stud. Surf. Sci. Catal.* 75 (1992) 1171.
- (32) J.E. Germain, R. Maurel, *C. R. Acad. Sci.* 247 (1958) 1854.
- (33) P.T. Dawson and P.C. Walker, *Experimental Methods in Catalytic research* eds. R.B. Anderson and P.T Dawson, Academic press, New York, (1976) 211.
- (34) J.W. Niemantsverdriet, *Spectroscopy in catalysis: an introduction*, VCH, Weinheim, Germany (1995) 24.
- (35) T. Ito, Kuramoto, M. Yoshida, M. Tokuda, T. J. *Phys. Chem.* 87 (1983) 411.
- (36) T. Ito, T. Murakami, T. J. Tokuda, *Chem. Soc. Trans. Faraday*. 79 (1983) 913.
- (37) J. Ham, *Chem. Soc.* 74 (1952) 811
- (38) J.C. Lavalley, *Catal. Today*, (1996) 27, 377.
- (39) D. Murphy, P. Massiani, R. Frank and D. Barthomeuf, *J. Phys. Chem.*, (1996) 100, 6731
- (40) A. Auroux, A. Gervasini, *J. Phys. Chem.*, 94 (1990) 6371.
- (41) H. Esemann, H. Forster, E. Geidel, K. Krause, *Microporous Mater.* 6 (1996) 321.
- (42) E. J. Doskocil, R. J. Davis, *J. Catal.* 12 (1999) 188, 353.
- (43) J. W. Hightower, K.W. J. M. Hall, *Chem. Soc.* 25 (1967) 89, 778.
- (44) A. Satoh, H. Hattori, *J. Catal.* 8 (1967) 77-89.
- (45) H. Hattori, M. Itoh, K. Tanabe, *J. Catal.* 2 (1976) 41.
- (46) G. A. Hussein, M. Sheppard, *N. J. Chem. Soc. Faraday Trans.* 17 (1989) 85.
- (47) F. Pepe, F. Stone, *J. Catal.* 56 (1979) 160.
- (48) M. Armendia, A. Borau, V. Jimenez, C. Marinas, J.M. Porras, A. Urbano, *F. J. Catal.* 161 (1996) 829.
- (49) Y. Fukuda, H. Hattori, K. Tanabe, *Bull. Chem. Soc. Jpn.* 51 (1978) 3150.
- (50) J. Anderson, R. M. Boudart, in *Catalysis Science And Technology*, 2 (1982) 232.
- (51) C. Lahousse, J. Bachelier, J. Lavalley, C. Lauron-Pernot, H.A. Govic, *J. Mol. Catal.* 87 (1994) 329.
- (52) A. Gordon, J. R. A. *The Chemist's Companion*, J. Wiley, New York, (1972) 115.

- (53) L. Scott, T. Naples, J. O. Synthesis; 168 (1973) 209.
- (54) P. Thomasson, O. S. Tyagi, H. Knözinger, Appl. Catal. 181 (1999) 181.
- (55) N. E. Fouad, P. Thomasson, H. Knözinger, Appl. Catal. 194/195 (2000) 213.
- (56) U. Meyer, W. F. Hoelderlich, J. Mol. Catal. 142 (1999) 213.
- (57) N. Foud, P. Thomasson, H. Knözinger, Appl. Catal. 196 (2000) 125.
- (58) Organic chemistry, S. 501f, New York. I (1999) 185.
- (59) B. M. Trost, Comprehensive organic synthesis, Pergamon Press, Oxford, 2 (1991) 133.
- (60) J. Muzart, Synth. Commun, 1985, 15, 285, J. Muzart, Synthesis, 1 (1982) 60.
- (61) A. L. Mckenzie, C. T. Fishel, R. J. Davis, J. Catal., 138 (1992) 547
- (62) A. Corma, V. Fornes, R.M. Martin-Aranda, H. Garcia and J. Primo, Appl.Catal. 88 (1990) 237.
- (63) J. Campelo, M. Climent, M. S. Marinas, J. M. React. Kinet. Catal. Lett. 47 (1992) 15.
- (64) J. Yamawaki, T. Ando, Chem. Lett. 24 (1979) 45.
- (65) J. Clark, H. Cork, D.G. Robertson, M. S. Chem. Lett. 13 (1983) 1145.
- (66) P. Laszlo, P. Peuneteau, Tetrahedron Lett. 22 (1983) 2645.
- (67) J. Clark, H. Cork, D. G. Robertson, M. S. Chem. Lett. 31 (1983) 1145.
- (68) D. Villemin, J. Chem. Soc. Chem. Commun, 15 (1983) 1092.
- (69) T. Ando, J. Clark, H. Cork, D. G. Hanafusa, T. Ichihara, J. Kimura, Tetrahedron Lett. 13 (1987) 1421.
- (70) T. Ushikubo, H. Hattori, K. Tanabe, Chem Lett. 7 (1984) 649.
- (71) Suzukamo, G., Fukao, M., Hibi, T., Chikaishi, K. In Acid-Base Catalysis; Tanabe, K., Hattori, H., Yamaguchi, T., Tanaka, T., Ed.; Kodansha (Tokyo)-VCH (Basel, Cambridge, New York, Weinheim) (1989) 405.
- (72) J. Kijenski, R. Hombek, J. Catal. 167 (1997) 503.
- (73) H. Knözinger, H. Ratnasamy, P. Catal. Rev.-Sci. Eng. 24 (1978) 31.
- (74) J. B. Peri, J. Phys. Chem. 1 (1956) 69, 220.
- (75) Gerhartz, Wolfgang, in Ullmann's Encyclopedia of Industrial Chemistry, Aluminum Oxide, Vol. A: (1985) 594.
- (76) K. Wefers, G. M. Bell: Oxides and hydroxides of aluminium, Alcoa T.P. Pittsburg (1972) 19.
- (77) H. Knözinger, In Handbook of Heterogeneous Catalysts, Volume 2 Weitkamp, J., Ed.; VCH (Weinheim) 194/195 (2000) 213.
- (78) M. P. Rosynek and J. W. Hightower, Proc. Int. Congr. Catal. 5<sup>th</sup>, Palm Beach, Fla. 2 (1973) 851.

- (79) H. C. Grange, P. Wiame, *J. Catal.* 50 (2000) 190, 406.
- (80) G. Busca, Lorenzelli, V. Porcile, G. Burton, M. R. Marchand, *Mater. Chem. Phys.* 14 (1986) 123.
- (81) P. Lendor, R. Ruiter, *J. Chem. Soc. Chem. Commun.*, 70 (1991) 1625.
- (82) A. Massinon, J. Odrozola, P. Bastians, R. Conanes, Marchand, R. Laurent, Y. and P. Grange, *Appl. Catal.* 137 (1996) 9.
- (83) P. Grange, P. Bastians, R. Conanec, R. Marchand, Y. Laurent, *Appl. Catal.* 191 (1994) 114
- (84) Granger, P. Lecomte, J. Leclercq, L. Leclercq, *Appl. Catal., A: General* 208 (2001) 369-379
- (85) P. Hathway, E. Davis, M. E. *J. Catal.* (1989) 119, 497.
- (86) P. Galich, N. Golubchenko, I. T. Gutray, V. S. Ilin, V. G. Naimark, I. E. *Ukr. Khim. Zh. Chem. Abst.* 64 (1966) 12571.
- (87) D. Bryant, E. Krancich, *J. Catal.* 8 (1967) 8.
- (88) T. Yashama, K. Yamazaki, H. Ahmad, M. Katsuta, N. Hara, *J. Catal.* 17 (1970) 151.
- (89) T. Yashima, K. Sato, T. Hayasaka, N. Hara, *J. Catal.* 26 (1972) 303-312.
- (90) R. Allmann, *Chimia* 24 (1970) 99.
- (91) H. F. Taylor, *W. Miner. Mag.* 37 (1969) 338.
- (92) F. Cavani, F. Trifirò, A. Vaccari, *Catal. Today*, 2 (1991) 11.
- (93) S. Miyata, *Clay Miner.* 23 (1975) 369.
- (94) V. R. Constantino, L. Pinnavaia, T. J. *Inorg. Chem.* 34 (1995) 883.
- (95) E. Narita, P. D. Kaviratna, T. J. Pinnavaia, *J. Chem. Soc.* (1993) 60.
- (96) J. Evans, M. Pillinger, J. Zhang, *J. Chem. Soc. Dalton Trans.* (1996) 2963.
- (97) R. Dziembaj, L. Chmielarz, A. Węgrzyn, P. Kuśtrowski, *Bull. Pol. Acad. Sci. Chem.* 50 (2002) 237.
- (98) B. Pérez, M. E. Ruano-Casero, R. Pinnavaia, T. J. *Catal. Lett.* 11 (1991) 55.
- (99) J.W. Boclair, P. Braterman, S. Brister, B. D. Wang, Z. F. Yarberry, *J. Solid State Chem.* 161 (2001) 249.
- (100) V. Rives, M. Ulibarri, *Coord. Chem. Rev.* 181 (1999) 61.
- (101) S. Miyata, T. Kumura, *Chem. Lett.* 24 (1973) 843.
- (102) M. Meyn, K. Beneke, G. Lagaly, *Inorg. Chem.* 29 (1990) 5201.
- (103) S. P. Newman, W. Jones, *New J. Chem.* (1998) 105.
- (104) B. Choudary, M. Kavita, B. Chowdari, N. S. Sreedhar, B. Kantam,

- Catal. Lett. (1988) 78.
- (105) J. C. Roelofs, A. Lensveld, D. J. van Dillen, A.J. de Jong, J. Catal. 203 (2001) 184.
- (106) J. I. Di Cosimo, C. R Apesteguía, M.Ginés, E. Iglesia, J. Catal. 190 (2000) 261.
- (107) R. Kaiser, Chromatography in the Gas Phase, Vol. 1: Gas Chromatography; Bibliographic Institute High School Pocketbooks, Vol. 22, Ed. 2 (1973) 220.
- (108) D. Mcauliffe, S. Barratt, R. J. Fay in Comprehensive Coordination Chemistry, Pergamon press, Oxford, 3 (1987) 363.
- (109) P. Kuśtrowski, L. Chmielarz, E. Bożek, M. Sawalha, F. Roessner, Advanced Mater. 39 (Nr.2) (2004) 263.
- (110) Y. Ono, T. Baba, Catal. Today 38 (1997) 321.
- (111) D. Martin, D. Duprez, J. Mol. Catal. A: Chemical, 118 (1997) 113.
- (112) A. Guida, M. Lhouty, M. H. Tichit, D. Figueras, F. P. Geneste, Appl. Catal. A: General 164 (1997) 251.
- (113) M. A. Drezdson, Inorg. Chem. 27 (1988) 4628.
- (114) K. Yoo, P. G. Smirniotis, Appl. Catal. A: General, 227 (220) 171.
- (115) J. Scherzer, Catal. Rev. Sci. Eng. 31 (3) (1993) 215.
- (116) J. Shen, M. Tu. Hu. J. Solid state Chem. 137 (1998) 295.
- (117) S. Velu, V. Ramkumar, A. Narayanan, C. S. Swamy, J. Mater. Sci. 32 (1997) 957.
- (118) E. Kanezaki, K. Kinugawa, Y. Ishikawa, Chem. Phys. Lett. 226 (1994) 325.
- (119) R. K. Kukkadapu, M.S. Witkowski, J.E. Amonette, Chem. Mater. 9 (1997) 417.
- (120) M. Badreddine. A. Legrouri, A. Barroug, A. De Roy, J.P. Besse, Mater. Lett. 38 (1999) 391.
- (121) J. Klopogge. T. R. L. Frost, J. Solid State Chem. 146 (1999) 506.
- (122) M. A. Ulibarri, F. M. Labajos, V. Rives, R. Trujillano, W. Kagunya, W. Jones, Inorg. Chem. 33 (1994) 2592.
- (123) M. J. Hernandez-Moreno, M. A. Ulibarri, J. L. Rendon, C. J. Serna, Phys. Chem. Minerals, 12 (1985) 34.
- (124) P. Kuśtrowski. A. Rafalska-Łasocha, D. Majda, D. Tomaszewska, R. Dziembaj, Solid State Ionics, 141-142 (2001) 237.
- (125) W. T Reichle, S.Y. Kang, D. S. Everhardt, J. Catal. 101 (1986) 352.
- (126) Malherbe. F. J.P. Besse, J. Solid State Chem. 155 (2000) 332.
- (127) J. Bernholc, J. A. Horsley, L. Murrel, L.G. sherman, S. Soled, J. Phys. Chem. 91 (1987) 1526.
- (128) M. Huang, S. Kaliaguine, Catal. Lett. 18 (1993) 373.
- (129) C. Mercier, G. Allmang, M. Aufrand, Appl. Catal. A: General 114 (1994) 51

- (130) M. Fernandez, X. Odriozola, J. Stud. Surf. Sci. Catal. G. Poncelet, J. Martens, 214 (1998) 73.
- (131) W. Daniell, H. Knözinger, Appl. Catal. A: General, 196 (2000) 247.
- (132) A. Brehm, Praktikumsanleitung Technische Chem., university of Oldenburg, 2003
- (133) A. Rausch, Diploma thesis, Hydroamination of ethanol, Oldenburg, (2003)
- (134) H. Knözinger, Huber, S. J. Chem. Soc. Faraday Trans. 94 (1998) 2047.
- (135) J. Gmehling, Dortmund Datenbank, DDBST GmbH, Oldenburg, (2004).
- (136) V. Keller, H. Lauron Pernot, J. Molec. Catal. A: Chemical 188 (2002) 163.
- (137) G. Zadrozna, E. Souvage, J. Kornatowski, J. Catal. 208 (2002) 270.
- (138) G. Busca, Catal. Today 41 (1998) 191.
- (139) T. Baba, G. Kim, J. Ono, Chem. Soc. Faraday Trans. 88 (1992), 891.
- (140) V. K. Díez, CR. Apesteguía, J. I. Di Cosimo, Catal. Today 63 (2000) 53.
- (141) D. Kulkarani, I. E. Wachs. Appl. Catal. A: General 237 (2002) 121.
- (142) K.C. Waugh, M. Bowker, R. W. Petts, H. D. Vanderwell, J. O Malley, Appl. Catal. 25 (1986) 21.
- (143) J. Skarzewski and J. Zon, Synth. Commun, 25, 2953 (1995).
- (144) M. j. Climent, A. Corma, R. Guil-Lopez, S. Iborra, J. Primo. Catal. Lett. 59 (1999) 33.

## 7. Appendix

### 7.1 - Empty reactor test for MBOH test reaction

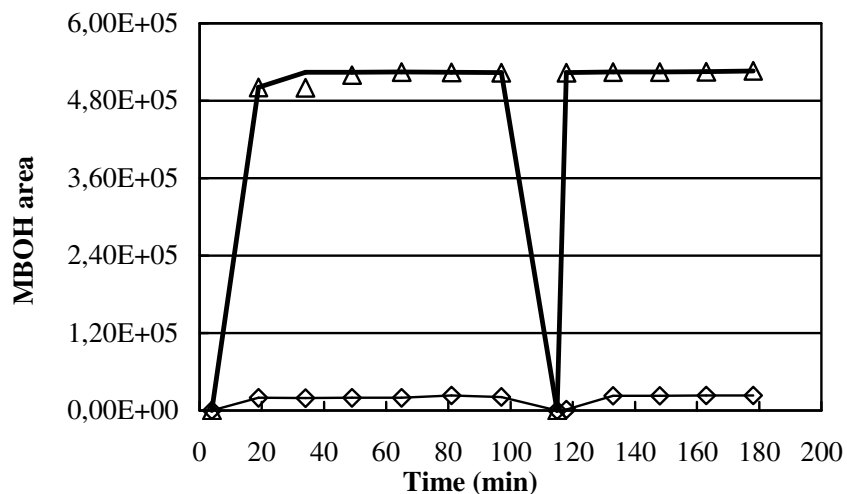


**Figure A-1. Test with empty reactor, T = 180 °C**

- △ Peak area of MBOH
- ◇ Peak area of n-hexane

### 7.2 Verification of carbon deposit for MBOH test reaction

**Table A-1.** Data from the calculating carbon deposition on basic catalyst (Puralox MG 70)

TOS (min)	Area MBOH	Area ACY	Area AON	A (MBOH)	A (ACY)	A (AON)	C actual	C target	C deposit
0	402439	60763	47018	442241	60763	70527	573531	594148	20618
17	416413	66746	51079	457597	66746	76619	600961	624462	23501
35	444935	67724	51629	488940	67724	77444	634107	658250	24143
53	432158	60264	46084	474899	60264	69126	604289	625559	21270
71	433747	59309	45869	476645	59309	68804	604758	624918	20160
90	450429	57135	44028	494977	57135	66042	618154	637814	19661
108	428035	59641	46356	470368	59641	69534	599543	619471	19928

A : area

ACY: acetylene , AON: acetone, C : Carbon

**Table A-2.** Data for the carbon deposit of MBOH conversion , carbon deposit of the selectivities of acetylene and acetone

TOS min	X(MBOH) %	S(ACY) %	S(AON) %	S(C deposit) %
0	25.6	40.0	46.4	13.6
17	26.7	40.0	45.9	14.1
35	25.7	40.0	45.7	14.3
53	24.1	40.0	45.9	14.1
71	23.7	40.0	46.4	13.6
90	22.4	40.0	46.2	13.8
108	24.1	40.0	46.6	13.4
126	21.8	40.0	46.6	13.4
144	22.1	40.0	46.5	13.5

TOS: time on stream

S : Selectivity, ACY: Acetylene, AON: Acetone

### 7.3 Analysis and calculations

#### 7.3.1 Report from Identification of MIPK

```

Area Percent Report

Data File : D:\HPCHEM\1\DATA\ROESSNER\MIPK.D          Vial: 1
Acq on   : 5 Jul 2002 10:23                          Operator:
Sample   : Produkt aus HMB-Reaktion                  Inst  : GC/MS Ins
Misc     :                                           Multiplr: 1.00
                                           Sample Amount: 0.00

MS Integration Params: autoint1.e

Method    : D:\HPCHEM\1\METHODS\AK20319M.M (Chemstation Integrator)
Title     :

Signal    : TIC

peak  R.T.  first  max  last  PK  peak  corr.  corr.  % of
#     min   scan  scan scan  TY  height area  % max. total
-----
1    4.100   852   874   915  BB 2  3159716 141905877 15.14%  8.766%
2    4.389   923   937   976  BB 2   117677   3481064   0.37%   0.215%
3    4.866  1026  1041  1076  BB   1241484 29319740  3.13%   1.811%
4    6.527  1377  1403  1444  BB   4355548 189691795 20.24%  11.718%
5    7.711  1642  1661  1677  BB 2    59712   1613932   0.17%   0.100%

6   10.179  2186  2199  2222  BV 2   103577   4204829   0.45%   0.260%
7   10.390  2222  2245  2299  VV 5   5913674 937400013 100.00% 57.906%
8   10.665  2299  2305  2332  VB 4   5142221 164917056  17.59%  10.187%
9   11.698  2514  2530  2572  BB    640813 15779875   1.68%   0.975%
10  12.115  2595  2621  2630  BV    66055   1348697   0.14%   0.083%

11  12.193  2630  2638  2648  VB    38946   715190   0.08%   0.044%
12  12.845  2760  2780  2803  BB    45371   886432   0.09%   0.055%
13  17.644  3801  3826  3853  BB   4797602 118131176  12.60%   7.297%
14  18.355  3966  3981  3991  BV    191220  3282579   0.35%   0.203%
15  18.506  3991  4014  4029  PV    268745   4727823   0.50%   0.292%

16  20.094  4339  4360  4402  BB    79377   1437526   0.15%   0.089%

Sum of corrected areas: 1618843604

MIPK.      Fri Jul 05 10:44:25 2002  GCMS]

```

## 7.4 Thermodynamic calculations for the basic pathway of the MBOH test reaction

### 7.4.1 Calculation of the thermodynamic equilibrium for the conversion of MBOH into acetone and acetylene (basic pathway)

For the formation of acetylene and acetone, the thermodynamic equilibrium was calculated within the temperature range of 423 to 573 K with the equilibrium constant  $K_b$ . Table A-3 gives the molar enthalpy of reaction at standard conditions and table A-4, is the stoichiometric table of the basic pathway of the MBOH reaction system.



**Table A-3.** Thermodynamic data for basic pathway of the MBOH test reaction calculated by group contribution method of Gani/Constantinou.

	Equilibrium constant	$\Delta H^{298}$ in kJ/mol	$\Delta G^{298}$ in kJ/mol
equation A-1	$K_b$	57.85	44.73

**Table A-4.** Stoichiometric table for the conversion of MBOH to acetylene and acetone.

Bond	Reaction time (min)	Equilibrium
MBOH	$N(\text{MBOH}, t=0)$	$N(\text{MBOH}, 0) * (1 - X_b)$
AON	$t=0$	$N(\text{MBOH}, 0) * X_b$
ACY	$t=0$	$N(\text{MBOH}, 0) * X_b$
Total P	$p(\text{MBOH})$	$p(\text{MBOH}, 0) + p(\text{MBOH}, 0) * X_b$

$X_{\text{basic}}$ : Amount of MBOH, that is converted to acetone and acetylene.

$p(\text{MBOH})$ : partial pressure of MBOH.

$X_b$  : Conversion of basic pathway,  $N(\text{MBOH}, t=0)$  : amount of MBOH at  $t=0$  min

AON : acetone, ACY : Acetylene

Equilibrium constant  $K_b$  was calculated by means of the partial pressures:

$$K_b = \frac{P_{\text{Acetone}} \cdot P_{\text{Acetylene}}}{P_{\text{MBOH}}} \quad \text{equation. A-2}$$



The equilibrium constant was calculated for different temperatures with van't Hoff's equation (equation A-3). The ratio of the equilibrium constants at temperatures  $T_1$  and  $T_2$ , can be calculated with the equation A-4, if the enthalpy of reaction is known at both temperatures.

$$\left( \frac{d \ln K_p}{dT} \right)_p = \frac{\Delta H_{rxn}^0(T)}{RT^2} \quad \text{equation A-3}$$

$$\ln \frac{K_p(T_2)}{K_p(T_1)} = \int_{T_1}^{T_2} \frac{\Delta H_{rxn}^0(T)}{RT^2} dT = -\frac{\Delta H_{rxn}^0(T)}{R} \cdot \left( \frac{1}{T_2} - \frac{1}{T_1} \right) \quad \text{equation A-4}$$

The temperature dependence of enthalpy of reaction  $\Delta H_{rxn}^0(T)$  is given through equation A-5

$$\Delta H_{rxn}^0(T) = \Delta H_{rxn}^0(298 K) + \int_{298 K}^{T_2} \Delta C_p(T) dT \quad \text{equation A-5}$$

The heat capacity  $C_p$  itself is temperature dependent too and this is indicated mostly in the form of equation A-6 with the parameters a, b, c and d. If this is not the case, it must be transformed into this form.

$$C_p(T) = a + b \cdot T + c \cdot T^2 + d \cdot T^3 \quad \text{equation A-6}$$

Therewith can be solved and one receives to one equation A-7 (100)

$$\begin{aligned} \ln \frac{K_p(T_2)}{K_p(T_1)} &= \frac{\Delta a}{R} \cdot \ln \frac{T_2}{T_1} + \frac{\Delta b}{2R} \cdot (T_2 - T_1) + \frac{\Delta c}{6R} \cdot (T_2^2 - T_1^2) + \frac{\Delta d}{12R} \cdot (T_2^3 - T_1^3) \\ &+ \frac{1}{R} \left[ -\Delta H_{rxn}^0(T_1) + \Delta a T_1 + \frac{\Delta b}{2} T_1^2 + \frac{\Delta c}{3} T_1^3 + \frac{\Delta d}{4} T_1^4 \right] \cdot \left[ \frac{1}{T_2} - \frac{1}{T_1} \right] \end{aligned} \quad \text{equation A-7}$$

With the resulting calculated values for  $K_b$ , for each temperature (equation 8) the conversion  $X(MBOH)$  can be determined by equation A-9:

$$p(AON) = \sqrt{\frac{K_b \cdot p(MBOH)^2}{1 + K_b}} \quad \text{equation A-8}$$

$$X(MBOH) = \frac{p(MBOH) - p(AON)}{p(MBOH)} \quad \text{equation A-9}$$

Summary results for the decomposition methylbutynol over Si/Al 5 and 10 calcined for 3h at 550 °C on time on stream.

**Table A-5. Si/Al 5**

time on stream	MBOH	Acetylene		Acetone		MBYNE		MIPK	
min	conversion	yield	selectivity	yield	selectivity	yield	selectivity	yield	selectivity
0	15,04	0,82	5,42	0,75	5,01	8,82	58,63	4,65	30,94
19	7,56	0,42	5,50	0,45	5,93	3,04	40,22	3,66	48,35
37	5,90	0,00	0,00	0,00	0,00	2,38	40,42	3,51	59,58
54	4,67	0,00	0,00	0,00	0,00	1,71	36,67	2,96	63,33
90	4,36	0,00	0,00	0,00	0,00	1,55	35,46	2,81	64,54
108	3,95	0,00	0,00	0,00	0,00	1,45	36,64	2,51	63,36
126	3,70	0,00	0,00	0,00	0,00	1,34	36,25	2,36	63,75

**Table A-6. Si/Al 10**

time on stream	MBOH	MBYNE		MIPK	
min	conversion	yield	selectivity	yield	selectivity
0	51,49	51,49	100,00	0,00	0,00
17	20,61	18,31	88,81	2,31	11,19
32	11,71	9,11	77,80	2,60	22,20
49	8,97	6,02	67,16	2,95	32,84
85	7,88	5,12	64,90	2,77	35,10
103	6,70	4,19	62,62	2,50	37,38
121	5,96	3,56	59,78	2,39	40,22
139	5,53	3,28	59,34	2,25	40,66
174	5,08	2,88	56,64	2,20	43,36
192	4,76	2,69	56,47	2,07	43,53

Summary results for the decomposition methylbutynol over Si/Al 20 and 40 calcined for 3h at 550 °C on time on stream.

**Temp reac. 120 °C**

time on stream	MBOH	Acetone		MBYNE		MIPK	
min	conversion	yield	selectivity	yield	selectivity	yield	selectivity
0	84,31	0,00	0,00	84,31	100,00	0,00	0,00
17	62,46	1,28	2,05	61,18	97,95	0,00	0,00
32	42,36	1,16	2,74	40,72	96,12	0,48	1,14
50	27,34	0,00	0,00	26,94	98,53	0,40	1,47
67	24,07	0,00	0,00	23,60	98,08	0,46	1,92
85	21,67	0,00	0,00	21,19	97,79	0,48	2,21
103	19,73	0,00	0,00	19,21	97,34	0,52	2,66
120	15,61	0,00	0,00	15,05	96,46	0,55	3,54
173	14,76	0,00	0,00	14,23	96,37	0,54	3,63

**Table A-8. Si/Al 40**

time on stream	MBOH	MBYNE		Prenal	
( min)	conversion	yield	selectivity	yield	selectivity
0	92,87	92,87	100,00	0,00	0,00
16	75,49	74,99	99,33	0,00	0,00
31	61,71	60,92	98,71	0,24	0,39
48	50,93	50,35	98,87	0,28	0,55
66	44,39	43,85	98,78	0,29	0,66
84	42,45	42,12	99,24	0,32	0,76
102	40,30	40,02	99,30	0,28	0,70
119	38,08	37,76	99,16	0,32	0,84
137	34,75	34,43	99,08	0,32	0,92
155	31,49	31,17	98,99	0,32	1,01
173	29,18	28,86	98,92	0,31	1,08
191	28,85	28,54	98,91	0,31	1,09

Summary results for the decomposition methylbutynol of Si/Al 5 and 10 calcined for 3h at 550 °C on time on stream.

**Temp reac. 180 °C**

**Table A-9. Si/Al 5**

time on stream	MBOH	Acetylene		Acetone		MBYNE		Prenal		MIPK	
min	conversion	yield	selectivity	yield	selectivity	yield	selectivity	yield	selectivity	yield	selectivity
0	79,39	55,00	69,28	0,00	0,00	24,39	30,72	0,00	0,00	0,00	0,00
20	65,86	21,79	33,08	14,34	21,78	25,14	38,16	0,49	0,74	4,11	6,24
35	42,82	10,90	25,46	8,43	19,68	15,97	37,30	0,27	0,64	7,24	16,92
53	36,35	8,34	22,94	6,45	17,73	13,67	37,59	0,30	0,81	7,61	20,92
71	34,81	7,49	21,52	5,92	17,00	13,39	38,47	0,26	0,76	7,75	22,25
89	32,37	6,59	20,35	5,18	16,00	12,90	39,85	0,00	0,00	7,71	23,81
125	26,09	4,86	18,63	3,87	14,84	10,52	40,33	0,00	0,00	6,84	26,20

**Table A-10. Si/Al 10**

time on stream	MBOH	Acetylene		Acetone		MBYNE		Prenal		MIPK	
min	conversion	yield	selectivity	yield	selectivity	yield	selectivity	yield	selectivity	yield	selectivity
0	73,78	10,83	14,67	7,68	10,41	51,40	69,66	0,49	0,66	3,39	4,60
15	59,15	7,30	12,35	5,88	9,94	40,07	67,74	0,49	0,84	5,41	9,14
33	45,92	4,95	10,79	4,10	8,93	29,98	65,29	0,25	0,55	6,63	14,44
51	39,47	3,90	9,87	3,31	8,39	25,50	64,60	0,00	0,00	6,77	17,14
69	35,86	3,39	9,45	2,83	7,88	22,83	63,66	0,22	0,60	6,60	18,40
87	31,47	2,66	8,46	2,26	7,17	20,08	63,82	0,25	0,78	6,22	19,77
105	29,67	2,50	8,44	2,09	7,03	18,88	63,64	0,28	0,94	5,92	19,94

Summary results for the decomposition methylbutynol over Si/Al 20 and 40 calcined for 3h at 550 °C on time on stream.

**Temp reac. 180 °C**

**Table A-11. Si/Al 20**

time on stream	MBOH	Acetylene		Acetone		MBYNE		MIPK	
min	conversion	yield	selectivity	yield	selectivity	yield	selectivity	yield	selectivity
0	90,59	14,83	16,37	5,72	6,31	70,04	77,31	0,00	0,00
15	95,45	2,17	2,28	1,60	1,68	91,67	96,04	0,00	0,00
30	95,49	1,65	1,73	1,41	1,48	92,43	96,79	0,00	0,00
48	95,49	1,42	1,49	1,33	1,39	92,73	97,11	0,00	0,00
66	95,34	1,34	1,40	1,27	1,33	92,46	96,98	0,26	0,28
84	94,00	1,16	1,24	1,16	1,23	91,24	97,07	0,44	0,47
102	92,67	1,11	1,20	1,14	1,23	89,84	96,94	0,59	0,64
120	91,57	1,05	1,14	1,04	1,13	88,63	96,79	0,70	0,77
138	90,88	1,00	1,10	1,00	1,10	87,91	96,73	0,77	0,85
157	88,98	0,94	1,05	0,97	1,09	85,94	96,58	0,88	0,99

**Table A-12. Si/Al 40**

time on stream	MBOH	Acetylene		Acetone		MBYNE		Prenal		MIPK	
min	conversion	yield	selectivity	yield	selectivity	yield	selectivity	yield	selectivity	yield	selectivity
0	89,03	44,46	49,94	15,48	17,39	29,09	32,68	0,00	0,00	0,00	0,00
19	92,86	2,08	2,24	2,02	2,18	88,01	94,78	0,00	0,00	0,74	0,80
34	93,89	1,87	1,99	1,90	2,02	89,31	95,12	0,00	0,00	0,82	0,88
51	93,35	1,53	1,64	1,81	1,94	88,78	95,11	0,28	0,30	0,95	1,01
70	93,50	1,34	1,44	1,61	1,72	89,46	95,68	0,28	0,29	0,81	0,87
88	93,42	1,27	1,36	1,52	1,63	89,69	96,01	0,00	0,00	0,94	1,00
106	93,52	1,16	1,24	1,42	1,52	90,09	96,34	0,00	0,00	0,84	0,90
124	92,74	1,04	1,12	1,41	1,52	89,12	96,10	0,30	0,32	0,87	0,94

Summary results for the decomposition methyl butynol over Si/Al 5,10 calcined for 3h at 900 °C on time on stream.

**Temp reac. 120 °C**

time on stream	MBOH	MBYNE		MIPK	
min	conversion	yield	selectivity	yield	selectivity
0	11,97	10,91	91,13	1,06	8,87
17	8,87	7,99	90,11	0,88	9,89
35	7,77	6,94	89,37	0,83	10,63
53	7,44	6,65	89,41	0,79	10,59
71	6,07	5,33	87,78	0,74	12,22
89	5,93	5,19	87,41	0,75	12,59
106	5,57	4,86	87,26	0,71	12,74
124	5,67	4,99	87,97	0,68	12,03
142	4,79	4,16	86,76	0,63	13,24
160	4,88	4,26	87,22	0,62	12,78
178	4,61	4,00	86,89	0,60	13,11

**Table A-14. Si/Al 10**

time on stream	MBOH	Acetylene		Acetone		MBYNE		MIPK	
min	conversion	0,00	0,00	yield	selectivity	yield	selectivity	yield	selectivity
0	47,52	0,00	0,00	23,16	48,75	24,13	50,77	0,23	0,48
32	24,00	0,00	0,00	0,00	0,00	24,00	100,00	0,00	0,00
50	22,96	0,00	0,00	0,00	0,00	22,96	100,00	0,00	0,00
68	18,88	0,00	0,00	0,00	0,00	18,88	100,00	0,00	0,00
85	17,13	0,00	0,00	0,00	0,00	17,13	100,00	0,00	0,00
103	17,08	0,00	0,00	0,00	0,00	17,08	100,00	0,00	0,00
121	15,34	0,00	0,00	0,00	0,00	15,12	98,53	0,23	1,47
139	14,33	0,00	0,00	0,00	0,00	14,10	98,39	0,23	1,61
156	14,25	0,00	0,00	0,00	0,00	14,02	98,36	0,23	1,64
174	10,30	0,00	0,00	0,00	0,00	10,06	97,73	0,23	2,27

Summary results for the decomposition methyl butynol over Si/Al 20 and 40 calcined for 3h at 900 °C on time on stream.

**Temp reac. 120 °C**

**Table A-15. Si/Al 20**

time on stream	MBOH	Acetylene		Acetone		MBYNE		Prenal		MIPK	
min	conversion	yield	selectivity	yield	selectivity	yield	selectivity	yield	selectivity	yield	selectivity
0	75,77	0,00	0,00	1,62	2,14	73,76	97,35	0,00	0,00	0,39	0,51
18	51,97	0,00	0,00	0,59	1,13	51,39	98,87	0,00	0,00	0,00	0,00
51	43,72	0,00	0,00	0,00	0,00	43,46	99,40	0,26	0,60	0,00	0,00
68	36,43	0,00	0,00	0,00	0,00	36,17	99,28	0,26	0,72	0,00	0,00
86	33,62	0,00	0,00	0,00	0,00	33,35	99,19	0,27	0,81	0,00	0,00
104	28,68	0,00	0,00	0,00	0,00	28,39	99,01	0,29	0,99	0,00	0,00
121	26,61	0,00	0,00	0,00	0,00	26,32	98,93	0,28	1,07	0,00	0,00
139	25,52	0,00	0,00	0,00	0,00	25,23	98,87	0,29	1,13	0,00	0,00
157	24,16	0,00	0,00	0,00	0,00	23,87	98,80	0,29	1,20	0,00	0,00

**Table A-16. Si/Al 40**

time on stream	MBOH	Acetylene		Acetone		MBYNE		MIPK	
min	conversion	yield	selectivity	yield	selectivity	yield	selectivity	yield	selectivity
0	83,44	0,00	0,00	1,42	1,70	81,54	97,71	0,48	0,58
18	59,13	0,00	0,00	0,61	1,03	58,13	98,31	0,00	0,00
35	45,24	0,00	0,00	0,00	0,00	44,72	98,86	0,00	0,00
53	38,43	0,00	0,00	0,00	0,00	37,88	98,56	0,00	0,00
71	33,47	0,00	0,00	0,00	0,00	32,87	98,20	0,00	0,00
89	29,48	0,00	0,00	0,00	0,00	28,87	97,90	0,00	0,00
106	27,51	0,00	0,00	0,00	0,00	26,86	97,63	0,00	0,00
133	25,26	0,00	0,00	0,00	0,00	24,58	97,28	0,00	0,00
166	23,76	0,00	0,00	0,00	0,00	23,08	97,14	0,00	0,00
184	21,47	0,00	0,00	0,00	0,00	20,80	96,86	0,00	0,00

Summary results for the decomposition methylbutynol over Si/Al 5 and 10 calcined for 3h at 900 °C on time on stream.

**Temp reac. 180 °C**

**Table A-17. Si/Al 5**

time on stream	MBOH	acetylene		Acetone		MBYNE		MIPK	
min	conversion	yield	selectivity	yield	selectivity	yield	selectivity	yield	selectivity
0	49,06	8,47	17,26	6,31	12,87	34,02	69,34	0,26	0,54
18	48,57	7,94	16,36	6,06	12,48	34,31	70,65	0,25	0,52
36	48,21	7,25	15,03	5,75	11,93	35,21	73,04	0,00	0,00
54	46,98	6,47	13,77	5,19	11,05	34,75	73,97	0,57	1,22
72	47,90	6,48	13,54	5,24	10,94	35,51	74,14	0,66	1,38
90	47,74	6,36	13,31	5,13	10,74	35,45	74,26	0,81	1,69
108	47,71	6,11	12,80	5,01	10,50	36,38	76,25	0,21	0,44
126	45,52	6,13	13,47	4,96	10,90	34,43	75,63	0,00	0,00

**Table A-18. Si/Al 10**

time on stream	MBOH	Acetylene		Acetone		MBYNE		Prenal		MIPK	
min	conversion	yield	selectivity	yield	selectivity	yield	selectivity	yield	selectivity	yield	selectivity
0	94,78	15,79	16,66	4,38	4,62	73,72	77,78	0,89	0,94	0,00	0,00
15	94,36	3,69	3,91	2,79	2,96	87,65	92,89	0,22	0,24	0,00	0,00
31	94,16	3,38	3,59	2,86	3,04	87,91	93,37	0,00	0,00	0,00	0,00
49	94,74	2,99	3,15	2,59	2,73	89,17	94,12	0,00	0,00	0,00	0,00
67	93,28	2,80	3,01	2,54	2,72	87,64	93,95	0,00	0,00	0,29	0,32
85	92,54	2,60	2,81	2,39	2,58	87,19	94,22	0,00	0,00	0,36	0,39
103	92,01	2,38	2,59	2,28	2,48	86,92	94,47	0,00	0,00	0,43	0,46
121	88,51	2,16	2,44	2,11	2,38	83,71	94,58	0,00	0,00	0,53	0,60
139	86,63	2,06	2,37	1,92	2,22	81,66	94,26	0,30	0,34	0,70	0,81
158	86,65	2,02	2,33	1,80	2,08	81,82	94,43	0,27	0,31	0,74	0,85
176	83,27	2,01	2,41	1,89	2,27	78,06	93,74	0,51	0,61	0,80	0,96
194	80,77	1,89	2,33	1,75	2,17	75,67	93,69	0,60	0,74	0,86	1,06



Summary results for the decomposition methylbutynol over Si/Al 20 and 40 calcined for 3h at 900 °C on time on stream

**Temp reac. 180 °C**

**Table A-19. Si/Al 20**

time on stream	MBOH	Acetylene		Acetone		MBYNE		MIPK	
min	conversion	yield	selectivity	yield	selectivity	yield	selectivity	yield	selectivity
0	90,19	1,60	1,77	1,80	2,00	85,93	95,27	0,86	0,95
41	90,48	1,32	1,46	1,59	1,76	86,77	95,90	0,79	0,88
59	90,53	1,15	1,27	1,43	1,58	87,18	96,31	0,76	0,84
77	90,60	1,01	1,12	1,32	1,45	87,61	96,70	0,66	0,73
95	90,57	0,91	1,00	1,23	1,36	87,84	97,00	0,58	0,64
113	90,34	0,83	0,92	1,15	1,27	87,82	97,21	0,53	0,59
131	90,50	0,87	0,96	1,22	1,35	87,84	97,07	0,56	0,62
149	90,26	0,81	0,89	1,07	1,19	87,86	97,34	0,52	0,58
167	90,05	0,80	0,89	1,06	1,18	87,48	97,15	0,54	0,60
185	89,52	0,80	0,90	1,04	1,16	86,96	97,13	0,56	0,63

time on stream	MBOH	Acetylene		Acetone		MBYNE		prenal		MIPK	
min	conversion	yield	selectivity	yield	selectivity	yield	selectivity	yield	selectivity	yield	selectivity
0	87,83	53,48	60,89	18,07	20,57	6,81	7,76	9,46	10,78	0,00	0,00
18	90,75	4,62	5,09	4,03	4,44	80,51	88,72	0,29	0,32	1,30	1,43
33	91,04	3,47	3,81	3,01	3,31	83,37	91,58	0,00	0,00	1,18	1,30
51	91,03	3,02	3,32	2,66	2,92	84,33	92,64	0,00	0,00	1,01	1,11
69	90,79	2,60	2,86	2,38	2,62	84,70	93,29	0,25	0,28	0,87	0,95
87	90,76	2,35	2,59	2,16	2,38	85,00	93,65	0,47	0,51	0,79	0,87
105	90,64	2,10	2,31	1,93	2,13	85,31	94,12	0,55	0,61	0,75	0,82
123	90,41	2,09	2,32	1,91	2,11	84,84	93,84	0,85	0,94	0,72	0,79
141	90,17	2,08	2,30	1,90	2,10	84,44	93,64	1,10	1,22	0,67	0,74
159	89,71	2,00	2,22	1,80	2,00	83,88	93,50	1,28	1,42	0,64	0,72
177	89,45	1,83	2,05	1,68	1,87	83,87	93,77	1,30	1,46	0,62	0,69

Summary results for the decomposition methylbutynol over pure titanium oxide and pure zirconia on time on stream

**Temp reac. 180 °C, Sub: MBOH**

**Table A-21. Pure TiO<sub>2</sub>**

time on stream	MBOH	Acetylene		Acetone		MBYNE		MIPK		HMB	
min	conversion	yield	selectivity	yield	selectivity	yield	selectivity	yield	selectivity	yield	selectivity
0	0,00	0,00	0,00	0,00	0,00	0,00	0,00	0,00	0,00	0,00	0,00
18	17,26	4,59	26,59	2,08	12,05	8,54	49,49	0,66	3,84	1,39	8,03
36	14,23	3,48	24,44	2,90	20,38	6,73	47,25	0,41	2,87	0,72	5,06
54	12,55	3,04	24,25	2,61	20,79	5,91	47,14	0,35	2,76	0,64	5,07
72	10,71	2,73	25,52	2,34	21,87	5,18	48,33	0,00	0,00	0,46	4,29
90	9,12	2,32	25,39	1,94	21,29	4,42	48,46	0,00	0,00	0,44	4,86
108	9,44	2,42	25,64	2,04	21,62	4,56	48,25	0,00	0,00	0,42	4,49
126	9,34	2,42	25,95	2,04	21,86	4,47	47,83	0,00	0,00	0,41	4,35
144	8,74	2,26	25,86	1,95	22,26	4,17	47,74	0,00	0,00	0,36	4,14

**Table A-22. Pure ZrO<sub>2</sub>**

time on stream	MBOH	Acetylene		Acetone		MBYNE		Prenal		MIPK	
min	conversion	yield	selectivity	yield	selectivity	yield	selectivity	yield	selectivity	yield	selectivity
0	98,09	0,10	0,10	0,08	0,08	0,00	0,00	97,89	99,79	0,03	0,03
18	97,86	0,10	0,10	0,08	0,08	0,00	0,00	97,66	99,79	0,02	0,02
36	97,14	0,09	0,10	0,08	0,08	0,00	0,00	96,94	99,80	0,02	0,02
54	97,04	0,00	0,00	0,09	0,09	0,00	0,00	96,93	99,89	0,02	0,02
68	96,89	0,10	0,10	0,00	0,00	0,00	0,00	96,77	99,88	0,02	0,02
86	96,31	0,10	0,10	0,08	0,09	0,00	0,00	96,11	99,79	0,02	0,02
104	96,50	0,10	0,10	0,08	0,09	0,00	0,00	96,30	99,79	0,02	0,02
122	99,98	0,10	0,10	0,08	0,08	0,00	0,00	99,77	99,79	0,03	0,03
140	95,99	0,09	0,09	0,08	0,08	0,00	0,00	95,80	99,80	0,02	0,03

Summary results for the decomposition methylbutynol over pure hafnium oxide and Pr<sub>6</sub>O<sub>11</sub> on time on stream

**Temp reac. 180 °C, Sub: MBOH**

**Table A-23. Pure TiO<sub>2</sub>**

time on stream	MBOH	Acetylene		Acetone		MBYNE		MIPK		HMB	
min	conversion	yield	selectivity	yield	selectivity	yield	selectivity	yield	selectivity	yield	selectivity
0	24,07	7,11	29,54	6,09	25,28	6,08	25,27	0,75	3,13	4,04	16,78
18	19,83	5,91	29,78	5,07	25,55	5,51	27,77	0,53	2,69	2,82	14,22
36	17,99	5,41	30,07	4,67	25,97	5,16	28,65	0,44	2,44	2,32	12,87
54	16,88	5,14	30,44	4,44	26,32	4,91	29,08	0,39	2,32	2,00	11,84
72	16,73	5,20	31,07	4,43	26,50	4,87	29,10	0,37	2,19	1,86	11,14
90	15,36	4,90	31,89	4,21	27,44	4,52	29,42	0,00	0,00	1,73	11,25
108	14,19	4,51	31,81	3,89	27,37	4,21	29,64	0,00	0,00	1,59	11,18
126	13,68	4,34	31,75	3,76	27,47	4,05	29,60	0,00	0,00	1,53	11,17
144	12,65	3,96	31,30	3,45	27,24	3,78	29,92	0,00	0,00	1,46	11,54
162	12,19	3,81	31,25	3,31	27,15	3,68	30,23	0,00	0,00	1,39	11,37
180	11,74	3,62	30,81	3,16	26,91	3,61	30,72	0,00	0,00	1,36	11,57

**Table A-24. Pure ZrO<sub>2</sub>**

time on stream	MBOH	Acetylene		Acetone		MIPK		HMB	
min	conversion	yield	selectivity	yield	selectivity	yield	selectivity	yield	selectivity
0	98,08	0,08	0,08	0,08	0,08	97,47	99,38	0,45	0,46
17	97,40	0,08	0,09	0,08	0,08	96,30	98,86	0,94	0,97
35	96,31	0,09	0,09	0,08	0,09	95,05	98,69	1,10	1,14
53	96,54	0,09	0,09	0,08	0,09	95,31	98,73	1,05	1,09
71	95,57	0,09	0,10	0,09	0,09	94,21	98,58	1,18	1,23
89	95,39	0,09	0,10	0,09	0,09	94,07	98,62	1,13	1,19
107	94,00	0,09	0,10	0,09	0,10	92,50	98,41	1,31	1,40
125	95,43	0,09	0,10	0,08	0,09	94,23	98,73	1,03	1,08
143	95,59	0,09	0,09	0,08	0,09	94,36	98,71	1,07	1,12

Summary results for the decomposition methylbutynol over  $ZrO_2/Al_2O_3$ ,  $TiO_2/Al_2O_3$  on time on stream

**Temp reac. 180 °C, Sub: MBOH+ H<sub>2</sub>O 2 wt.%**

**Table A-25.  $ZrO_2/Al_2O_3$**

time on stream	MBOH	Acetylene		Acetone		MBYNE		Prenal		MIPK	
min	conversion	yield	selectivity	yield	selectivity	yield	selectivity	yield	selectivity	yield	selectivity
0	48,04	13,06	27,20	11,38	23,69	12,80	26,64	0,00	0,00	10,80	22,47
17	40,09	10,60	26,43	9,11	22,72	10,42	26,00	0,00	0,00	9,97	24,86
34	33,50	8,57	25,57	7,32	21,85	8,72	26,04	0,00	0,00	8,89	26,54
52	32,24	8,26	25,62	7,12	22,09	8,30	25,75	0,00	0,00	8,56	26,54
70	32,92	8,70	26,42	7,49	22,76	8,24	25,03	0,00	0,00	8,49	25,79
88	30,37	7,95	26,17	6,84	22,51	7,57	24,94	0,00	0,00	8,01	26,39
106	27,60	6,98	25,29	6,07	22,00	7,03	25,46	0,00	0,00	7,52	27,25
124	27,08	6,85	25,31	5,94	21,94	6,91	25,51	0,00	0,00	7,38	27,24
142	26,31	6,74	25,61	5,78	21,98	6,64	25,22	0,00	0,00	7,15	27,19
160	24,88	6,33	25,44	5,46	21,95	6,26	25,15	0,00	0,00	6,83	27,46

**Table A-26.  $TiO_2 /Al_2O_3$**

time on stream	MBOH	Acetylene		Acetone		MBYNE		Prenal		MIPK	
min	conversion	yield	selectivity	yield	selectivity	yield	selectivity	yield	selectivity	yield	selectivity
0	53,20	17,50	32,89	13,74	25,83	18,32	34,44	0,00	0,00	3,65	6,85
18	51,05	14,58	28,56	11,74	23,00	16,97	33,23	0,00	0,00	7,76	15,21
36	50,33	13,84	27,50	11,20	22,26	16,90	33,59	0,25	0,50	8,13	16,16
54	49,47	13,37	27,03	10,75	21,73	16,39	33,13	0,31	0,63	8,64	17,47
72	47,87	12,49	26,08	10,20	21,31	15,94	33,30	0,36	0,76	8,88	18,55
90	46,73	11,87	25,41	9,75	20,88	15,54	33,25	0,40	0,85	9,17	19,62
108	48,42	12,04	24,86	9,86	20,35	16,37	33,80	0,43	0,89	9,73	20,09
126	48,42	12,04	24,86	9,86	20,35	16,37	33,80	0,43	0,89	9,73	20,09
144	44,04	10,99	24,96	9,05	20,56	14,65	33,26	0,42	0,96	8,92	20,26
162	43,17	10,71	24,82	8,75	20,27	14,39	33,33	0,45	1,04	8,87	20,55

Summary results for the decomposition methylbutynol over  $ZrO_2/Al_2O_3$ ,  $TiO_2/Al_2O_3$  on time on stream

Temp reac. 180 °C, Sub: MBOH

Table A-27.  $ZrO_2/Al_2O_3$

time on stream	MBOH	Acetylene		Acetone		MBYNE		Prenal		MIPK	
min	conversion	yield	selectivity	yield	selectivity	yield	selectivity	yield	selectivity	yield	selectivity
0	68,10	30,56	44,88	26,20	38,47	7,93	11,64	0,00	0,00	3,41	5,01
18	36,17	13,87	38,33	11,49	31,78	5,32	14,70	0,00	0,00	5,49	15,19
36	31,72	11,94	37,64	9,90	31,20	4,85	15,28	0,00	0,00	5,04	15,88
54	31,24	11,69	37,41	9,70	31,06	4,80	15,38	0,00	0,00	5,05	16,15
72	28,53	10,69	37,47	8,87	31,08	4,33	15,17	0,00	0,00	4,65	16,29
90	23,12	8,41	36,36	7,01	30,33	3,67	15,89	0,00	0,00	4,03	17,41
108	23,68	8,61	36,37	7,18	30,32	3,80	16,04	0,00	0,00	4,09	17,27
126	21,97	7,88	35,89	6,59	29,98	3,55	16,17	0,00	0,00	3,95	17,97
144	19,67	7,09	36,03	5,92	30,07	3,17	16,09	0,00	0,00	3,50	17,81

Table A-28.  $TiO_2/Al_2O_3$

time on stream	MBOH	Acetylene		Acetone		MBYNE		Prenal		MIPK	
min	conversion	yield	selectivity	yield	selectivity	yield	selectivity	yield	selectivity	yield	selectivity
0	43,97	14,79	33,63	12,35	28,09	7,35	16,70	0,00	0,00	9,49	21,58
17	35,56	11,37	31,98	9,53	26,79	6,07	17,08	0,00	0,00	8,58	24,14
35	34,68	10,98	31,67	9,22	26,58	6,09	17,57	0,00	0,00	8,39	24,18
53	30,97	9,64	31,11	8,18	26,42	5,41	17,48	0,00	0,00	7,74	24,99
71	28,26	8,82	31,23	7,44	26,34	4,98	17,63	0,00	0,00	7,01	24,80
89	23,81	7,18	30,16	6,08	25,55	4,33	18,19	0,00	0,00	6,21	26,10
107	21,77	6,53	30,00	5,53	25,39	4,06	18,66	0,00	0,00	5,65	25,95
125	22,17	6,74	30,41	5,68	25,61	4,08	18,41	0,00	0,00	5,67	25,57
143	20,07	5,93	29,56	5,05	25,17	3,83	19,10	0,00	0,00	5,25	26,16
161	21,77	6,71	30,82	5,60	25,71	4,00	18,36	0,00	0,00	5,47	25,11

Summary results for the decomposition methylbutynol over  $\text{HfO}_2/\text{Al}_2\text{O}_3$  with different ratios on time on stream.

**Temp reac. 180 °C, Sub: MBOH**

**Table A-29.**  $\text{HfO}_2/\text{Al}_2\text{O}_3$  (5:95 wt.%)

time on stream	MBOH	Acetylene		Acetone		MBYNE		Prenal		MIPK	
min	conversion	yield	selectivity	yield	selectivity	yield	selectivity	yield	selectivity	yield	selectivity
0	93,22	41,32	44,33	32,18	34,52	11,99	12,86	0,00	0,00	7,74	8,30
18	42,27	16,13	38,15	13,26	31,37	5,40	12,77	0,00	0,00	7,49	17,71
36	33,23	12,25	36,86	10,10	30,41	4,49	13,51	0,00	0,00	6,39	19,23
54	29,74	10,79	36,26	8,83	29,69	4,33	14,57	0,00	0,00	5,79	19,48
72	25,28	8,92	35,26	7,36	29,10	3,72	14,71	0,00	0,00	5,29	20,92
90	22,23	7,58	34,12	6,30	28,34	3,46	15,58	0,00	0,00	4,88	21,96
107	22,68	7,89	34,79	6,53	28,77	3,50	15,43	0,00	0,00	4,77	21,01
125	21,08	7,26	34,45	6,01	28,52	3,26	15,45	0,00	0,00	4,55	21,58
143	19,72	6,77	34,32	5,59	28,36	3,06	15,54	0,00	0,00	4,29	21,78
161	18,23	6,14	33,69	5,09	27,95	2,93	16,07	0,00	0,00	4,06	22,29
179	17,93	6,06	33,80	5,03	28,04	2,87	16,01	0,00	0,00	3,97	22,15

**Table A-30.**  $\text{HfO}_2/\text{Al}_2\text{O}_3$  (10:90 wt.%)

time on stream	MBOH	Acetylene		Acetone		MBYNE		Prenal		MIPK		HMB	
min	conversion	yield	selectivity	yield	selectivity	yield	selectivity	yield	selectivity	yield	selectivity	yield	selectivity
0	63,75	28,71	45,04	21,40	33,57	12,72	19,95	0,00	0,00	0,92	1,44	0,00	0,00
18	61,50	23,33	37,93	18,41	29,93	14,47	23,53	0,00	0,00	5,30	8,61	0,00	0,00
36	58,12	22,73	39,10	18,09	31,12	11,43	19,66	0,00	0,00	5,88	10,12	0,00	0,00
54	57,13	22,08	38,65	17,50	30,63	11,17	19,55	0,00	0,00	6,14	10,76	0,24	0,42
72	49,83	18,44	37,01	14,83	29,76	9,65	19,36	0,31	0,62	6,60	13,25	0,00	0,00
90	49,22	18,15	36,87	14,50	29,47	9,58	19,46	0,28	0,58	6,44	13,09	0,27	0,54
108	48,60	17,86	36,75	14,28	29,38	9,46	19,46	0,28	0,58	6,44	13,25	0,28	0,57
126	46,82	17,00	36,30	13,64	29,13	9,12	19,49	0,30	0,64	6,46	13,81	0,30	0,64
144	46,76	17,16	36,70	13,69	29,28	9,13	19,51	0,31	0,65	6,48	13,86	0,00	0,00

Summary results for the decomposition methylbutynol over hydrotalcites (HT) intercalated different anions on stream.

**Temp reac. 120 °C, Sub: MBOH**

**Table A-31. HT-Cl**

time on stream	MBOH	Acetylene		Acetone	
min	conversion	yield	selectivity	yield	selectivity
11	9,95	9,95	100,00	0,00	0,00
26	19,10	5,54	29,01	4,87	25,49
44	11,41	6,31	55,30	5,10	44,70
62	11,43	6,36	55,64	5,07	44,36
80	11,24	6,05	53,86	5,18	46,14
98	10,96	6,11	55,76	4,85	44,24
116	8,84	4,80	54,24	4,05	45,76
134	8,85	4,81	54,28	4,05	45,72
162	8,84	4,80	54,26	4,04	45,74

**Table A- 32. HT-TA**

time on stream	MBOH	Acetylene		Acetone	
min	conversion	yield	selectivity	yield	selectivity
14,00	62,32	28,62	45,93	12,40	19,90
32,00	43,22	17,50	40,49	13,42	31,05
68,00	28,82	16,22	56,26	12,61	43,74
86,00	29,19	16,32	55,92	12,87	44,08
104,00	26,78	14,86	55,49	11,92	44,51
122,00	26,72	14,69	55,00	12,02	45,00
140,00	27,19	15,21	55,94	11,98	44,06

Summary results for the decomposition methylbutynol over hydrotalcites (HT) intercalated different anions on stream.

**Temp reac. 120 °C, Sub: MBOH**

**Table A-33. HT-CO<sub>3</sub>**

time on stream	MBOH	Acetylene		Acetone	
min	conversion	yield	selectivity	yield	selectivity
16	43,89	26,12	59,50	17,78	40,50
32	38,72	22,78	58,81	15,81	40,82
48	40,57	23,96	59,07	16,47	40,59
66	39,45	23,46	59,47	15,87	40,22
86	35,55	20,85	58,65	14,58	41,02
120	35,92	21,09	58,71	14,72	40,97
138	37,36	22,02	58,93	15,24	40,78
157	35,60	20,95	58,85	14,54	40,86

**Table A-34. HT-SO<sub>4</sub>**

time on stream	MBOH	Acetylene		Acetone		Yace/Yacetone
min	conversion	yield	selectivity	yield	selectivity	
18	8,14	6,64	81,61	1,50	18,39	4,44
36	5,31	5,31	100,00	0,00	0,00	0,00
54	1,94	0,98	50,74	0,95	49,26	1,03
72	1,70	0,81	47,84	0,89	52,16	0,92
90	1,99	1,05	53,05	0,93	46,95	1,13
108	1,72	0,90	52,26	0,82	47,74	1,09
154	1,63	0,83	51,04	0,80	48,96	1,04
172	1,71	0,87	50,88	0,84	49,12	1,04

**Table A-35. HT-HPO<sub>4</sub>**

time on stream	MBOH	Acetylene		Acetone	
min	conversion	yield	selectivity	yield	selectivity
15	14,32	8,05	56,25	6,17	43,11
33	13,69	7,33	53,59	6,35	46,41
51	14,46	8,01	55,38	6,45	44,62
69	13,75	7,71	56,10	6,04	43,90
87	13,18	7,17	54,43	6,00	45,57
105	14,32	8,19	57,17	6,13	42,83
150	12,73	7,03	55,23	5,70	44,77
168	11,55	6,45	55,85	5,10	44,15



Summary results for the decomposition methylbutynol over hydrotalcites (HT) intercalated different anions on stream

**Temp reac. 160 °C, Sub : MBOH**

**Table A-36. HT-Cl**

time on stream	MBOH	Acetylene		acetone	
min	conversion	yield	selectivity	yield	selectivity
16	61,68	59,70	96,78	1,99	3,22
31	81,09	49,08	60,52	31,79	39,20
49	83,36	49,48	59,35	33,62	40,33
67	80,56	46,18	57,32	34,13	42,37
86	82,10	46,94	57,18	34,90	42,52
104	81,65	46,49	56,94	34,92	42,77
122	80,69	45,85	56,82	34,63	42,92
141	80,72	45,81	56,75	34,70	42,99
159	76,17	42,74	56,12	33,23	43,63
177	73,16	41,20	56,31	31,83	43,51
196	77,48	43,63	56,31	33,68	43,47

**Table A-37 HT-TA**

time on stream	MBOH	Acetylen		Acetone	
min	conversion	yield	selectivity	yield	selectivity
15	42,60	41,68	97,84	0,92	2,16
30	91,80	59,22	64,51	32,42	35,31
48	90,49	54,03	59,71	36,25	40,06
86	89,91	52,07	57,91	37,62	41,84
104	89,60	51,56	57,55	37,82	42,21
122	85,27	53,83	63,12	31,30	36,71
140	88,99	50,69	56,96	38,09	42,80
158	88,59	50,20	56,66	38,18	43,10
177	85,97	48,38	56,27	37,42	43,52
216	85,90	48,08	55,97	37,63	43,81
231	85,19	47,58	55,86	37,43	43,94

Summary results for the decomposition methylbutynol over hydrotalcites (HT) intercalated different anions on stream.

**Temp reac. 160 °C, Sub: MBOH**

**Table A-38 HT-CO<sub>3</sub>**

time on stream	MBOH	Acetylene		Acetone	
min	conversion	yield	selectivity	yield	selectivity
17	70,96	70,43	99,24	0,54	0,76
32	56,99	31,17	54,70	25,82	45,30
49	82,89	51,76	62,44	30,96	37,35
67	98,98	63,39	64,05	35,35	35,72
85	82,15	48,59	59,15	33,37	40,62
103	88,70	51,30	57,84	37,19	41,93
121	84,78	49,34	58,20	35,23	41,56
139	82,49	48,28	58,53	34,01	41,23
157	82,29	47,54	57,78	34,55	41,99
193	84,23	48,66	57,77	35,39	42,01
210	84,10	48,49	57,66	35,41	42,11

**Table A-39 . HT-SO<sub>4</sub>**

time o stream	MBOH	Acetylen		Actone	
min	conversion	yield	selectivity	yield	selectivity
9	17,65	9,73	55,16	7,91	44,84
27	19,92	10,78	54,10	9,14	45,90
45	19,06	10,35	54,30	8,71	45,70
81	19,46	10,73	55,13	8,73	44,87
99	20,72	11,25	54,31	9,47	45,69
117	19,82	11,11	56,06	8,71	43,94
136	20,43	11,14	54,51	9,30	45,49
154	17,99	9,73	54,09	8,26	45,91

**Table A-40. HT-HPO<sub>4</sub>**

time on stream	MBOH	Acetylene		Acetone	
min	conversion	yield	selectivity	yield	selectivity
15	76,54	48,54	63,42	27,80	36,33
33	48,80	41,89	85,84	6,91	14,16
51	76,33	44,25	57,98	31,76	41,61
69	78,21	46,05	58,89	31,84	40,71
77	75,52	43,23	57,24	32,01	42,39
105	75,07	43,05	57,35	31,70	42,22
141	75,36	43,12	57,21	31,98	42,43
159	75,91	43,00	56,64	32,59	42,94
177	71,71	39,65	55,29	31,78	44,32

Summary results for the Knoevenagel condensation over Si/Al 5 and 10 calcined for 3h at 550 °C.

**Table A-41.** Si/Al (5:95 wt.%)

time on stream	Malononitrile	Benzaldehyde	Benzylidenmalononitrile	Maximal conversion Malonitrile=
min	Conversion [mol%]		Yield [mol%]	X/X(max) [*100]
0	0,00	0,00	0,00	0,00
5	11,16	32,82	32,82	14,06
10	16,74	49,57	49,57	23,54
15	20,74	62,80	62,80	31,50
20	23,20	71,33	71,33	32,86
30	27,09	83,68	83,68	41,49
45	32,20	94,26	94,26	66,84
60	32,78	97,26	97,26	69,06
75	31,66	98,45	98,45	79,47
90	32,73	99,19	99,19	85,71
120	34,01	100,00	100,00	100,00
255	34,18	100,00	100,00	100,00

**Table A-42.** Si/Al (10:90 wt.%)

time on stream	Malononitrile	Benzaldehyde	Benzylidenmalononitrile	Maximal conversion Malonitrile=
min	Conversion [mol%]		Yield [mol%]	X/X(max) [*100]
0	0,00	0,00	0,00	0,00
5	4,68	13,13	13,13	14,06
10	7,84	21,68	21,68	23,54
15	10,49	29,50	29,50	31,50
20	10,94	34,56	34,56	32,86
30	13,81	43,78	43,78	41,49
45	22,25	68,01	68,01	66,84
60	22,99	72,72	72,72	69,06
75	26,46	80,35	80,35	79,47
90	28,53	88,75	88,75	85,71
120	31,28	98,48	98,48	93,97
255	32,23	99,21	99,21	96,81

Summary results for the Knoevenagel condensation over Si/Al 20 and 40 calcined for 3h at 550 °C.

**Table A-43.** Si/Al (20:80 wt.%)

time on stream	Malononitrile	Benzaldehyde	Benzylidenmalononitrile	Maximal conversion Malonitrile=
min	Conversion [mol%]		Yield [mol%]	X/X(max) [*100]
0	0,16	0,43	0,43	0,47
5	1,22	3,39	3,39	3,66
10	2,09	6,01	6,01	6,29
15	2,71	7,49	7,49	8,15
20	3,35	9,33	9,33	10,06
30	4,69	13,70	13,70	14,10
45	6,13	17,77	17,77	18,43
60	7,54	21,40	21,40	22,65
75	9,36	27,17	27,17	28,12
90	10,65	30,89	30,89	31,99
120	13,53	39,85	39,85	40,64
255	22,27	68,05	68,05	66,88

**Table A-44.** Si/Al (40:60 wt.%)

time on stream	Malononitrile	Benzaldehyde	Benzylidenmalononitrile	Maximal conversion Malonitrile=
min	Conversion [mol%]		Yield [mol%]	X/Xmax malononitrle (max) [*100]
0	0,00	0,00	0,00	0,00
5	0,76	2,01	2,01	2,30
10	2,04	5,56	5,56	6,13
15	2,67	7,67	7,67	8,01
20	2,40	7,00	7,00	7,20
30	2,71	7,49	7,49	8,15
45	3,58	9,97	9,97	10,76
60	4,19	11,61	11,61	12,58
75	5,10	14,00	14,00	15,32
90	5,84	16,60	16,60	17,55
120	7,54	21,40	21,40	22,65
255	13,51	39,33	39,33	40,58

Summary results for the Knoevenagel condensation over Si/Al 20 and 40 calcined for 3h at 550 °C.

**Table A-43.** Si/Al (20:80 wt.%)

time on stream	Malononitrile	Benzaldehyde	Benzylidenmalononitrile	Maximal conversion Malonitrile=
min	Conversion [mol%]		Yield [mol%]	X/X(max) [*100]
0	0,16	0,43	0,43	0,47
5	1,22	3,39	3,39	3,66
10	2,09	6,01	6,01	6,29
15	2,71	7,49	7,49	8,15
20	3,35	9,33	9,33	10,06
30	4,69	13,70	13,70	14,10
45	6,13	17,77	17,77	18,43
60	7,54	21,40	21,40	22,65
75	9,36	27,17	27,17	28,12
90	10,65	30,89	30,89	31,99
120	13,53	39,85	39,85	40,64
255	22,27	68,05	68,05	66,88

**Table A-44.** Si/Al (40:60 wt.%)

time on stream	Malononitrile	Benzaldehyde	Benzylidenmalononitrile	Maximal conversion Malonitrile=
min	Conversion [mol%]		Yield [mol%]	X/Xmax malononitrile (max) [*100]
0	0,00	0,00	0,00	0,00
5	0,76	2,01	2,01	2,30
10	2,04	5,56	5,56	6,13
15	2,67	7,67	7,67	8,01
20	2,40	7,00	7,00	7,20
30	2,71	7,49	7,49	8,15
45	3,58	9,97	9,97	10,76
60	4,19	11,61	11,61	12,58
75	5,10	14,00	14,00	15,32
90	5,84	16,60	16,60	17,55
120	7,54	21,40	21,40	22,65
255	13,51	39,33	39,33	40,58

Summary results for the Knoevenagel condensation over Si/Al 20 and 40 calcined for 3h at 900 °C.

**Table A-47. Si/Al (20:80 wt.%)**

time on stream	Malononitrile	Benzaldehyde	Benzylidenmalononitrile	Maximal conversion Malnonitrile=
min	Conversion [mol%]		Yield [mol%]	X/Xmax malonitrile (max) [*100]
0	1,05	2,79	2,79	3,16
5	1,42	3,75	3,75	4,25
10	1,45	3,90	3,90	4,37
15	1,68	4,60	4,60	5,04
20	1,74	4,76	4,76	5,22
30	2,24	6,51	6,51	6,73
45	2,55	6,77	6,77	7,66
60	2,36	6,55	6,55	7,09
75	2,61	7,04	7,04	7,83
90	2,79	7,53	7,53	8,39
120	3,34	9,57	9,57	10,03
255	4,52	12,19	12,19	13,57

**Table A-48. Si/Al (40:60 wt.%)**

time on stream	Malononitrile	Benzaldehyde	Benzylidenmalononitril	Maximal conversion Malnonitrile=
min	Conversion [mol%]		Yield [mol%]	X/Xmax malonitrile (max) [*100]
0	1,09	3,01	3,01	3,27
5	1,10	3,08	3,08	3,30
10	1,16	3,29	3,29	3,47
15	1,27	3,69	3,69	3,83
20	1,42	3,97	3,97	4,25
30	1,36	3,84	3,84	4,08
45	1,44	4,07	4,07	4,32
60	1,61	4,54	4,54	4,85
75	1,58	4,37	4,37	4,74
90	1,56	4,33	4,33	4,69
120	1,66	4,62	4,62	4,98
255	2,28	6,39	6,39	6,84

Summary results for the Knoevenagel condensation over hydrotalcites intercalated different anions.

**Table A-49. HT-CO<sub>3</sub>**

time on stream	Malonitrile	Benzaldehyde	Benzylidenmalonitrile	Maximal conversion Malonitrile=
min	Conversion [mol%]		Yield [mol%]	X/X(max) [*100]
0	0,58	1,53	1,53	1,74
5	12,20	36,73	36,73	36,63
10	18,22	53,47	53,47	54,74
15	20,82	60,67	60,67	62,54
20	22,21	65,89	65,89	66,72
30	25,78	76,27	76,27	77,45
45	27,61	82,54	82,54	82,92
60	30,14	90,47	90,47	90,52
75	30,86	92,79	92,79	92,70
90	30,30	94,73	99,80	91,01
120	30,70	96,93	99,90	92,21
255	32,47	100,00	100,00	97,53

**Table A-50. HT-Cl**

time on stream	Malonitrile	Benzaldehyde	Benzylidenmalonitrile	Maximal conversion Malonitrile=
min	Conversion [mol%]		Yield [mol%]	X/X(max) [*100]
0	0,13	0,35	0,35	0,39
5	8,75	25,15	25,15	26,29
10	8,75	25,15	25,15	26,29
15	9,95	28,39	28,39	29,88
20	11,14	31,88	31,88	33,47
30	12,91	36,40	36,40	38,79
45	15,19	44,12	44,12	45,64
60	16,74	49,07	49,07	50,27
75	19,06	55,25	55,25	57,24
90	19,05	56,88	56,88	57,21
120	21,82	64,32	64,32	65,54
255	22,44	74,98	74,98	67,42

Summary results for the Knoevenagel condensation over hydrotalcites (HT) intercalated different anions.

**Table A-51. HT-HPO<sub>4</sub>**

time on stream	Malononitrile	Benzaldehyde	Benzylidenmalononitrile	Maximal conversion Malnonitrile=
min	Conversion [mol%]		Yield [mol%]	X/X(max) [*100]
0	0,13	0,35	0,35	0,39
5	8,75	25,15	25,15	26,29
10	8,75	25,15	25,15	26,29
15	9,95	28,39	28,39	29,88
20	11,14	31,88	31,88	33,47
30	12,91	36,40	36,40	38,79
45	15,19	44,12	44,12	45,64
60	16,74	49,07	49,07	50,27
75	19,06	55,25	55,25	57,24
90	19,05	56,88	56,88	57,21
120	21,82	64,32	64,32	65,54
255	22,44	74,98	74,98	67,42

**Table A-52. HT-TA**

time on stream	Malononitrile	Benzaldehyde	Benzylidenmalononitrile	Maximal conversion Malnonitrile=
min	Conversion [mol%]		Yield [mol%]	X/X(max) [*100]
0	0,31	1,03	1,03	0,93
5	1,39	3,95	3,95	4,18
10	1,62	4,62	4,62	4,88
15	2,12	5,52	5,52	6,37
20	2,05	5,70	5,70	6,16
30	2,28	6,25	6,25	6,86
45	2,56	6,92	6,92	7,70
60	3,36	9,41	9,41	10,10
75	3,49	9,69	9,69	10,48
90	3,16	10,16	10,16	9,50
120	3,46	9,36	9,36	10,39
255	4,47	12,23	12,23	13,42



Summary results for the Knoevenagel condensation over hydrotalcites intercalated different anions.

**Table A-53.** HT-SO<sub>4</sub>

time on stream	Malononitrile	Benzaldehyde	Benzylidenmalononitrile	Maximal conversion Malnonitrile=
min	Conversion [mol%]		Yield [mol%]	X/X(max) [*100]
0	0,00	0,00	0,00	0,00
5	0,36	0,98	0,98	1,07
10	0,30	0,81	0,81	0,89
15	0,29	0,80	0,80	0,88
20	0,48	1,38	1,38	1,44
30	0,77	2,25	2,25	2,32
45	0,66	1,80	1,80	1,98
60	0,70	1,93	1,93	2,11
75	0,77	2,10	2,10	2,30
90	0,93	2,63	2,63	2,81
120	1,25	3,64	3,64	3,74
255	1,85	5,13	5,13	5,55

## Curriculum Vitae

### Personal details

Family name: Alsawalha  
Name : Murad  
Date of birth: 14.03.1973  
Place of birth: Kuwait  
Status : Single  
Nationality : Jordanian

### Education :

Oct. 1980- Jun. 1984 Elementary education school ( in Kuwait)  
Oct. 1984- Jun. 1988 Low secondary school (in Kuwait)  
Oct. 1988- Jun. 1993 High and school leaving examination (matriculation, Jordan)  
Oct. 1993- Sep. 1999 Study Chemistry at the technical university Lodz-Poland  
Sep.1999 M. Eng., Note: very good  
  
January 2000 PhD student at Ossietsky universität Oldenburg (Germany)  
Faculty of Mathematics and Science, Institute for Pure and Applied Chemistry /Industrial Chemistry.  
  
PhD research title Characterization of acidic and basic properties of heterogeneous Catalysts by test reactions  
  
10. Dec. 2004 Doctor of Science (Dr. rer. nat).

### Occupational career :

Practice 2 weeks Chemistry practical in fabric–Poland  
Nov. 1999- Apr. 2000 Work in Rivage fabric (Supervisor: Production line, Jordan)

Sep. 2001- Jan 2005      Work at the university (Industrial measurements)  
Oct. 2001- Sep.2004      Supervising laboratory work for master students in frame  
of European Exchange Programs.

### **Publication**

Materials Research Bulletin 39 (2004) 263–281

Publication title      “Acidity and basicity of hydrotalcite derived mixed Mg-Al  
Oxides” corporation work with Jagiellonian University  
(Cracow- Poland).

Poster:                      1.09.03 Europa Cat-VI-in Innsbruck (Austria)

### **Awards**

1997 and 1998              Given by the deputy Rector for Students Affairs  
Technical university of Lodz; in recognition of very good results  
in the study.

Sep. 2004- Jan. 2005      Financial grant from German Academic Exchange  
Service (DAAD).

### **Language skills**

Arabic                      : native language  
German                      : very good (four year practice in Germany)  
English                      : very good ( PhD Study in English language)  
Polish                        : very good

## **ERKLÄRUNG**

Hiermit versichere ich, dass ich die vorliegende Dissertation selbständig angefertigt habe und  
Keine anderen als die angegebenen Quellen verwendet habe.

Murad Alsawalha

Oldenburg, den 16. Dezember 2004